CRANFIELD UNIVERSITY

ZHIJUN SHI

PREDICTING FATIGUE CRACK GROWTH LIFE IN INTEGRAL METALLIC SKIN-STRINGER PANELS

SCHOOL OF ENGINEERING
MSc by Research

MSc
Academic Year: 2011 - 2012

Supervisor: Dr. Xiang Zhang
January 2012

CRANFIELD UNIVERSITY

SCHOOL OF ENGINEERING
MSc by Research

MSc

Academic Year 2011 - 2012

ZHIJUN SHI

Predicting Fatigue Crack Growth Life in Integral Metallic Skin-stringer Panels

Supervisor: Dr. Xiang Zhang
January 2012

ABSTRACT

During the past few years, in comparison to traditional riveted structures, integral metallic skin stringer structures have played more and more important roles in aircraft design due to the fact they are economical and also have the ability to reduce weight. Their wide application in aircraft, especially large integral structures is limited because of the fact that they have shortcomings in damage tolerance performance. Hence, calculating the crack growth lives and improving the damage tolerance performance of integral structures by selecting appropriate materials or choosing rational structures is a critical work. Therefore the purpose of this thesis is to find effective analysis methods of integral metallic skin-stringer panels for the use in engineering.

There are two important steps in crack growth lives calculation: Stress intensity factor (SIF) calculation and crack growth calculation. Both shell element models (2D) and three dimensional element models (3D) are built separately to get SIF results through the displacement extrapolation method (DE) using the ABAQUS. During the second step, both Paris law and AFGROW tabular input are used to represent crack growth rates and taken into the life prediction. Three integral metallic skin-stringer panels machined from monolithic aluminium alloys are under investigation with two kinds of materials 2024-T351and 2027-T351. Cracks are beginning from central panel with broken stiffener. Then they grow straight along the skin up to a certain length. When the cracks reach the joint region, it will grow in panel and stiffener respectively. Constant amplitude loads are applied to each specimen, material properties and experimental results regarding the structures are also provided. The results of the calculation show that these methods are all suitable for SIF calculation.

New interactive procedure method is used in SIF calculation. 2D model is built in this new method. In this process, both SIF values of panel and stiffener are calculated when the crack reach the stiffener. Then given a certain cycles, crack growth at both stiffener and panel will be calculated. New model could be built with new crack at panel and stiffener, and SIF values can be calculated. Repeating this work until the crack crosses the stiffener. Although the method is time consuming, the result is more accurate than 2D model.

The author also involved in a Group Design Program (GDP) on conceptual design phase of a 200-seats Flying-wing aircraft. During the period, the author was in charge of the market analysis, 3D view and also took part in structure layout, which would be introduced in appendix.

Keywords: Stress intensity factor, Crack growth, Skin-stringer panels, Displacement extrapolation method

ACKNOWLEDGEMENTS

Dr. Xiang Zhang played an important role in developing the calculations and ideas described in this dissertation. Her ingenuity, hard-working attitude, inquisitiveness, skills as a mentor and ability to distil knowledge to useful elements has impressed me greatly. I have learned a great deal from her about fatigue and damage tolerance analysis. I also admire the successful balance she has achieved between her professional and personal life.

Meanwhile, I would also want to give my appreciation to Aviation Industry Corporation of China (AVIC) and the China Scholarship Council for providing a chance to study at Cranfield University.

There are many other people that I have interacted with during my graduate career that also deserve acknowledgment. I would like to thank Yang Yang, Jian Wang, Huahua Pang for numerous help of life, and I learn a lot from them. I would also like to express my gratitude to the staff of the School of engineering, especially for their help during my GDP process. Furthermore, it was an unforgettable memory to study with my colleagues during this year.

My family and friends also deserve many thanks for their continued support and understanding during the pursuit of my graduate degree. Lastly, for her unwavering encouragement and patience, I thank my girlfriend, to whom this work is dedicated.

TABLE OF CONTENTS

LIST OF FIGURES

LIST OF TABLES

NOTATIONS

Symbols

a	Half of the crack length
a1	Half crack length at the panel
a2	Crack length at the stiffener
Δ a	Crack increment
C_{th}	Empirical constant
da/dN	Crack propagation rate
ds	Element of arc along the integration contour
E	Modulus of elasticity
K	Stress intensity factor
ΔK_0	Threshold intensity factor
N	Cycles
r	Element size
R	Ratio of cyclic load
T	Traction
u	Displacement
W	Width of the plate
β	Non-dimensional function of structural geometry
θ	Coordinate in the local cylindrical coordinate system
μ	Shear modulus
v	Poisson's ratio
σ	Stress

Abbreviations

2D	Two-dimensional
3D	Three-dimensional
CGL	Crack Growth Life
DE	Displacement extrapolation method
DOC	Direct operating cost
FEM	Finite element method
GDP	Group design program
IAS	Integral Airframe Structures
M (T)	Middle crack tension
SIF	Stress intensity factor

1 Introduction

1.1 Back ground

Typical riveted skin-stringers structures have been introduced in aircraft fuselage assemblies since the 1940's, and then widely used in many parts of the aircraft (as shown in Figure 1-1). It seems that it is difficult to get significant improvement in this technology because of the advancement made during the last century. Integral skin-stringer structures which make skin and stringers as a continuum are suitable to change the situation, even though they are poor at damage tolerance performance. Compared with the conventional riveted structures, integral skin-stringer structures have many advantages, such as lower weight and lower cost to manufacture. It is worthy of note that, fewer components mean they are easy to inspect and no holes in riveted joints improve fatigue crack initiation life.

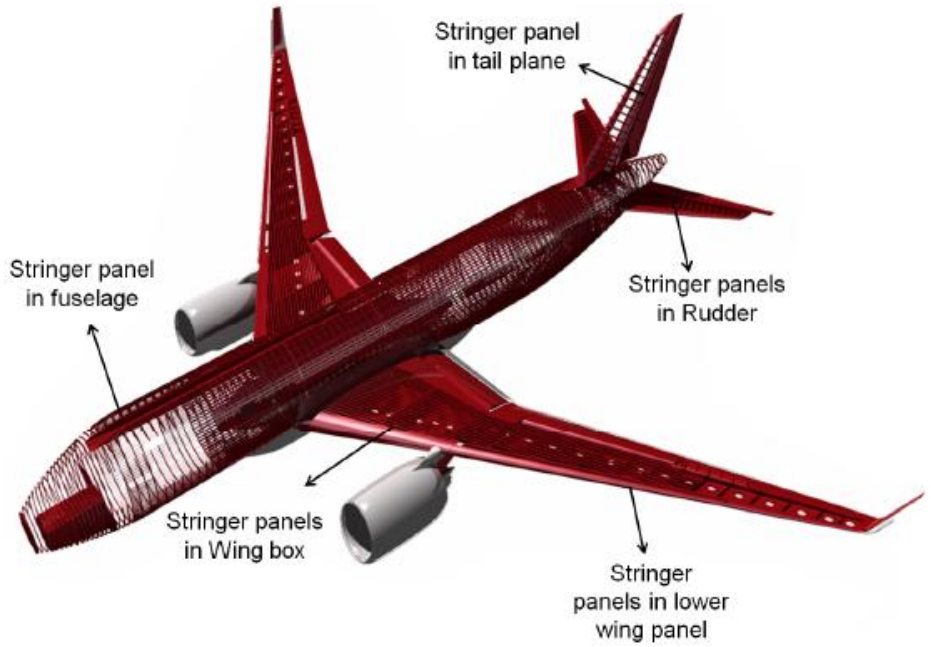

Figure 1-1 Locations of stringer panels in the aircraft

NASA began Integral Airframe Structures (IAS) Program to develop integral metallic structures in 1966 [1]. The purpose of the program was to design and test structures which were lower in price than the current structures and

improvement in structural weight and performance. The IAS program obtained satisfactory results with the improvement and the application of integrally stiffened fuselage structure. The configuration of integral aircraft fuselage structure and conventional fuselage structure are compared in Figure 1-2.

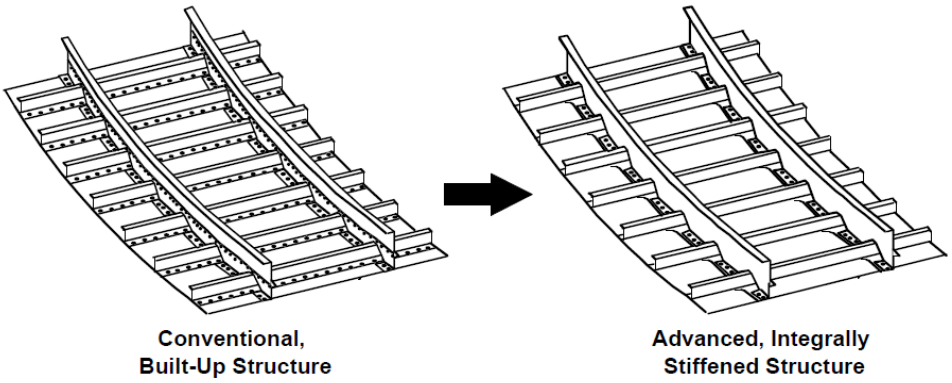

Figure 1-2 Integral aircraft structure and conventional structure [1]

In recent years, the technology of design, analysis integral structures have become one of the key technologies for the widespread use of the integral metallic skin-stringer structures in the aerospace field. Two different methods are used in order to optimize the damage tolerance performance of the integral skin-stringer panels. The first one is to apply new alloy materials with lower crack propagation rate and higher fracture toughness. Another one is to design or optimize new structure conformation. In order to achieve the latter objective, many researchers have been done research to develop efficient and reliable methods to improve the damage tolerance performance of integral skin-stringer panels [2].

1.2 Aim and objectives

Since the lack of damage tolerance behaviour, the life expectancy becomes especially important to the integral metallic skin-stringer panels. The purpose of this paper is to find an effective way for fatigue crack growth life prediction in integral metallic skin-stringer panels for the use in engineering. To achieve this purpose, panels with different aluminium alloys and shapes were analyzed

using finite element method by ABAQUS to calculate various stress intensity factors at different crack length. Then the life of the panels could be computed using several methods, and these results were compared with published experimental results to check the rationality of the calculation process.

The first objective is to study published theory and learn the methods about SIF calculation and crack growth live prediction.

The second one is to compute SIF values of three integral panels using displacement extrapolation methods, then get crack growth lives.

The third one is to compare the results with published test results to determine the feasibility of this method.

1.3 Outline of thesis

Chapter 1 is a brief introduction of the background of this thesis including the development from the skin-stringers riveted structures to integral structures.

Chapter 2 introduces the advantages of integral structures and methods to improve them. Several finite element methods for modelling the integral skin-stringer panels were also introduced, which agreed well with theoretical or experimental results.

Chapter 3 describes several methods used in SIF calculation and life prediction; focus on methods used in this article.

Chapter 4 gives the results of the calculation of 3 panels. At first, several methods were used in middle crack tension geometry to calculate the values of stress intensity factor. After comparison, Displacement extrapolation method was chosen for the SIF calculation of skin-stringer panels. And all the SIF results and life prediction were presented in this chapter.

Chapter 5 discusses some of the difficulties encountered in the calculation process.

Chapter 6 is the conclusions of the thesis and also illustrates some recommendations for the future work.

During this year, the author also took part in the Students' Group Design Project of a conceptual design of a Flying-wing aircraft. This is a new kind of 250-seat commercial aircraft, mainly used in the international air transport market. The author was the coordinator of the market analysis and 3D drawing, besides the author also took part in the work of structure layout. The detail is presented in Appendix A.

2 Literature Review

2.1 Design of Integral Structures

According to NASA's research, "About a third of the airlines' direct operating cost (DOC) of an airplane is associated with the manufacturing cost, which is probably the most critical competitive parameter with regard to market share"[3]. It means that it is an effective way to cut down the manufacturing cost to reduce the acquisition cost of an aircraft. The skin-stringers riveted structures have been used in aircraft fuselage for more than 60 years. These kind of riveted structures have advantages in damage tolerance performance and also fail-safe, since stringers gives another path for load passing, which delays the speed of crack growth. But this kind of design makes it difficult to reduce in cost significantly because they are highly refined and mature with associated construction details and fabrication processes. Nevertheless, metallic structure is well proved, and it will likely retain extensive metallic production capability and skills in the foreseeable future. Hence, the conception of designing renewed large integral metallic skin-stringer panels for aircraft fuselage for low acquisition cost and the emergence of high speed machining is imminent. A typical integral structure made by NASA's ISA program shows in Figure 2-1.

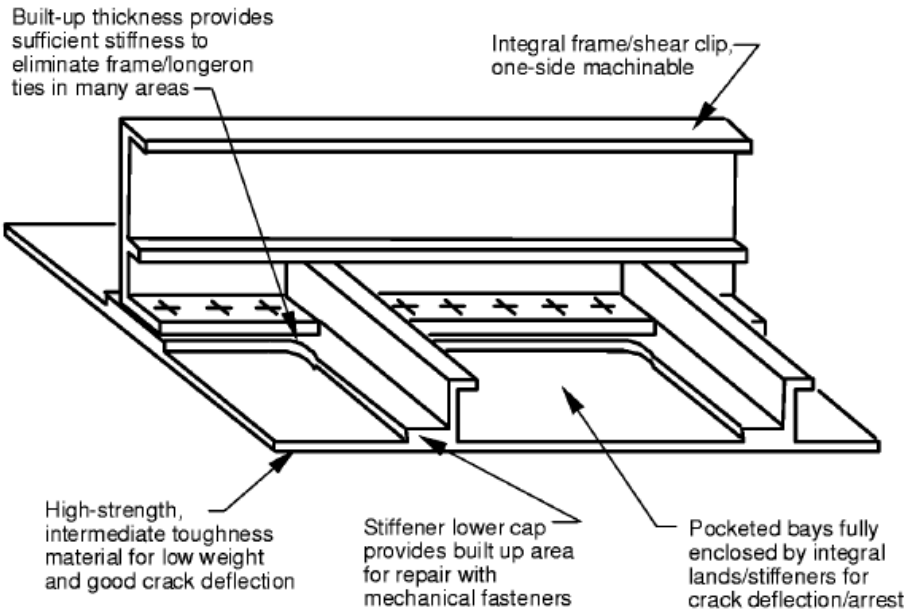

Figure 2-1 Typical integral fuselage [3]

The results were exciting when machined integral structures were taken into Boeing 747 fuselage. It was found to be superior in terms of part count and cost, and almost equivalent in terms of weight when compared with riveted structure. These results are summarized in Table 2-1 [1].

Table 2-1 Results of riveted and integral panels [1]

Factor	Riveted Panel	Integral Panel	Integral Change From Riveted	Target Savings Over Riveted
Number of Parts	78	7	91% reduction	50%
Weight	179 pounds	186 pounds	4% increase	Neutral
Estimated Cost	$33,000	$14,000	58% reduction	25%

2.2 Comparison of riveted and integral structures

It is necessary to investigate the integral panels in details in order to ascertain the possible high benefits over riveted panels.

Figure 2-2 below gives the difference between conventional riveted stringer fuselage panel and the new integral skin-stringer fuselage panel. Figure 2-3 describes the riveted stringer panel and the integral skin-stringer panel.

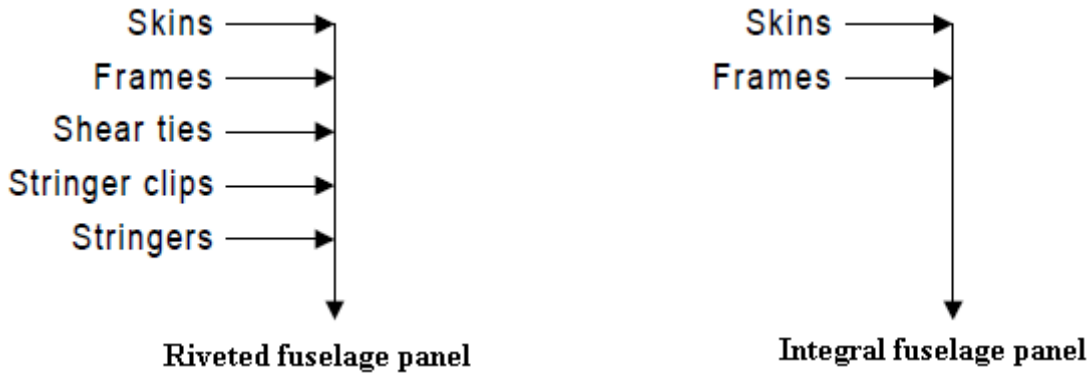

Figure 2-2 Structure of riveted panel and integral fuselage panel [3]

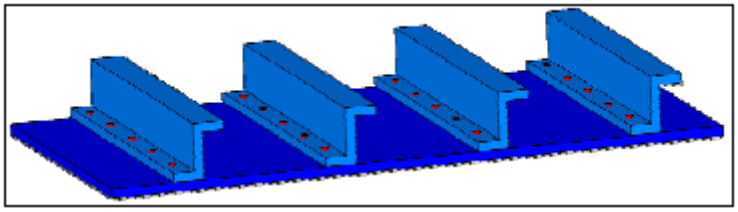

(a) Riveted Stringer Panel

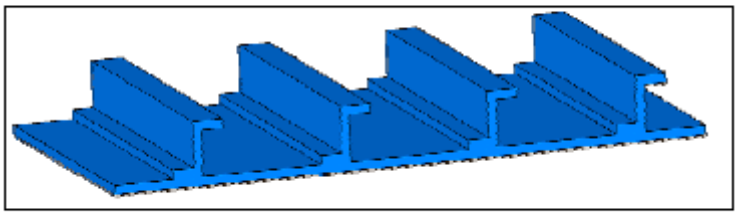

(b) Integral Stringer Panel

Figure 2-3 Riveted stringer panel and integral stringer panel [4]

Nesterenko [4] compared the damage tolerance behaviour of integrally skin-stringer structures and riveted structures, and gave the pros and cons as follow:

For riveted stringer panel, the pro is offering fail safety for the hard of crack going to the stiffener. The cons are causing premature initiation of fatigue cracks, thousands of fasteners to be used and the fact that they are difficult to manufacture and inspect.

For integral stringer panel, the pro are reducing part count and structural complexity, automated processing and improving visual inspection capability. The cons are lacking of redundant structural members, lacking of damage tolerance behaviour and increasing crack growth rates in heat affected zones.

2.3 Improvement of Integral Structures

In order to optimize the damage tolerance performance of integral metallic structures, two particular aspects should be considered.

The first one is developing new kinds of materials with a better fracture toughness property [5]. Although the 7000 series aluminium alloys have sensational mechanical performance, toughness sharp reduction at low temperatures which is especially dangerous for the integral metallic structures

limits its use. Since 2000 series aluminium alloys are not so sensitive to very low temperature, they can be exploited to overcome the disadvantage.

Another one is designing or optimizing structures. In recent years, researchers analysed many different methods for the structure design optimization. It is an effective way to save the time and money for the prototype building through the development of methods to simulate the crack growth behaviour of the components. Retarders of crack growth, which are bonded to integral metallic panels, were investigated in order to overcome the lack of a fail safety performance. In order to create a failsafe design feature, a hybrid structure bonding two different materials together is created in critical zone [6]. These bonded straps still have some disadvantages, even though they have advantages in delaying the fatigue crack growth. Another way for optimization is to reduce crack growth speed in the integral panels through the investigation of the optimized shapes. Stringers which play important roles in the damage tolerance behaviour of integral panels are the most promising fields to analysis [7]. According to the research, the stress intensity factor (SIF) decreases when the crack approaches a stiffener and it increases when the stiffener has been crossed. The overall result is the crack grows slow, because the crack growth depends on SIF variation. Besides, stiffeners increase T-stress, which may cause crack turning. Hence, it is important to build an effective model to describe the SIF evolution during the crossing of the stiffener, in an accurate way.

A phenomenon must be taken seriously enough, crack turning. It is considered to be an important way to Prevent crack propagation. This phenomenon is most likely to happen in thin narrow fuselage skin, and has also been tested in Boeing 707, as shown in Figure 2-4 [8]. Swift [9, 10] observed this phenomenon in cylindrical plates. Pettit [11] did the research on crack turning in riveted panels.

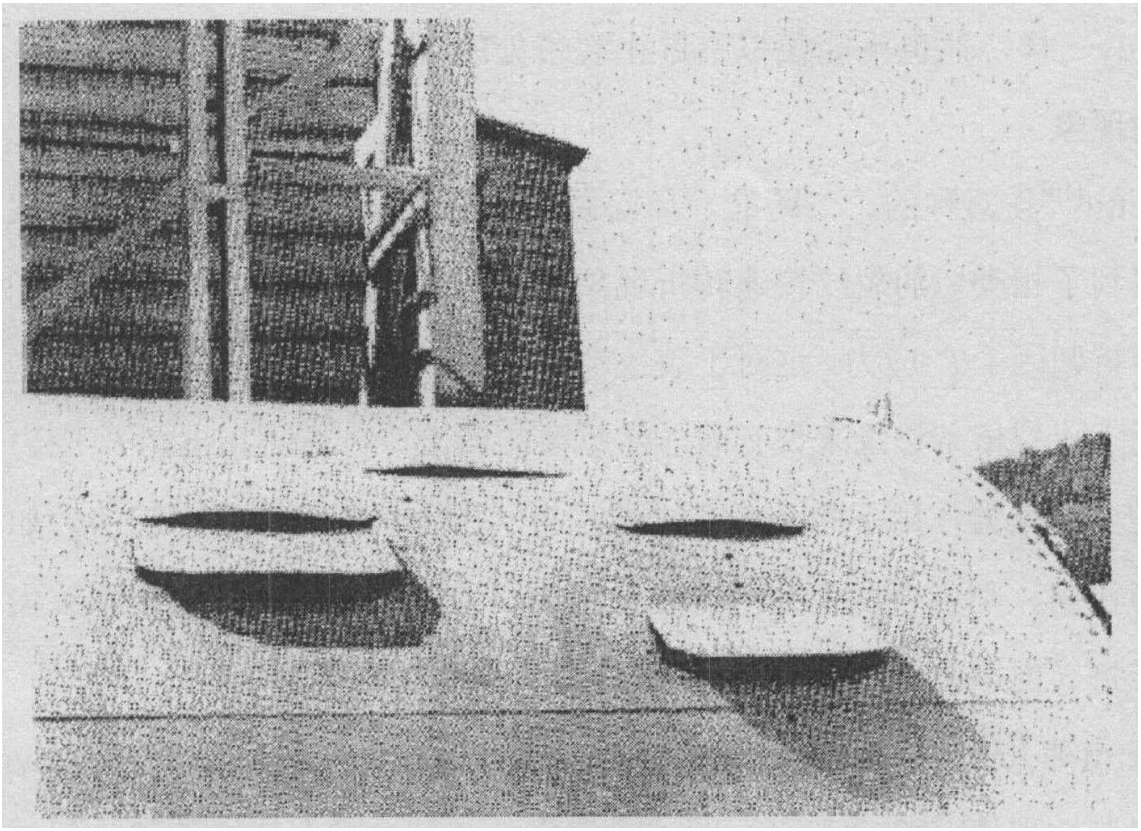

Figure 2-4 Crack turning and flapping in Boeing 707 test [8]

2.4 Model approach

During the last 20 years, SIF in cracked stiffened panels have been calculated in many studies. Several authors [12, 13, and 14] did their research on structures involving cracks in infinite and semi-infinite panels with integral stiffeners. According to their results, the effect of nearby boundaries should be taken seriously into account through numerical methods.

The finite element method (FEM) together with strain energy release rate method and the crack tip opening displacement method were used to calculate SIF for riveted stiffened cracked panels [15]. Utukuri [16] applied the complex variable method together with compatible deformations to finite stiffened structures through boundary collocation method.

Moreira and Pastrama [17] built three-dimensional (3D) models to calculate SIF for two plates using finite element method. They did the work on a through the thickness central crack plate at the beginning. The SIF along the thickness

direction of the panel was calculated, and compared with the literature [18] and 2D finite element analysis. The results showed that the SIF at mid-plane in 3D model were higher than 2D SIF except for very thick plates, in which they were comparable, when thickness was less than half crack length. Similar results were also achieved by Kwon [19].

They then calculated the SIF for a double-stiffened integral panel with uniform traction load (cross section as Figure 2-5). The crack tip was defined as A, B respectively, and J-Integral technique was used in SIF calculation for both crack tips.

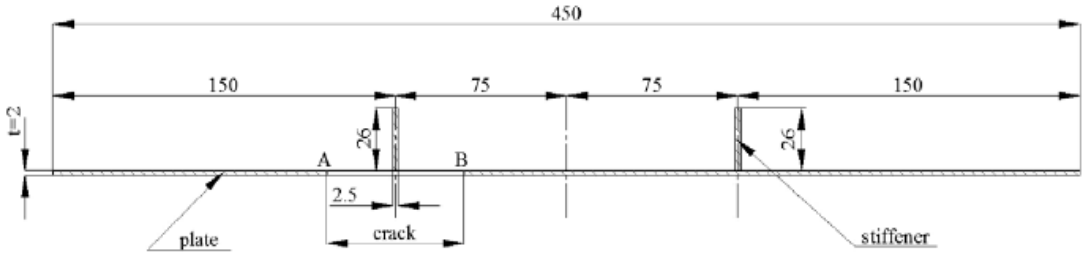

Figure 2-5 Cross section of the integral panel [17]

During their calculation, some values of SIF were negative in the back layer (elements opposite to the stiffener surface). This was caused by negative σ_y values (Figure 2-6).

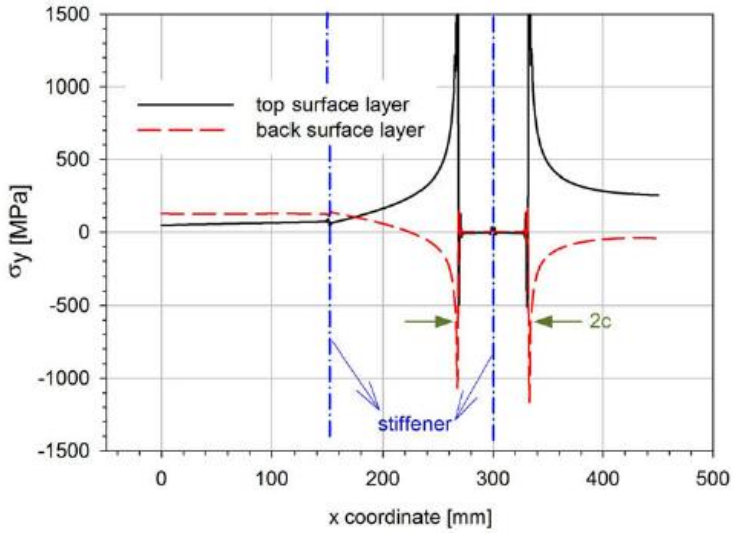

Figure 2-6 Variation of the opening stress [17]

The conclusion of the article [17] gave two important suggestions: First, for the unbroken stiffener panel, the SIF results from the back layer (elements opposite to the stiffener) were the best agreement with results of compounding technique. Second, for the broken stiffener panel, the SIF results from the middle layer were the best agreement with results of compounding technique. Although the results are exciting and helpful in SIF calculation using 3D models, one key important technology about SIF evolution during the crossing of the stiffener is not mentioned in the paper.

Two methods to calculate the behaviour of integrally metallic skin-stringer structures of crack growth were introduced by Fossati and Colombo [20], which agreed well with experimental results. The first one was a finite element model but no constraints on crack front, which meant that the shape of the crack front would modify automatically during the growth of the crack. Given a fixed cycles, the growth on every point depended on the local SIF K. The second one was a finite element model with line crack front, which meant that the growth of the crack with a linear front. The value of K would no longer modify the figure of the front but the propagation speed.

According to the results of the first method, the crack front was far from the straight configuration, Figure 2-7, while the K value was only a slightly bigger than the mean values of the straight configuration. This meant that only a slight difference in propagation rates for those two methods before the crack reached the stringer. The first method reflected the crack growth behaviour profoundly and improved the accuracy in estimation of the fatigue life of the panel. However, the approach was complex and spent a lot of time. Especially when the crack was near the stringer, sudden change in thickness might cause numerical problems in automatic propagation.

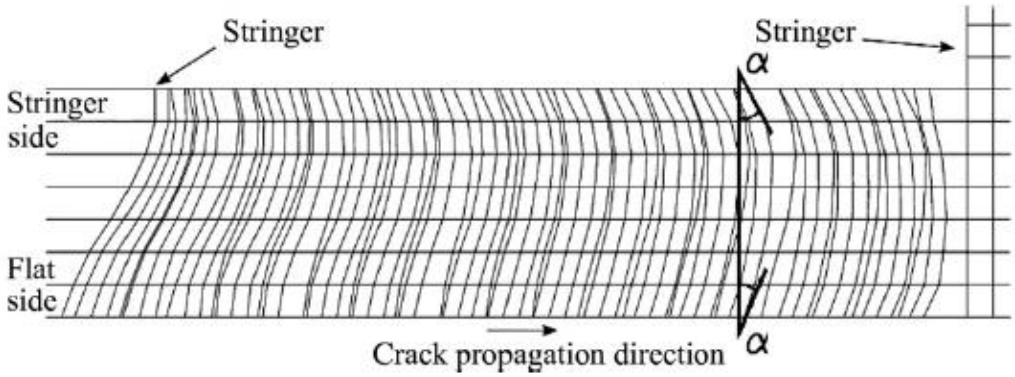

Figure 2-7 Crack front shape [20]

When the crack went into the stringer zone, the front shape shown as Figure 2-8, and the use of second method might cause a significant error. The sudden increase of the section caused a decrease of K values.

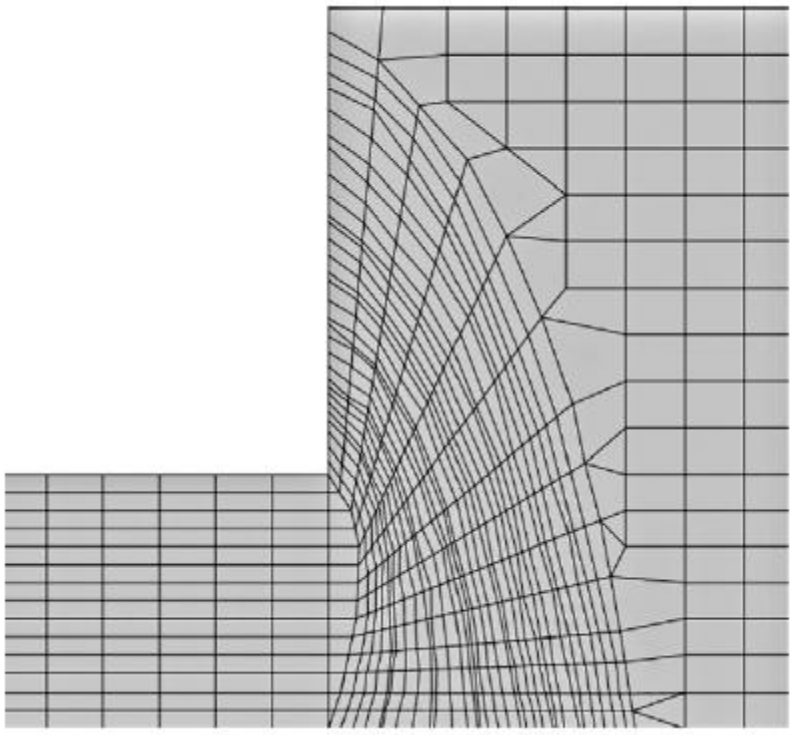

Figure 2-8 Crack front shape in stringer zone [20]

In order to solve the problem of inaccuracy SIF data of the stringer, three different methods were assumed in the article [20]: “Full stringer”, “Half stringer” and “one third stringer”, which were distinguished by the steps taken into

account inside the stringers. The final results showed that the “one third stringer” model is better than the other, as Figure 2-9. The author suggested that ignoring the step of the crack front in the entry of stringer could get a better result except an accurate simulation of the crack front could be done.

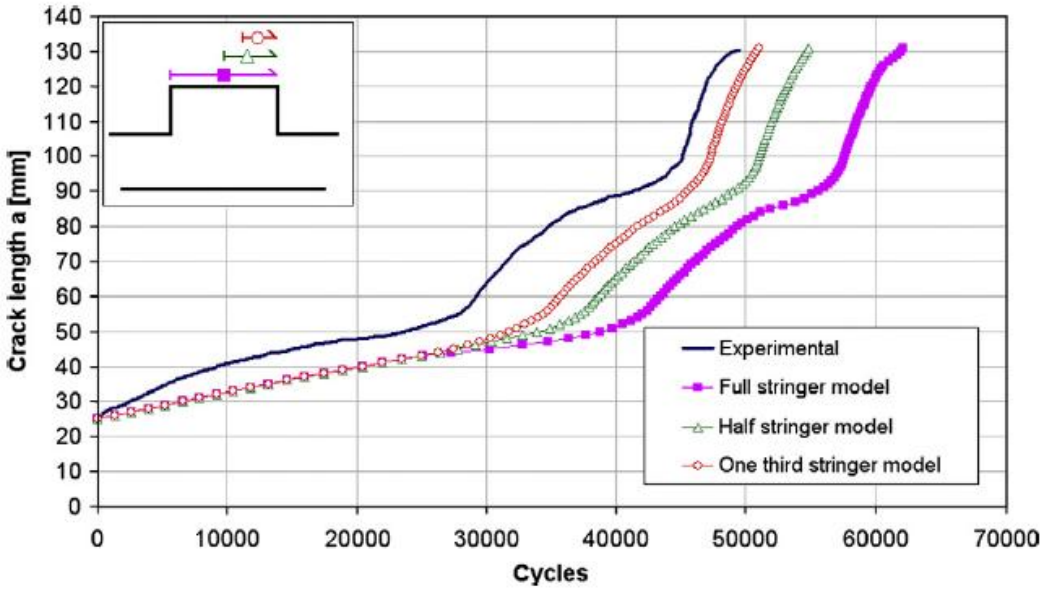

Figure 2-9 Comparison of crack growth behaviour [20]

3 Methodology

This chapter introduces the analysis methods for SIF calculation and crack growth life prediction for integral stiffened panels.

There are three possible forms of classic mode [21]. Three types of mode tensile mod shear mode and tearing mode are shown in Figure 3-1. In this thesis, all the SIF evaluations are using Mode I.

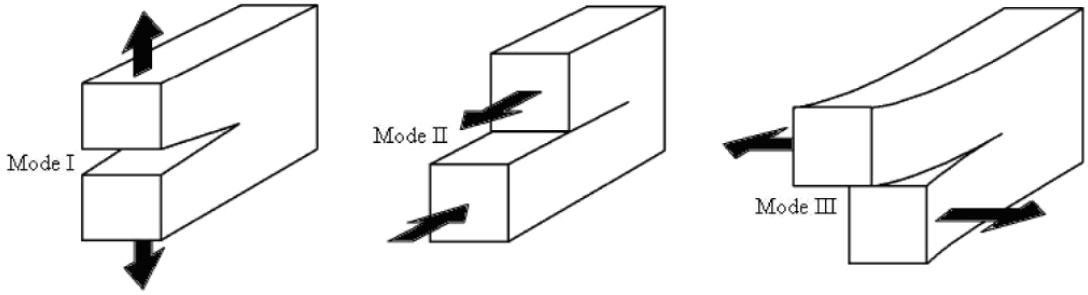

Figure 3-1 Fracture modes

3.1 Method of SIF calculation

3.1.1 Stress extrapolation method [22]

Stress extrapolation method is show to be a direct method to get stress intensity factor using Finite element analysis software. A sufficiently fine mesh is required in the vicinity of the crack, and the theory can be described briefly.

It is very easy to get stress σ_{yi} and the corresponding coordinates r_i from finite element analysis software. Schematic diagram of stress distribution at the crack tip is shown in Figure 3-2, K_{I} is the stress intensity factor at the crack tip corresponding to the value of r = 0.

For each σ_{yi}, the equation is,

$$\mathrm{K_{Ii}} = \sigma_{\mathrm{yi}} \sqrt{2\pi \mathrm{r_i}} \qquad \textbf{(3-1)}$$

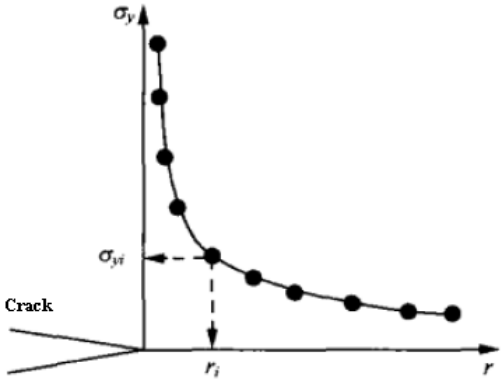

Figure 3-2 Stress around the crack tip

Suppose the relationship between r_i and K_{Ii} are linear, another equation can be deduced.

$$\hat{K}_I = Ar + B \tag{3-2}$$

When r=0, $K_I \approx \hat{K}_I(r=0) = B$.

According to least square method, the result of equation below should be Min.

$$S = \sum \left(K_{Ii} - \hat{K}_{Ii}\right)^2 = \sum (Ar_i + B - K_{Ii})^2 \tag{3-3}$$

Then the equations are,

$$\frac{\partial S}{\partial A} = 2\sum (Ar_i + B - K_{Ii})^2 r_i = 0 \tag{3-4}$$

$$\frac{\partial S}{\partial B} = 2\sum (Ar_i + B - K_{Ii}) = 0 \tag{3-5}$$

Solve two equations above,

$$A = \frac{\sum r_i \sum K_{Ii} - N\sum r_i K_{Ii}}{(\sum r_i)^2 - N\sum {r_i}^2} \tag{3-6}$$

$$K_I \approx B = \frac{\sum r_i \sum r_i K_{Ii} - \sum {r_i}^2 \sum K_{Ii}}{(\sum r_i)^2 - N\sum {r_i}^2} \tag{3-7}$$

B is equal to stress intensity factor.

3.1.2 Displacement extrapolation method [22]

Displacement extrapolation is another direct method in SIF calculation. The significant advantage is that it can get more accurate results than Stress extrapolation method, because displacement is the primary variable in most finite element analysis software and stress is linked to displacement through stress. The same as Stress extrapolation method, the relationship between displacement and distance can be calculated, as show in Figure 3-3.

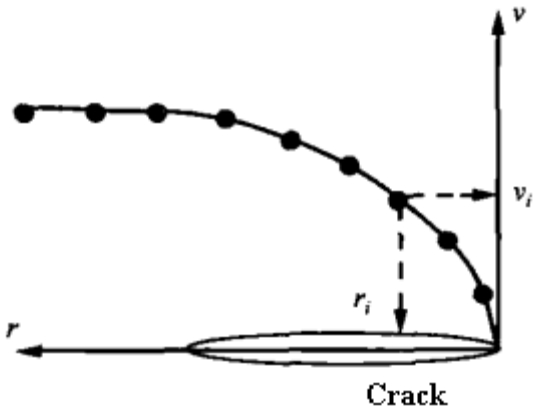

Figure 3-3 Displacement around the crack tip

The equation can be derivate as below,

$$\mathrm{K_{Ii}} = \frac{2\mu}{\kappa + 1} v_i \sqrt{\frac{2\pi}{r_i}} \qquad \textbf{(3-8)}$$

Where, μ is the Shear modulus. κ is the Expansion modulus. v_i is the displacement for point i.

In plane strain situation, κ=3-4ν.

In plane stress situation, $\kappa = \frac{3-\nu}{1+\nu}$.

ν is Poisson's ratio.

The data near the crack tip are not correct, which is the main reason of the error caused. Several points near the crack tip should be deleted. Figure 3-4[22] explains the reason of getting rid of several points around the crack tip.

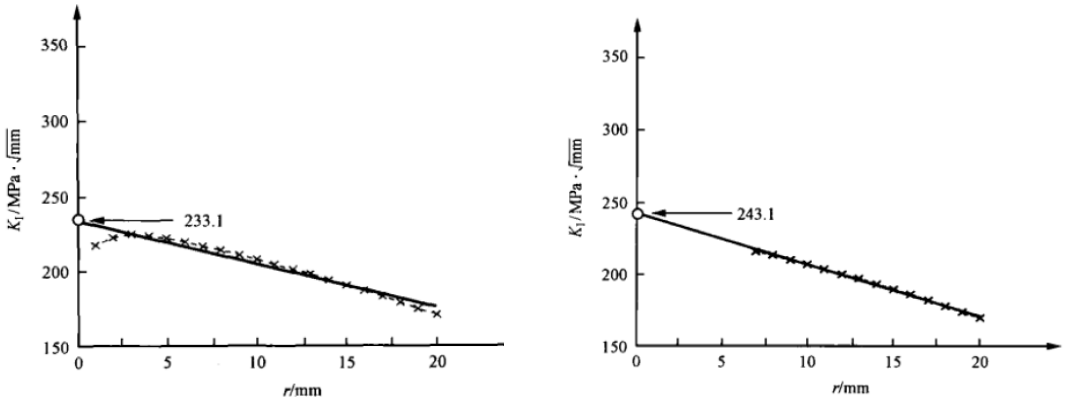

Figure 3-4 Results of displacement extrapolation

3.1.3 J-integral method

J-integral is a parameter to deal with Non-linear fracture problem which is proposed by Rice [23]. J-integral is less dependent on crack tip stress singularity for it is based on the concept of conservation of energy, which means there is no need to do special treatment on the mesh around crack tip.

As shown in Figure 3-5, the equation of J-integral is

.

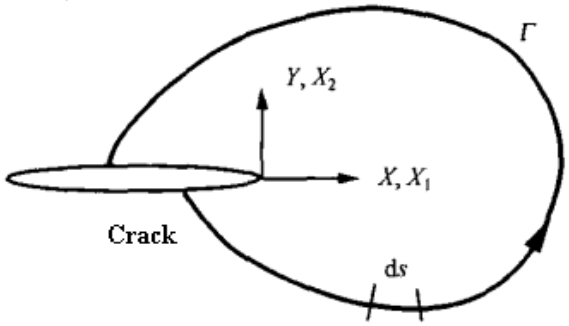

Figure 3-5 Counterclockwise loop around the crack tip

$$J = \int_{\Gamma} \left(w dx_2 - T_i \frac{\partial u_i}{\partial x_i} \right) ds \quad \textbf{(3-9)}$$

Where w is the strain energy density, T_i is the traction vector, u_i is the displacement vector, ds is an element of arc along the integration contour.

3.2 Life prediction Methods

The fatigue life as a whole can be divided into three parts: crack initiation, crack propagation, and final failure. Several conventional fatigue analysis methods are used in first phase life estimation such as the S-N curve approach and detail fatigue rating approach. A small crack is assumed in the beginning of fatigue life calculation. Although the small flaw may not be fracture critical under static loads, it will gradually increase under cyclic loads. Therefore, the ability of the prediction of a component under cyclic loads becomes particularly important. During the crack propagation process, stress intensity factor plays a decisive role. It is assumed that the crack growth rate is determined by the stress intensity factor range, and different cracks have same rate of propagation if they have the same stress intensity factor. Thus, the crack propagation rate, da/dN, has the relationship with stress intensity factor range,

$$\Delta K = K_{max} - K_{min} \quad \textbf{(3-10)}$$

$$da/dN = f(\Delta K) \quad \textbf{(3-11)}$$

3.2.1 Paris Equation

Paris, etc were the first to find the relationship between the crack growth rate and the SIF, and began to compare it with test data [24]. They gave the equation in the following form:

$$da/dN = C(\Delta K)^n \quad \textbf{(3-12)}$$

This is Paris law, where C and n were constants related to the material.

3.2.2 Forman's Equation

Forman's law is also a kind of life prediction method, which considers the mean stress effect of a fatigue stress cycle [25]. The equation is in the following form:

$$\frac{\mathrm{da}}{\mathrm{dN}} = \frac{\mathrm{C}(\Delta\mathrm{K})^{\mathrm{n}}}{(1-\mathrm{R})\mathrm{K_c} - \Delta\mathrm{K}} \quad \textbf{(3-13)}$$

Where R= $S_{\min}/S_{\max}$ reflects the mean stress effect. K_c is the fracture toughness which describes the effect when K_I near to K_{IC}.

As the result of fatigue testing experience, ΔK_{th} is also related to the stress ratio and material property. Hence, Forman's equation can be modified as follow:

$$\frac{\mathrm{da}}{\mathrm{dN}} = \frac{\mathrm{C}(\Delta\mathrm{K} - \Delta\mathrm{K_{th}})^{\mathrm{n}}}{(1-\mathrm{R})\mathrm{K_c} - \Delta\mathrm{K}} \quad \textbf{(3-14)}$$

3.2.3 NASGRO Equation

NASGRO equation is another formula which is often used in crack growth analysis [26]. The equation is in the following form:

$$\frac{\mathrm{da}}{\mathrm{dN}} = \mathrm{C}\left[\left(\frac{1-\mathrm{f}}{1-\mathrm{R}}\right)\Delta\mathrm{K}\right]^{\mathrm{n}} \frac{\left(1-\frac{\Delta\mathrm{K_{th}}}{\Delta\mathrm{K}}\right)^{\mathrm{p}}}{\left(1-\frac{\mathrm{K_{max}}}{\mathrm{K_{Ie}}}\right)^{\mathrm{q}}} \quad \textbf{(3-15)}$$

Where R is the stress ratio. ΔK is the stress intensity factor range. p, n, q and C are constants. f is the Newman closure function, given as:

$$\mathrm{f} = \frac{\mathrm{K_{op}}}{\mathrm{K_{max}}} = \begin{cases} \max(\mathrm{R},\ \mathrm{A_0} + \mathrm{A_1R} + \mathrm{A_2R^2} + \mathrm{A_3R^3}) & \mathrm{R} \geq 0 \\ \mathrm{A_0} + \mathrm{A_1R} & -2 \leq \mathrm{R} \leq 0 \end{cases} \quad \textbf{(3-16)}$$

Where,

$$A_0 = (0.825 - 0.34\alpha + 0.05\alpha^2)\left[\cos\left(\frac{\pi}{2}\frac{\mathrm{S_{max}}}{\sigma_0}\right)\right] \quad \textbf{(3-17)}$$

$$A_1=(0.415-0.071\alpha)\frac{S_{max}}{\sigma_0} \quad \textbf{(3-18)}$$

$$A_2=1\text{-}A_0\text{-}A_1\text{-}A_3 \quad \textbf{(3-19)}$$

$$A_3=2A_0+A_1\text{-}1 \quad \textbf{(3-20)}$$

ΔK_{th} is the threshold SIF:

$$\Delta K_{th}=\frac{\Delta K_0\left(\frac{a}{a+a_0}\right)^{0.5}}{\left(\frac{1-f}{(1-A_0)(1-R)}\right)^{(1+C_{th}R)}} \quad \textbf{(3-21)}$$

Where a_0 is the intrinsic crack length, a is the crack length, α is Plane stress/strain constraint factor, ΔK_0 is the threshold intensity factor, and C_{th} is the empirical constant.

A typical crack growth curve is illustrated in Figure 3-6, which describes crack growth rate da/dN versus SIF range.

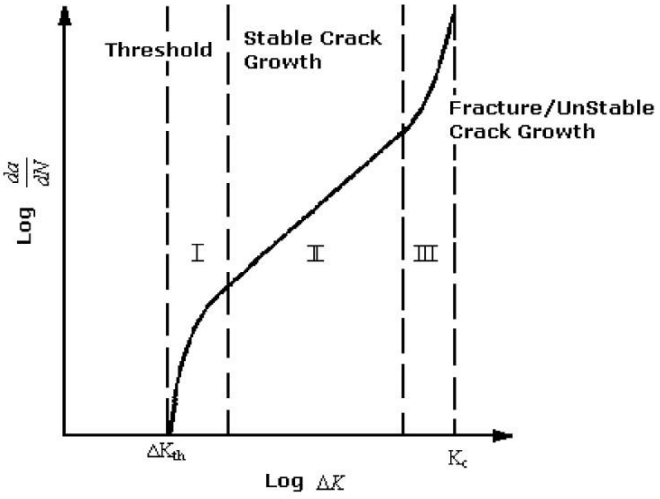

Figure 3-6 Crack growth rate curve [27]

3.3 Methods used in this article

3.3.1 SIF calculation of ABAQUS

In this article, software ABAQUS is used for SIF calculation. The whole data input includes Part, property, load and so on. The modules of ABAQUS are described in the Figure 3-7.

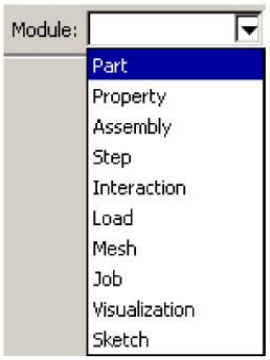

Figure 3-7 Modules in ABAQUS/CAE

A brief introduction about SIF calculation through ABAQUS was as follows:

1. Create the model in ABAQUS (input dimension data).
2. Input material data including elasticity, and Poisson's ratio for the panel in the property module, and also define the thickness in section choice.
3. Establish an independent assembly of the part in the Assembly module.
4. Make a step for the ABAQUS analysis in the Step module.
5. Choose elements type, and then create the mesh of the panel.
6. Add boundary conditions and load.
7. Submit the job to write a"*.inp" file.
8. Modify the"*.inp" document; add some output information, including the displacement and coordinate of the crack edge points.
9. submit the"*.inp" document in command window to get the displacement and coordinate.
10. Calculate the SIF of the panel using DE method.

The process of SIF calculation through ABAQUS is presented in the Figure 3-8.

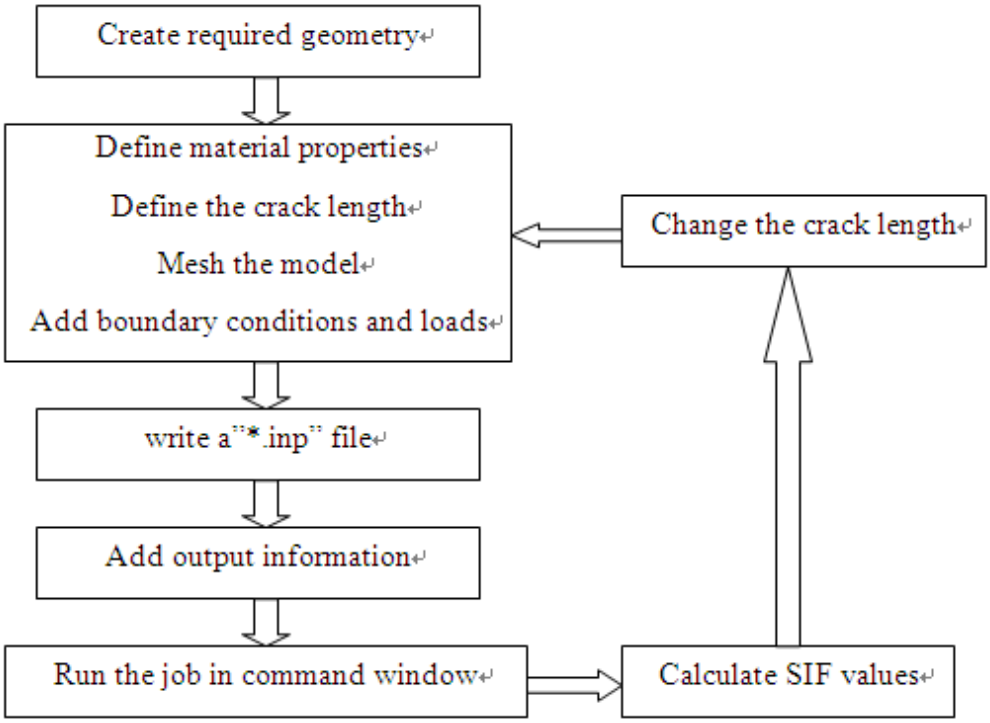

Figure 3-8 Flowchart of SIF calculation

Considering the load always changes in different situation, the geometry factor β is always used for any stresses to describe the stress intensity conditions instead of K. It is calculated using the following formula:

$$\beta = \frac{K}{\sigma\sqrt{\pi a}} \tag{3-22}$$

Where, a is half crack length, σ is remote stress.

During all above calculation, the crack growth rate in the skin and stiffeners was supposed to be the same when the crack tip reaches the stiffener. But the real situation is not always the same, and the assumption may cause less accurate results.

3.3.2 New procedure

Considering the potential problem, a new interactive procedure is applied in SIF calculation. In this situation, crack growth rate in the skin and stiffeners was not assumed to be the same. Instead, they will be calculated respectively, and then

the crack grows separately, it is show as Figure 3-9. The flow chart of the whole process is show as Figure 3-10.

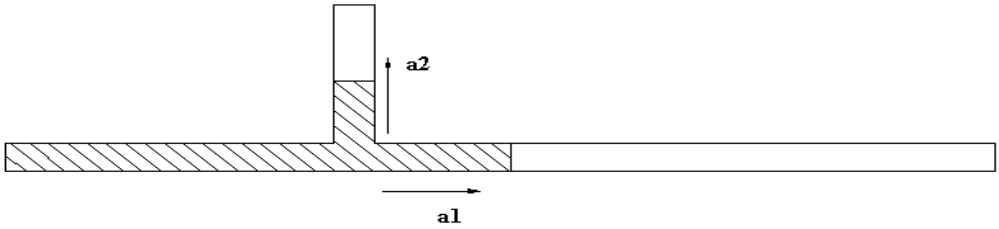

Figure 3-9 Crack growth rate in the skin and stiffener

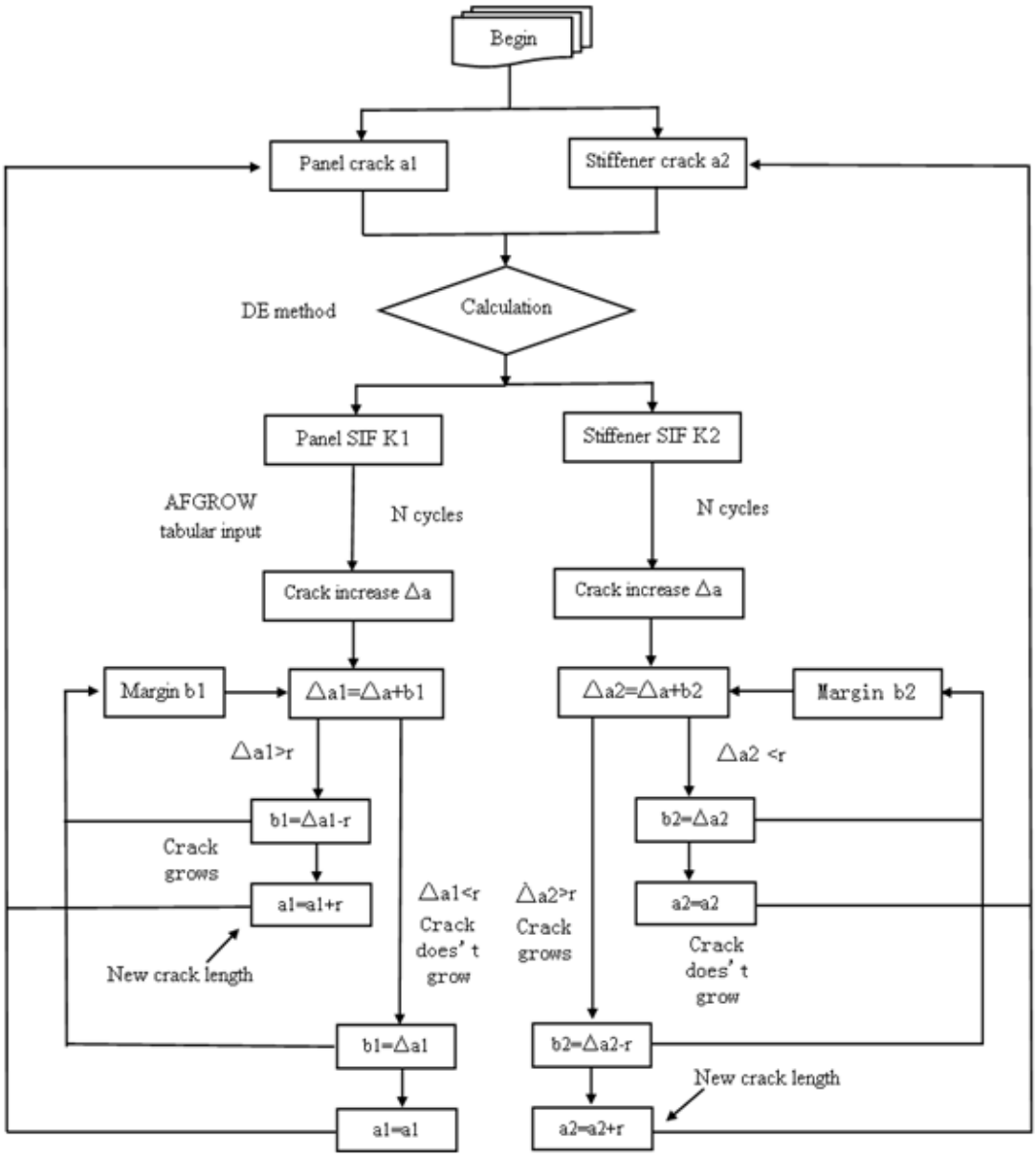

Figure 3-10 Flow chart of the new method

Where, a1 is the half crack length at the panel, a2 is the crack length at the stiffener, K1 is the stress intensity factor corresponding to a1, K2 is the stress intensity factor corresponding to a2, N is load cycles. r is element size, Δ a is crack increment after certain cycles, Δ a1 is real increment accumulation in panel crack, Δ a2 is real increment accumulation in stiffener crack, b1 is margin of a1 after the crack propagation, b2 is margin of a2 after the crack propagation.

A brief introduction of process of the flow chart is as follow:

The calculation begins when the crack reaches the stiffener, and a1 and a2 are supposed to be cracks in panel and stiffener separately. Displacement extrapolation method is applied in stress intensity factor calculation, and K1 and K2 are calculated. Then, the crack growth rate da/dN at that point can be calculated through Δ K -da/dN curve. For a certain cycles, the increment in panel and stiffener will be calculated separately. After that, the increment will be compared with element size r. If the increment is greater than r, then the crack will grow one grid size. If the increment is less than r, then the crack does not grow. The function of b1 and b2 are error correction. If the crack growth less than r, it will be ignored in next step SIF calculation. But it will be accumulated to the next crack growth.

3.3.3 Analysis of Crack Growth Life

AFGROW was used in the Crack Growth Life prediction. There are many built-in models available for the user to choose. The user needs to choose crack cases and dimensions. The crack growth calculation process in AFGROW is below:

1. Choose the proper geometry, defined as through crack and input plate length, crack length about the plate.
2. Define the material while the predefined Tabular input is used in this analysis of crack growth models.
3. Input the stress level, and retardation models are not applied during the whole process.
4. Give the final crack length of the plate.

5. Calculate to get the results.

The procedure of Crack Growth Life prediction is shown in Figure 3-11.

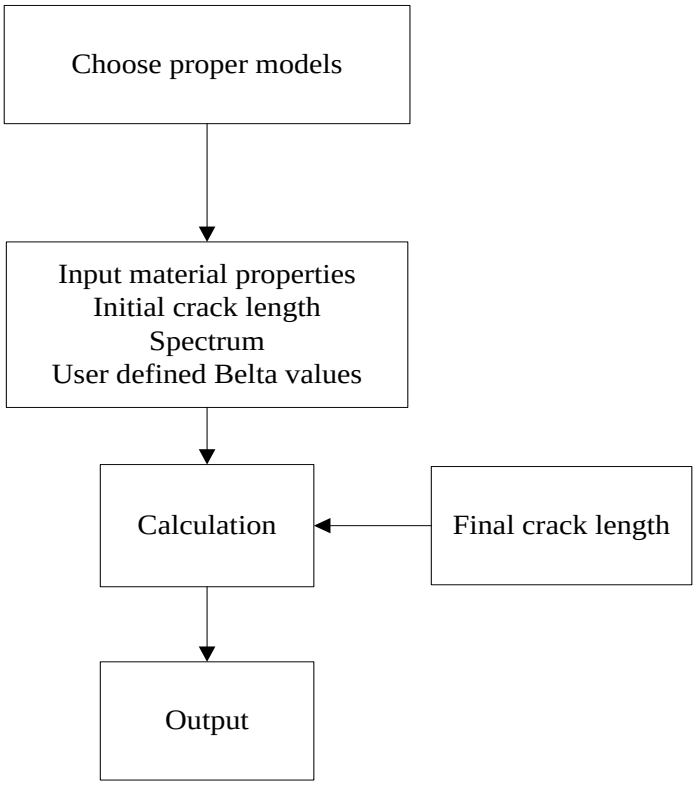

Figure 3-11 Flowchart of Crack Growth Life prediction procedure

3.4 Middle crack tension geometry

3.4.1 Description

In order to choose a better method to calculate SIF values of integral structures, a simple example of a finite plate under tension is discussed in several methods. The width of the plate is W=300mm, initial crack length is 2a=105mm, and the stress is σ =62.5Mpa. The geometry configuration is shown as Figure 3-12. Because it is a symmetry panel, and loading condition is also symmetry, only a quarter of the panel is used in model building.

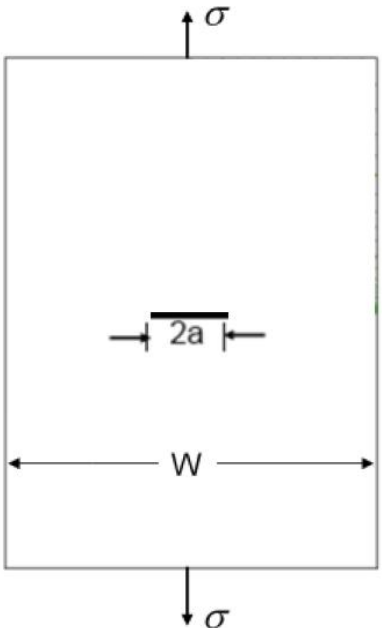

Figure 3-12 Middle crack tension geometry

It is easy to calculate the theoretical solution for the plate with the half crack length from 52.5mm to 92.5mm, using the formula below, and the results are presented in Table 3-1.

$$\beta=\frac{1}{\left(\cos\left(\frac{\pi a}{W}\right)\right)^{0.5}} \tag{3-23}$$

$$K=\beta\cdot\sigma\cdot\sqrt{\pi\cdot a} \tag{3-24}$$

Table 3-1 Theoretical results of plate

a (mm)	K ($MPa\sqrt{m}$)
52.5	27.489
62.5	31.093
72.5	35.022
77.5	37.171
82.5	39.483
87.5	41.999
92.5	44.768

3.4.2 Convergence test

Half crack a= 82.5mm was taken in order to do the research to find out the relationship between Grid size and the accuracy in different calculation method. Grid size length cuts down gradually from 8mm to 2mm. The calculation results are in Table 3-2, and curves are drawn as Figure 3-13.

Table 3-2 Convergence test results

element size mm	DE		DE（remove points）		J-integral		Theoretical
	Results	Error	Results	Error	Results	Error	Result
8	37.847	-4.14%	39.33	-0.39%	39.52	0.09%	39.483
5	38.404	-2.73%	39.40	-0.22%	39.52	0.09%	
4	38.648	-2.11%	39.46	-0.06%	39.51	0.07%	
2	39.161	-0.81%	39.50	0.04%	39.51	0.07%	

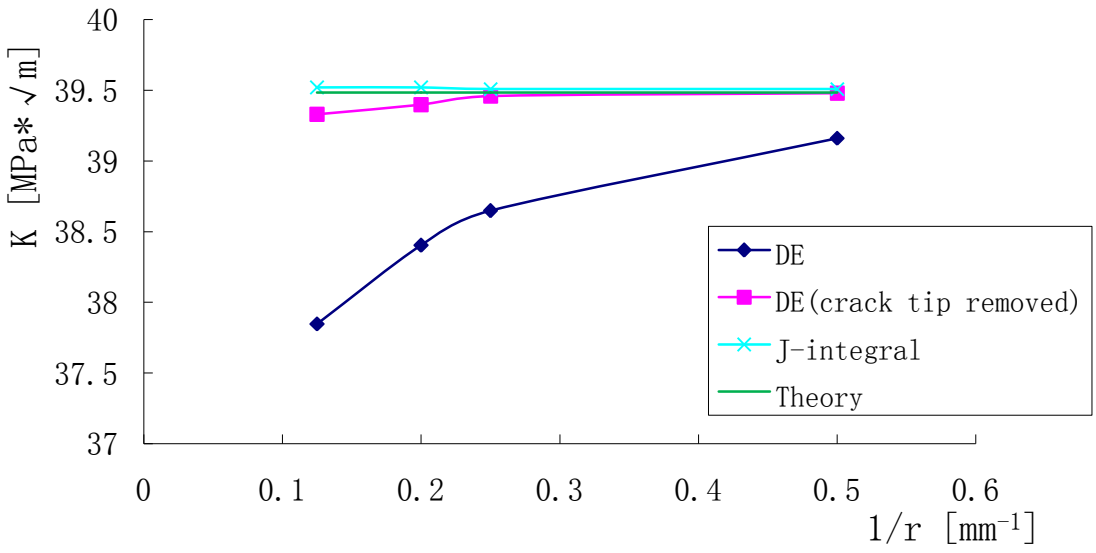

Figure 3-13 Curves of convergence test

According to the test, element size 2mm is suitable for the SIF calculation when using DE method (remove two points around the crack tip) and J-integral method.

3.4.3 Displacement extrapolation results

ABAQUS 6.10-1 was chosen for the model building. Considering the symmetry of the panel, a quarter of the structure was used in FE model. The element size around crack tip was 2×2 mm and the mesh is shown in Figure 3-14. There were 4122 elements with the element type is CPS8R. CPS is plane stress element and it is used in very thin structure. The final results are presented in Table 3-3.

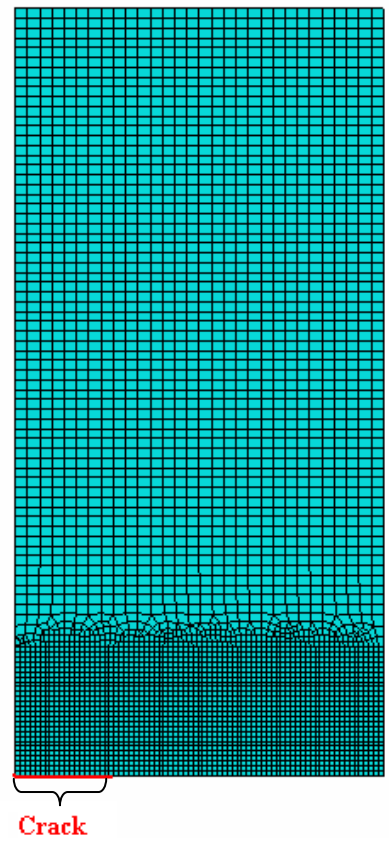

Figure 3-14 Mesh of the panel (DE method)

Table 3-3 SIF values with different crack length (DE method)

a (mm)	K ($MPa\sqrt{m}$)
52.5	27.480
62.5	31.085
72.5	35.020
77.5	37.175
82.5	39.497
87.5	42.031
92.5	44.821

3.4.4 J-integral results

ABAQUS 6.10-1 was chosen for the model building. Considering the symmetry of the structure, a quarter of the structure was used in FE model. The element size was also 2 ×2mm near the crack (1mm at crack tip), and the mesh was shown in Figure 3-15.There were 4114 elements with the element type is CPS8R. The calculation results are list in Table 3-4.

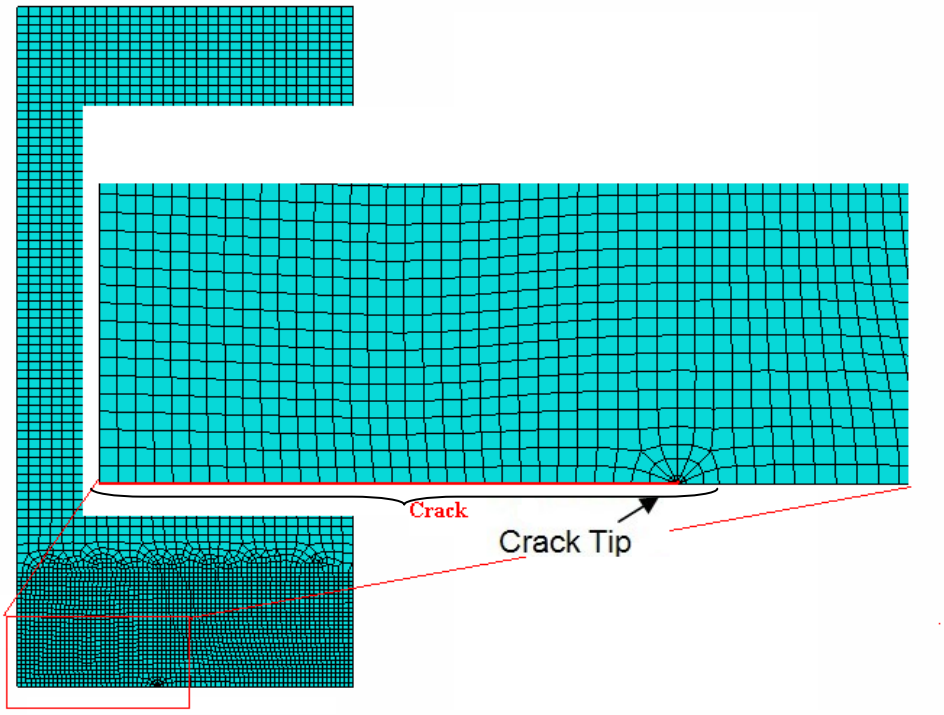

Figure 3-15 Mesh of the panel (J-integral method)

Table 3-4 SIF values with different crack length (J-integral method)

a (mm)	K ($MPa\sqrt{m}$)
52.5	27.55
62.5	31.14
72.5	35.06
77.5	37.21
82.5	39.51
87.5	42.05
92.5	44.83

3.4.5 Comparison

The results of comparison with theoretical solution are shown in Table3-5, and curves are shown in Figure 3-16.

Table 3-5 SIF results comparison

Half-crack mm	Theoretical solution	J-integral method		DE	
		result	error	result	error
52.5	27.489	27.550	0.222%	27.480	-0.032%
62.5	31.093	31.140	0.151%	31.085	-0.0253%
72.5	35.022	35.060	0.094%	35.020	-0.006%
77.5	37.171	37.210	0.105%	37.175	0.011%
82.5	39.483	39.510	0.068%	39.497	0.035%
87.5	41.999	42.050	0.121%	42.031	0.076%
92.5	44.768	44.830	0.138%	44.821	0.118%

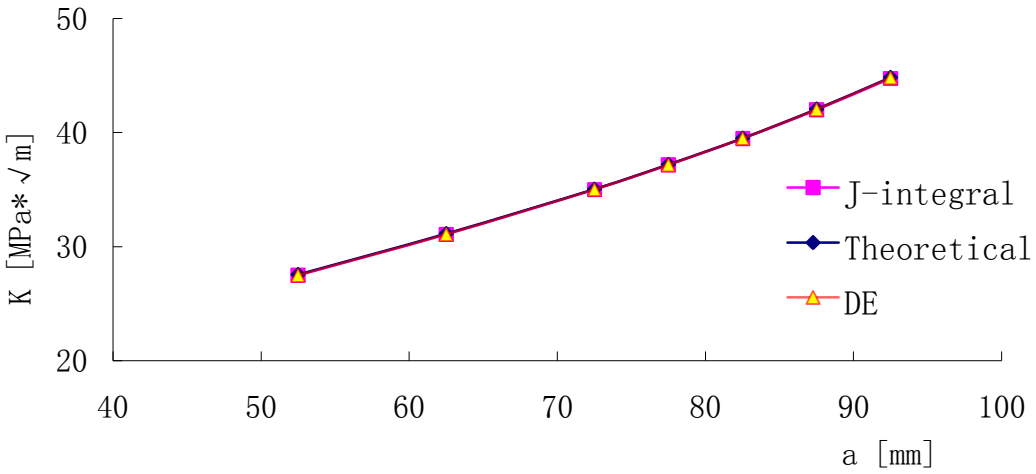

Figure 3-16 Curves of SIF results

According to the Table 3-5, the results calculated by two methods are all acceptable for use in engineering, but displacement extrapolation method gets more accurate results than J-integral method. Although J-integral method has many advantages in SIF calculation, for example, it does not need close grids to get accurate results, the following two deficiencies limit its application in crack growth SIF calculation. First, it cannot get more accurate result by using fine mesh when reaching certain value. Second, you have to mesh the model once again after the crack growth. So, for the more complex integral structures, displacement extrapolation method is applied to compute SIF values.

4 Results

4.1 Overview of configurations modelled in thesis

Three integral stiffened structures are investigated in this thesis. Panel 1 and panel 2 are part of an ongoing Round Robin exercise organized by the ASTM Task Group E08.04.05. The first one is a 2024-T351 integral plate, with five stringers. The second one is 2027-T351 integral plate, with nine stringers. The third one is a very thin plate with only three stringers, and the material is also 2024-T351.

4.1.1 Structure Configurations

4.1.1.1 Panel 1 configuration

The first structure under investigation is an integral metallic skin-stringer panel, which is part of an ongoing Round Robin program organized by the ASTM Task Group E08.04.05. Panel 1 is a 2024-T351 panel with main dimensions 508 mm $\times$1270 mm and thickness of 38.1 mm. At the beginning, the initial crack length is 127 mm in the centre of the panel cross the central stringer. The final crack is near the second stringer with the crack length 293.4mm.In order to achieve the maximum stress 41.4MPa, an axial load with a ratio R=$\sigma_{min}/\sigma_{max}$=0.1 was exerted to the ends of the panel under displacement control. The overall dimensions are shown in Figure 4-1 (All dimensions in mm). Material properties are given in Table 4-1, provided by ASTM [28].

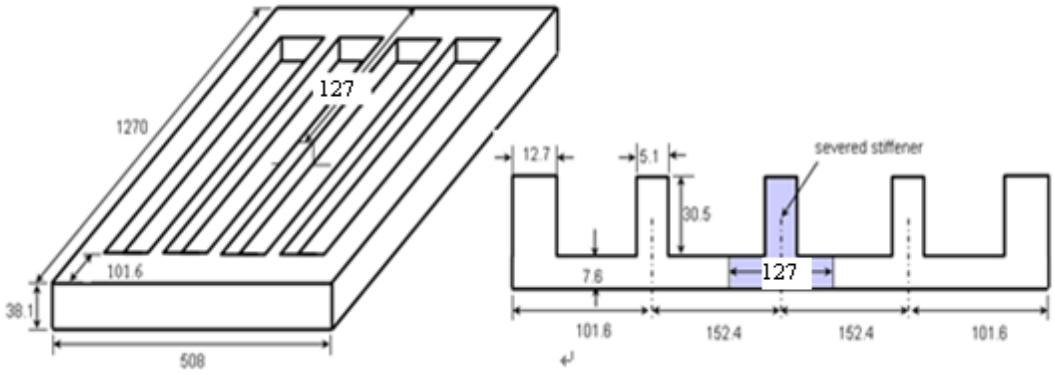

Figure 4-1 Geometry configuration of Panel 1 [28]

Table 4-1 Material properties of Alloy 2024-T351

	Longitudinal Direction (L)	Transverse Direction (LT)
UTS [MPa]	490	485
YS [MPa]	388	342
% Elong	17.3	18.3

4.1.1.2 Panel 2 configuration

The Panel 2 is a 2027-T351 plate with main dimensions 490 mm ×1000 mm and thickness of 23.9 mm. At the beginning, the initial crack length is 50 mm in a middle position through the central stringer while the final crack length is 260mm. In order to get a maximum stress equal to 69.5MPa, an axial load with a ratio R=0.1 was exerted to the ends of the panel under displacement control. The overall dimensions are shown in Figure 4-2 (All dimensions in mm). Material properties are given in Table 4-2, provided by ASTM [28].

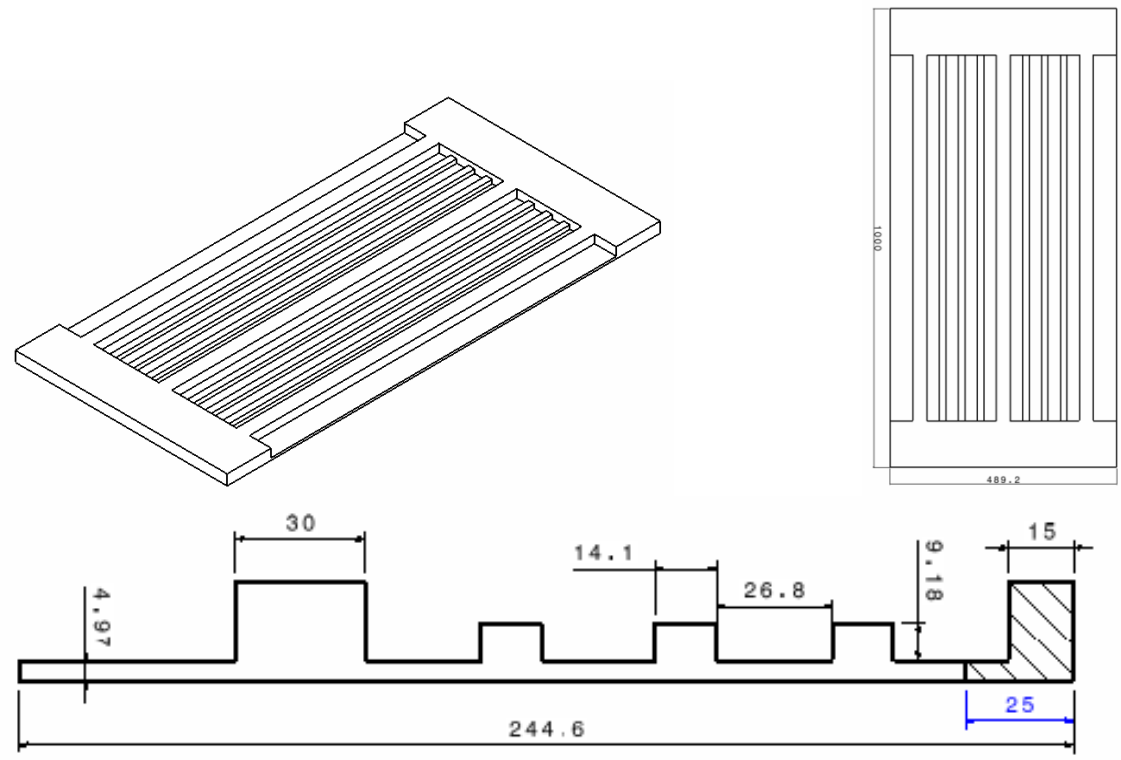

Figure 4-2 Geometry configuration of Panel 2 [28]

Table 4-2 Material properties of Alloy 2027-T351

	Longitudinal Direction (L)	Transverse Direction (LT)
UTS [MPa]	494	471
YS [MPa]	375	334
% Elong	18.0	20.9

4.1.1.3 Panel 3 configuration

The Panel 3 is also a 2024-T351 plate with main dimensions 490 mm ×590 mm and thickness of 4.79 mm. At the beginning, the initial crack length is 24 mm in a symmetrical position under the central stringer. In order to obtain a maximum stress equal to 100MPa, an axial load with a ratio R=0.1 was exerted to the ends of the panel under displacement control. The overall dimensions are shown in Figure 4-3 (All dimensions in mm) [33].

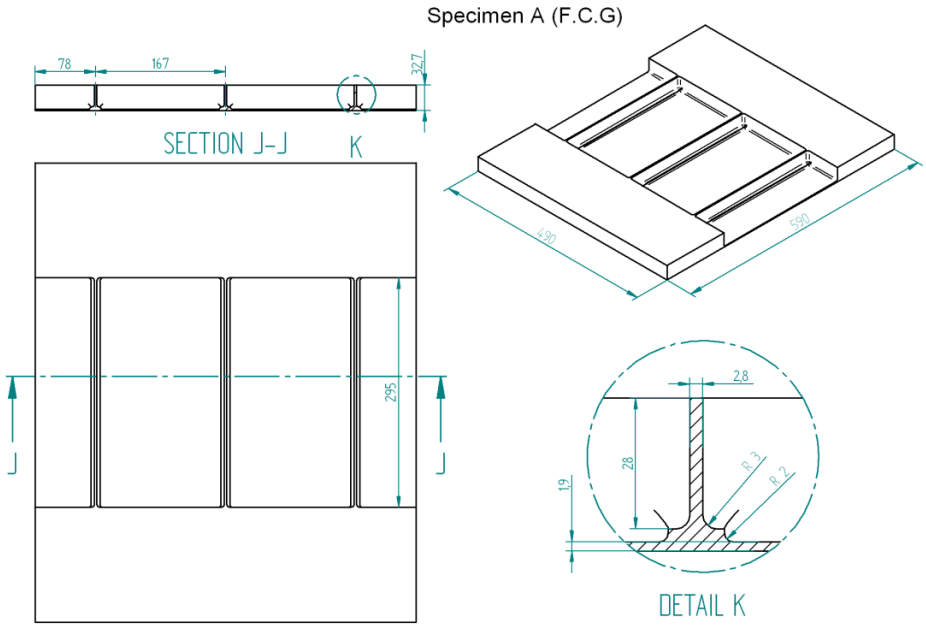

Figure 4-3 Geometry configuration of Panel 3 [33]

4.1.2 Test Results

4.1.2.1 Panel1

The crack growth results of panel 1 were provided by the ASTM Round Robin organiser, and it was shown in Figure 4-4 [28].

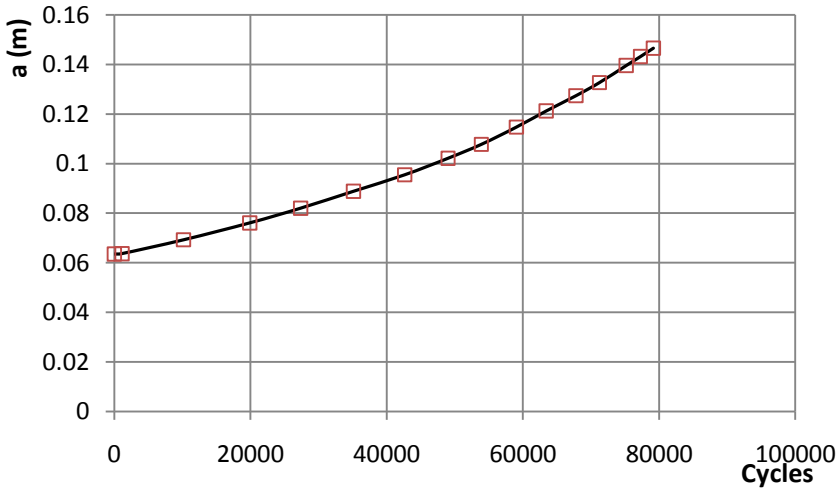

Figure 4-4 Crack Growth Curve of Panel1

4.1.2.2 Panel2

The crack growth results of panel 2 were plotted in Figure 4-5 [28].

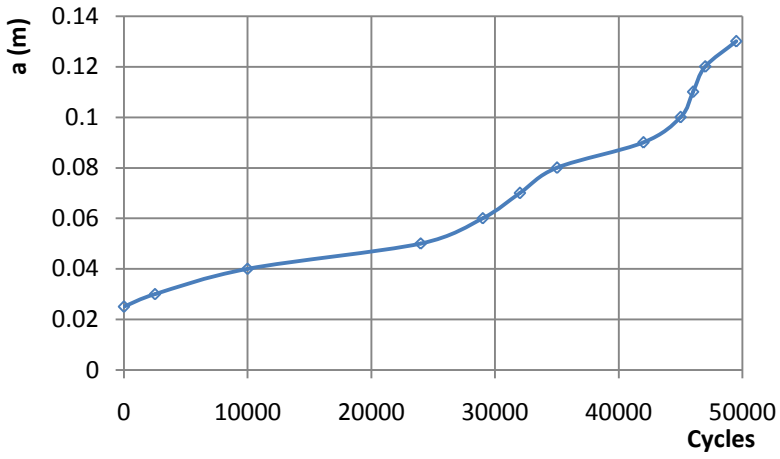

Figure 4-5 Crack Growth Curve of Panel2

4.1.2.3 Panel3

The crack growth results of panel 3 were plotted in Figure 4-6 [33].

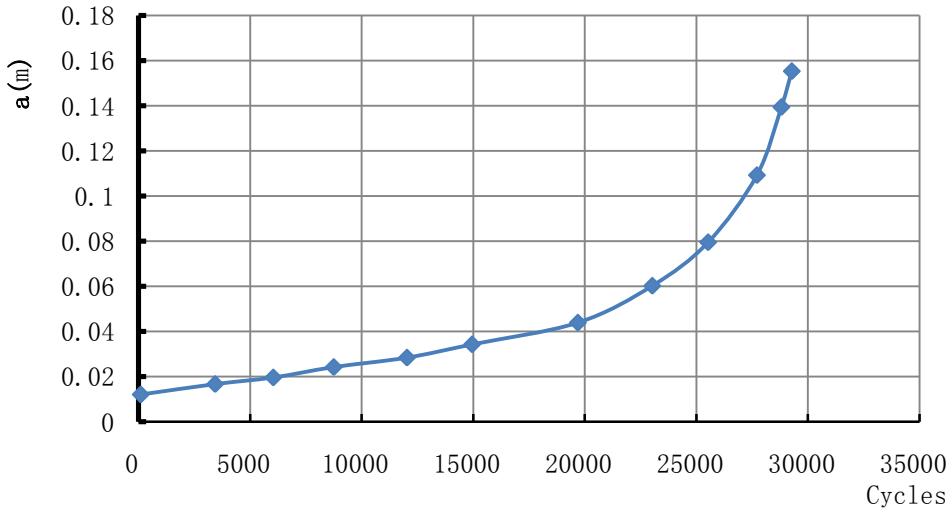

Figure 4-6 Crack Growth Curve of Panel3

4.2 Panel 1

The configuration of Panel1 is shown in Figure 4-1.The calculation is including SIF calculation and life prediction.

4.2.1 2D Model

4.2.1.1 Model building

Considering the geometry and loading condition, only one fourth of the panel was modelled due to geometric symmetry.

The plane was built at the central of the section of panel 1, as shown in Figure 4-7.

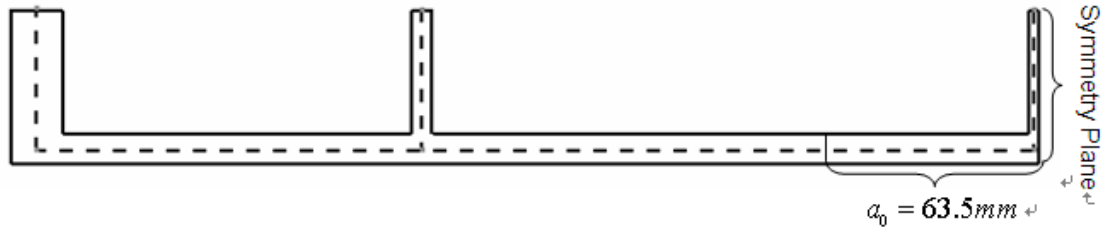

Figure 4-7 Placement of the shell reference surface

The FE package ABAQUS 6.10-1 was taken in model is building and SIF calculation. The load and boundary conditions was shown in Figure 4-8. A tensile load with the stress 41.4MPa was applied in Z direction on the top shell edge. Two types of boundary conditions were added into the geometry. In Y-Z symmetry, X displacements and Y and Z rotations were constrained. In X-Y symmetry, Z displacements and X and Y rotations were constrained except the crack location.

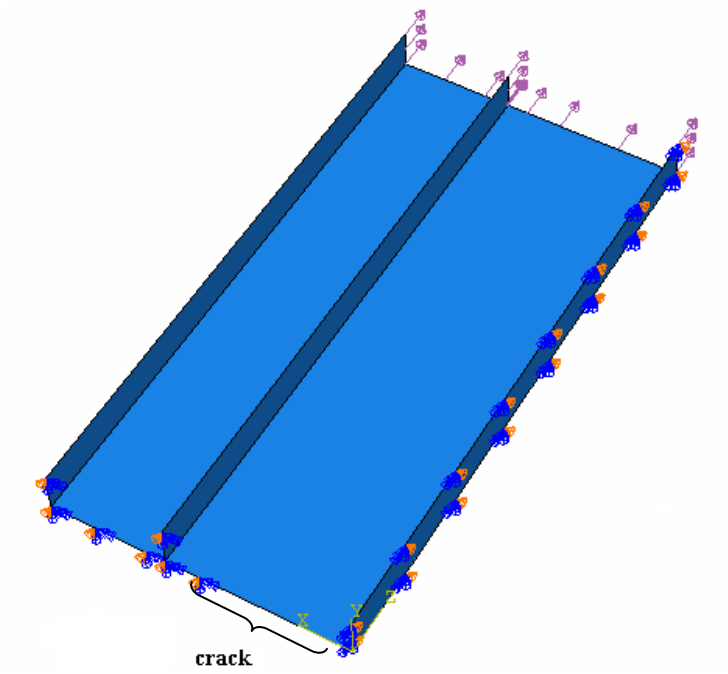

Figure 4-8 2D model of Panel 1 (one quarter)

4.2.1.2 Convergence test

In order to get a proper grid size to do the calculation of panel 1, half crack a= 63.5mm was taken to do the research to find out the relationship between grid size and the result using DE method. Grid size length would cut down gradually from 8mm to 1mm. The calculation results are list in Table 4-3, and curves are plotted in Figure 4-9. Considering both accuracy and time consuming, element size 2mm was taken in the calculation.

Table 4-3 Convergence test results of panel 1 (2D)

r (mm)	K ($MPa\sqrt{m}$)
8	19.072
6	19.293
4	19.576
3	19.732
2	19.881
1	20.097

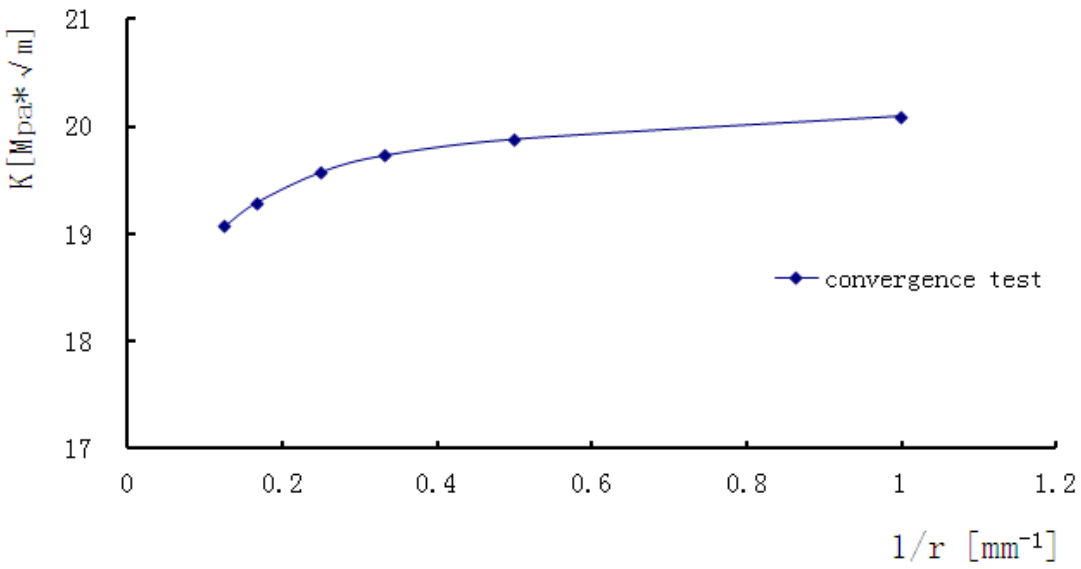

Figure 4-9 Convergence test curve of panel 1 (2D)

4.2.1.3 SIF result

The mesh of panel 1 is shown in Figure 4-10. Altogether 5928 elements with the element type S8R were in the model. The element sizes were 2 mm near the crack tip fields and 6 mm in the other parts.

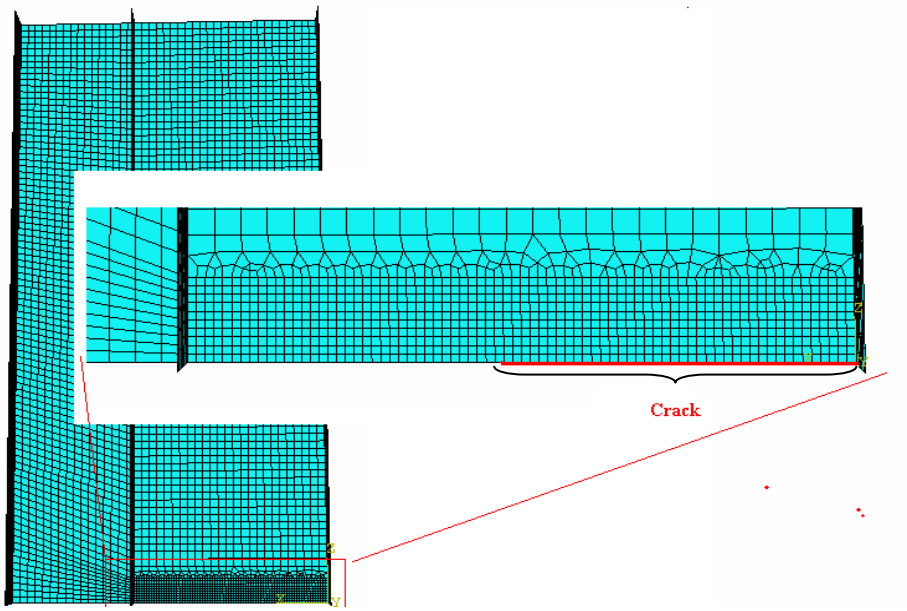

Figure 4-10 Mesh of panel 1 (2D)

At first, the stress state and distribution was checked to confirm that the edge loads and constrains were correct. The stress diagram results are shown in Figure 4-11.

Then, the SIF values were calculated at different crack lengths. The results are given in Table 4-4 and drawn in Figure 4-12.

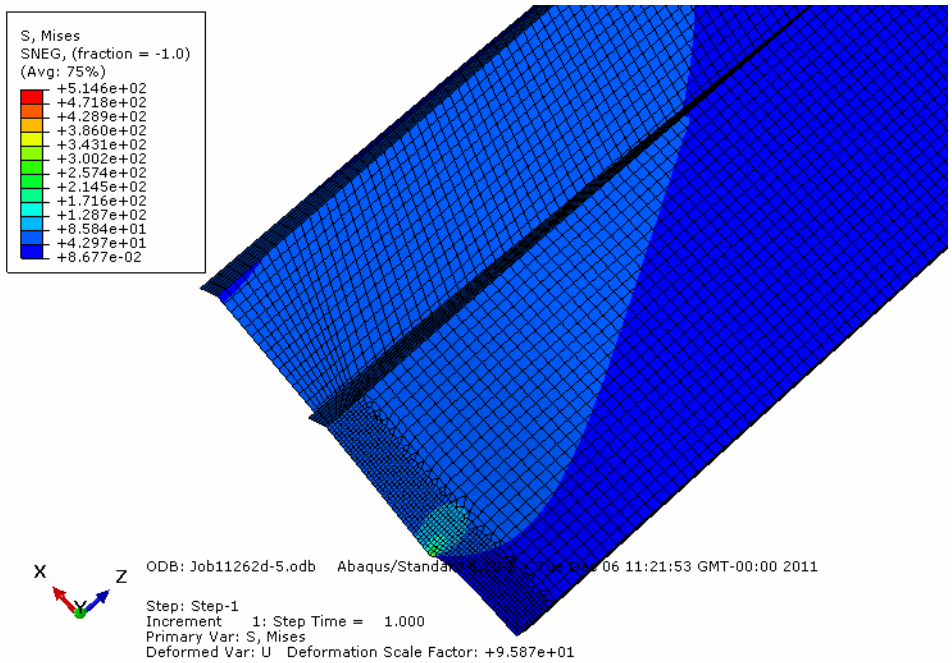

Figure 4-11 Stress distribution diagram of Panel 1 (2D)

Table 4-4 SIF values with different crack length of Panel1 (2D)

a (mm)	K ($MPa\sqrt{m}$)	β
63.5	19.881	1.062
73.5	21.227	1.069
83.5	22.832	1.078
93.5	24.441	1.091
103.5	26.072	1.106
113.5	27.74	1.124
123.5	29.46	1.144
133.5	31.196	1.165
143.5	32.823	1.183

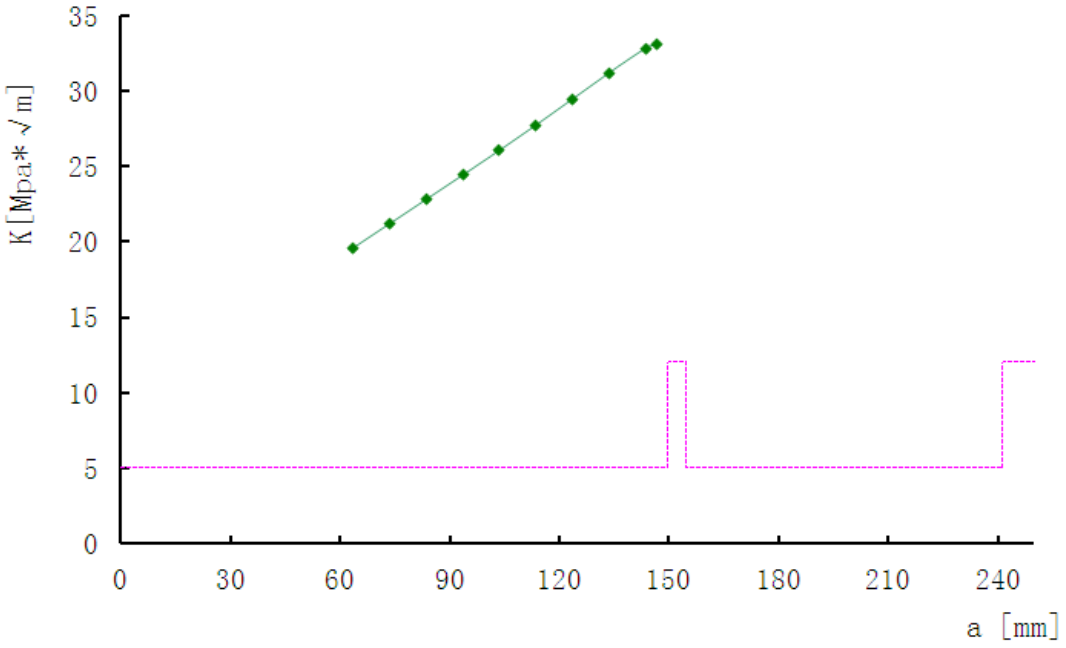

Figure 4-12 SIF curve of Panel 1 (2D)

The geometry factor β values of different crack lengths are plotted in Figure 4-13. It would be used in life prediction.

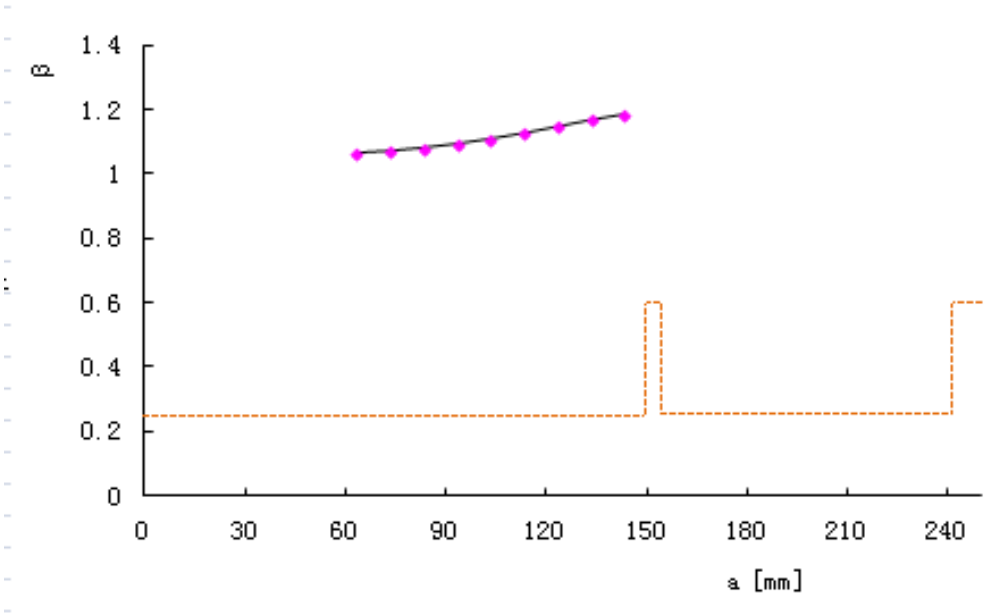

Figure 4-13 Geometry factor β curve of Panel 1 (2D)

4.2.1.4 Crack Growth Life Prediction Results

Paris law and AFGROW tabular input were used in life prediction. When using Paris law, C=0.534e-011 and n=3.9 were applied [29], and according to the Paris law equation $\mathrm{d}a/dN = C(\Delta K)^n$, crack growth life was calculated. When using AFGROW Tabular input method, Constant loading ($\sigma_{\max} = 41.4\mathrm{MPa}$,) $\mathrm{R} = 0.1$ was chosen. The β value was defined by user, which calculated in former calculation. This means using AFGROW Tabular input facility but not using any correlated equations like Paris law, but use the raw test data. The model taken to calculation is drawn in Figure 4-14. At the beginning, the initial crack length is $\mathrm{a}_0 = 63.5\mathrm{mm}$, while the width b=254mm.

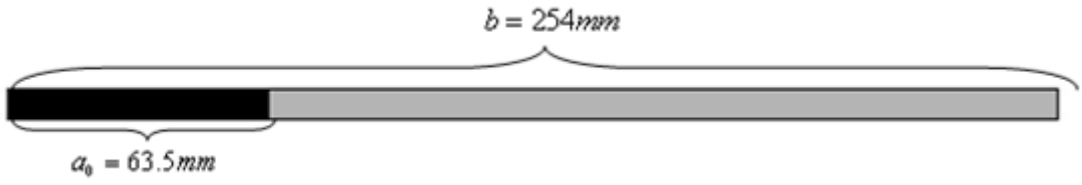

Figure 4-14 AFGROW crack growth model of Panel 1

Crack propagation would stop while the crack length reached the final crack length a=143.5mm. The method of AFGROW Tabular input chose the same data with the ASTM experiment [30], as shown in Figure 4-15.

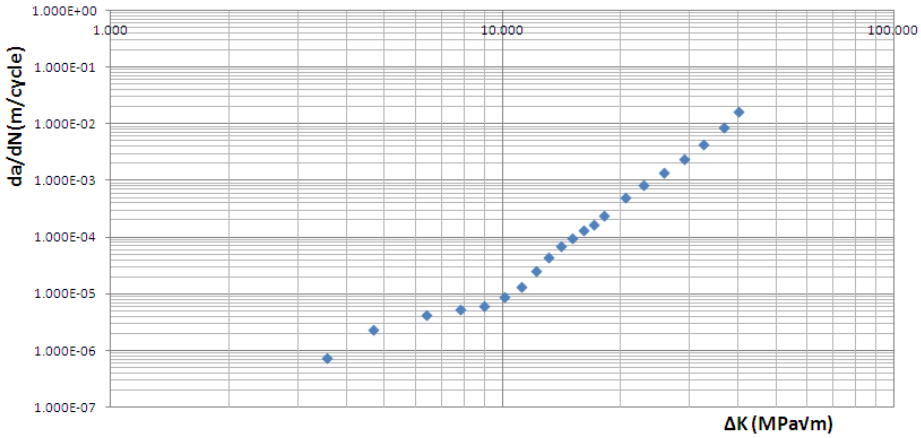

Figure 4-15 $\Delta K - da/dN$ **curve of Al 2024-T351**

The CGL (Crack Growth Life) calculation results of Panel 1 were written in Table 4-5 and drawn in Figure 4-16.

Table 4-5 Prediction results of crack growth life of Panel 1

Method	Crack Growth Life (Cycles)	error
Experiment	79159	
Paris Equation	83476	5.45%
Tabular Input	118687	49.93%

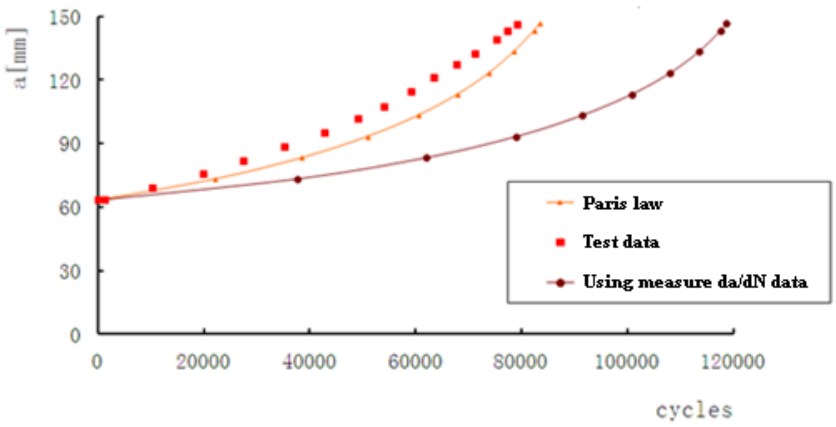

Figure 4-16 Prediction of crack growth curves and experiment

From Figure 4-16, it is quite clear that the result calculated by Paris law is much better than the tabular input result. This may be caused by the $\Delta K - da/dN$ curve provided by ASTM since there is a significant lower region in the curve. This will be discussed in detail in chapter 5.

4.2.2 3D models

4.2.2.1 Model building

Considering the geometry and loading condition, only a quarter of the panel was modelled in favour of calculation.

The load and boundary conditions was shown in Figure 4-17.Two types of boundary conditions were added into the geometry. In Y-Z symmetry, X displacements and Y and Z rotations were constrained. In X-Y symmetry, Z displacements and X and Y rotations were constrained except the crack location. A pressure load with the stress 41.4MPa was applied in Z direction on the top surface.

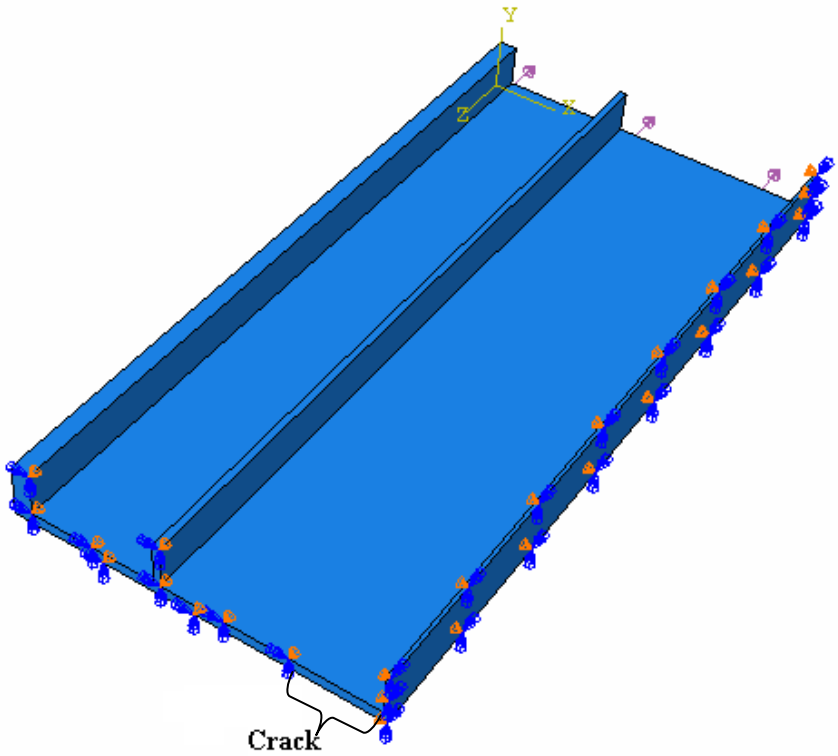

Figure 4-17 3D model of Panel 1 (one quarter)

4.2.2.2 Convergence test

In order to get a proper grid size to do the calculation of panel 1, half crack a= 63.5mm was taken to do the research to find out the relationship between grid size and the result using DE method. Grid size length would cut down gradually from 8mm to 1mm. The calculation results are list in Table 4-6, and curves are plotted in Figure 4-18. Considering both accuracy and time consuming, element size 3mm was taken in the calculation.

Table 4-6 Convergence test results of panel 1 (3D)

r (mm)	K ($MPa\sqrt{m}$)
8	19.482
6	19.687
4	19.923
3	19.991
2	20.044

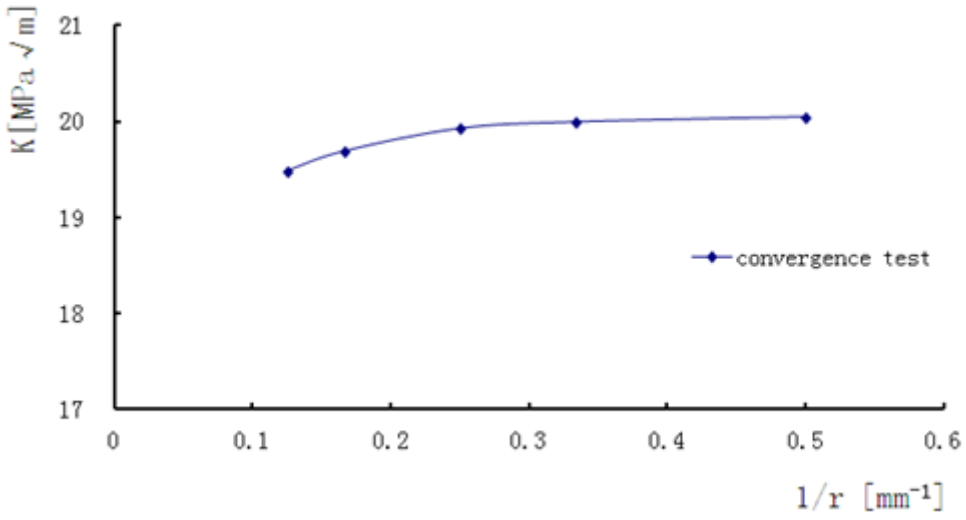

Figure 4-18 Convergence test curve of panel 1 (3D)

4.2.2.3 SIF result

The mesh of panel 1(3D) is shown in Figure 4-19. Altogether 22344 elements with the element type C3D20R were in the model. The element sizes were 3mm.

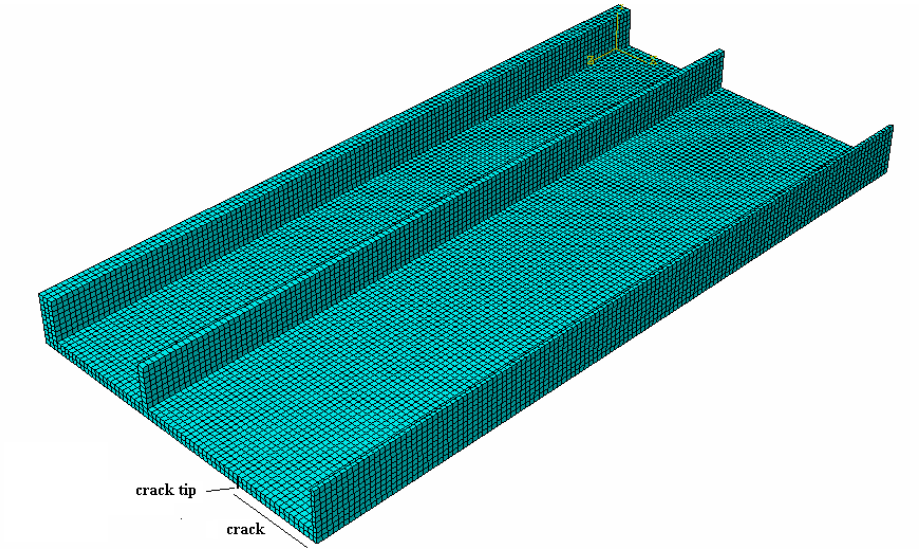

Figure 4-19 3D element mesh of panel 1

At first, the stress state and distribution is checked to confirm if the edge loads and constrains are correct. The calculation results are shown in Figure 4-20.

Then, the SIF values were calculated at different crack lengths. The results are given in Table 4-7 and drawn in Figure 4-21 (in comparison with 2D results).

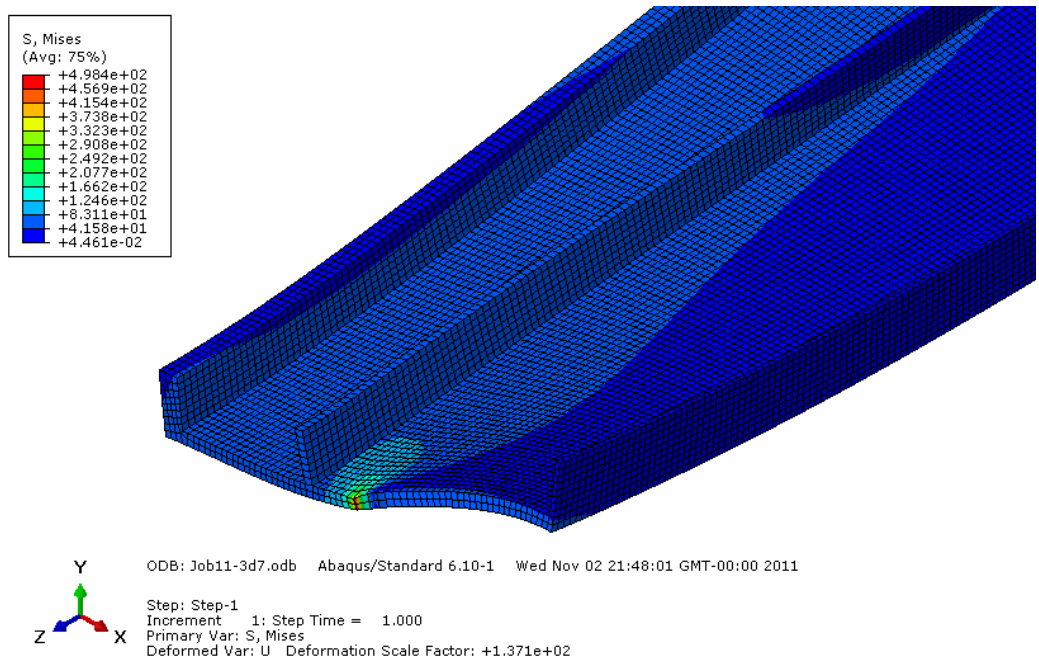

Figure 4-20 Stress distribution diagram of Panel 1 (3D)

Table 4-7 SIF values with different crack length of Panel1 (3D)

a (mm)	K ($MPa\sqrt{m}$)	β
63.5	19.991	1.083
73.5	21.623	1.088
83.5	23.194	1.095
93.5	24.828	1.108
103.5	26.472	1.123
113.5	28.158	1.141
123.5	29.881	1.160
133.5	31.742	1.186
143.5	33.422	1.204

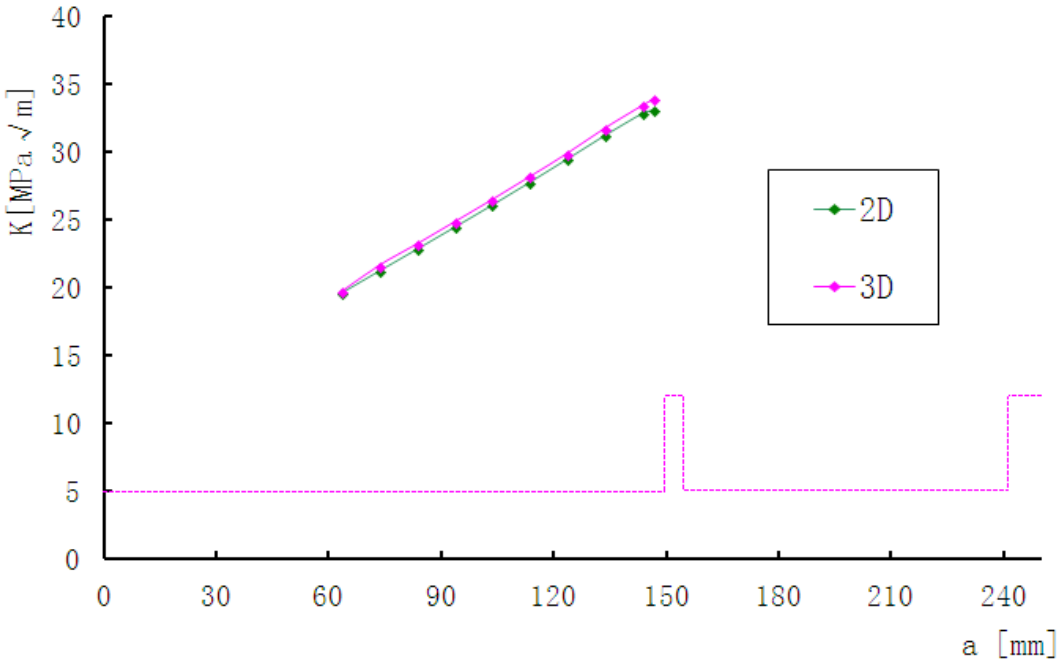

Figure 4-21 SIF results comparison of Panel 1 (2D and 3D)

The geometry factor β values of different crack lengths were plotted in Figure 4-22(compared with 2D results).

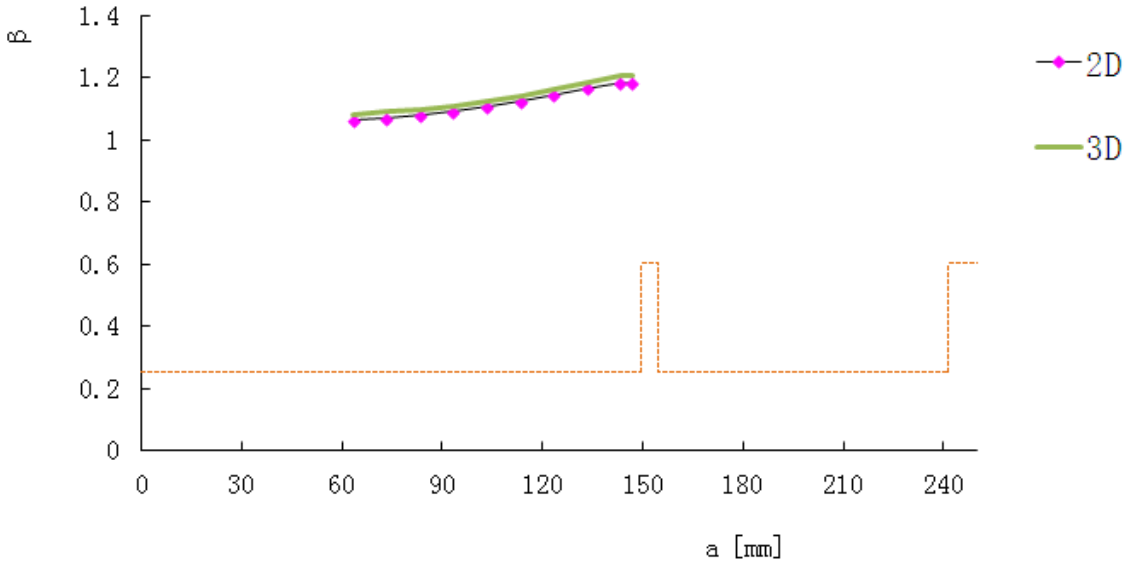

Figure 4-22 β values comparison of Panel 1 (2D and 3D)

The comparison results showed that, the results of 3D model are always slightly bigger than 2D model.

4.2.2.4 Crack Growth Life Prediction Results

Paris law and AFGROW tabular input were used in life prediction. When using Paris law, C=0.534e-011 and n=3.9 were applied [29], and according to the Paris law equation $\mathrm{d}a/dN = C(\Delta K)^n$, crack growth life was calculated. When using AFGROW Tabular input method, Uniform amplitude loading ($\sigma_{\max} = 41.4\mathrm{MPa}$,) $\mathrm{R} = 0.1$ was chosen. The β value was defined by user, which calculated in former calculation. The model taken to calculation is shown in Figure 4-23. At the beginning, the initial crack length is $\mathrm{a}_0 = 63.5\mathrm{mm}$, while the width b=254mm.

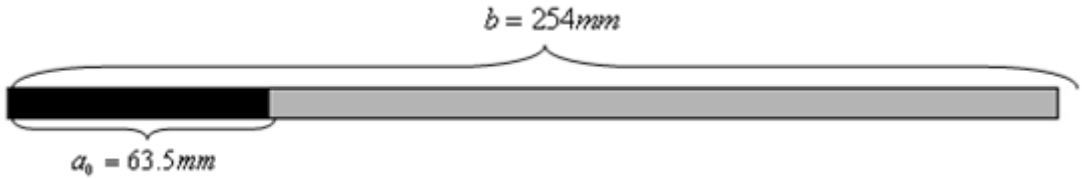

Figure 4-23 AFGROW crack growth model of Panel 1

Crack propagation would stop while the crack length reached the final crack length a=143.5mm.

The CGL prediction results of Panel 1 were written in Table 4-8 and drawn in Figure 4-24 (compared with 2D model).

Table 4-8 Prediction results of crack growth life of Panel 1

Method	Crack Growth Life (Cycles)	error
Experiment	79159	
Paris law	78797	-0.46%
Using da/dN data	110140	39.14%

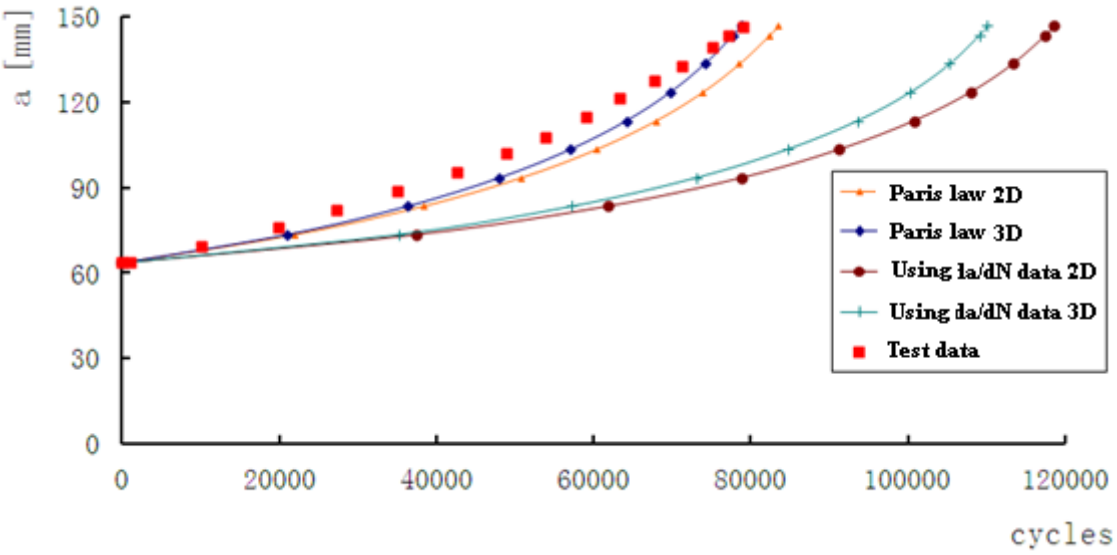

Figure 4-24 Crack growth curves (2D and 3D) and experiment results

The results show that Tabular Input method gets a much longer life than the test result. It may be caused by $\Delta K - da/dN$ curve of 2024-T351 material, which has a significant pit in the middle region, resulting in a longer life at the beginning of the crack growth. This phenomenal will be discussed in chapter 5.

4.3 Panel 2

4.3.1 2D Model

4.3.1.1 Model building

According to the geometry and loading condition, a quarter of the panel is modelled in favour of calculation.

The plane of shell reference is built in the central of the section of panel 2, as shown in Figure 4-25.

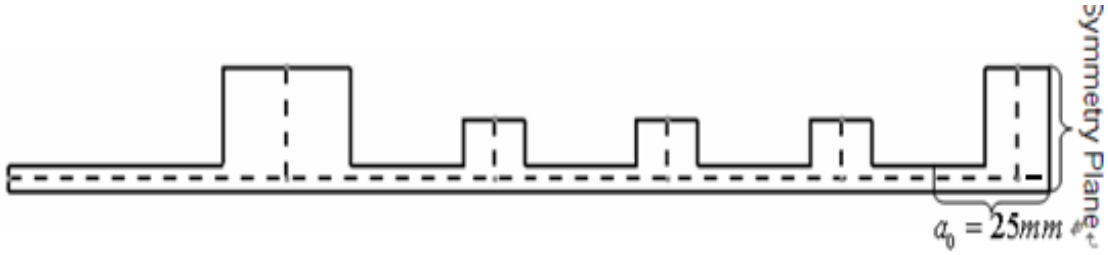

Figure 4-25 Placement of the shell reference surface

The code pack ABAQUS 6.10-1 was taken in model is building and SIF calculation. The load and boundary conditions was shown in Figure 4-26. A tensile load with the stress 69.5MPa was applied in Z direction on the top shell edge. Two types of boundary conditions were added into the geometry. In Y-Z symmetry, X displacements and Y and Z rotations were constrained. In X-Y symmetry, Z displacements and X and Y rotations were constrained except the crack location.

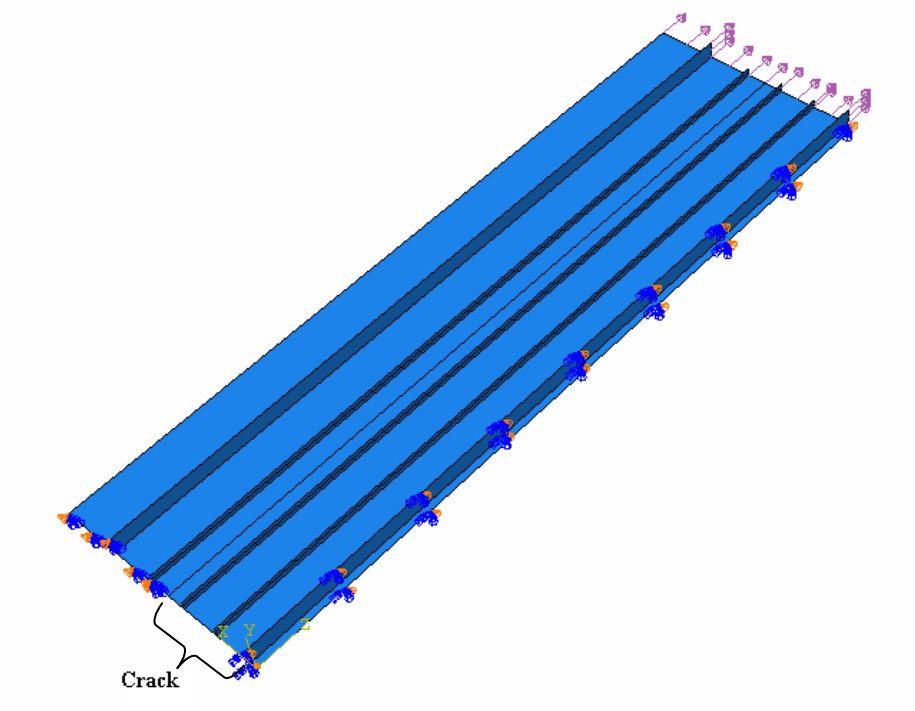

Figure 4-26 2D model of Panel 2 (one quarter)

4.3.1.2 Convergence test

In order to get a proper grid size to do the calculation of panel 2, half crack a= 30mm was taken to do the research to find out the relationship between grid size and the result using DE method. Grid size length would cut down gradually from 8mm to 1mm. The calculation results are list in Table 4-9, and curves are plotted in Figure 4-27. Considering both accuracy and time consuming, element size 2mm was taken in the calculation.

Table 4-9 Convergence test results of panel 2 (2D)

r (mm)	K ($MPa\sqrt{m}$)
8	27.093
6	27.383
4	27.704
3	27.903
2	28.108
1	28.252

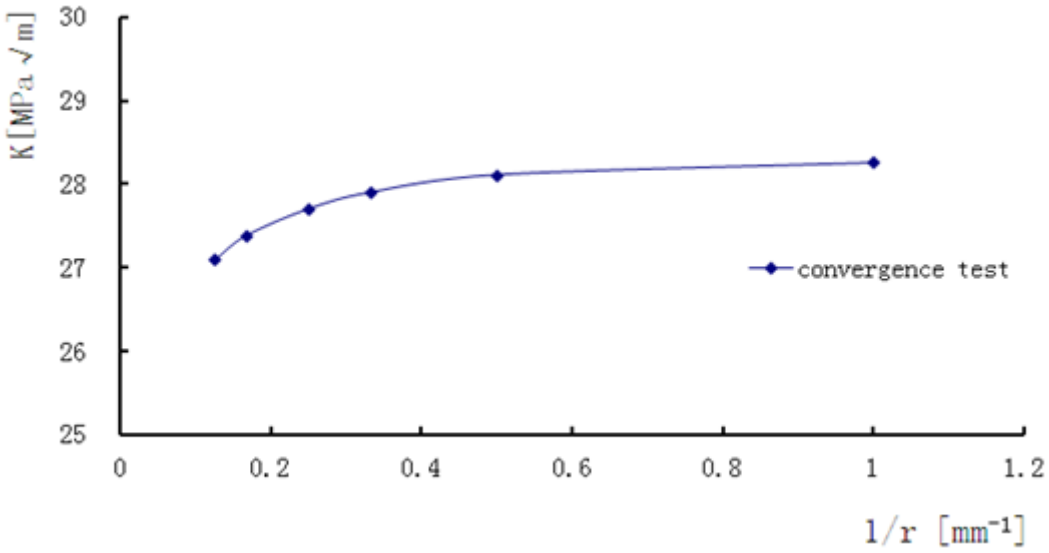

Figure 4-27 Convergence test curve of panel 2 (2D)

4.3.1.3 SIF result

The mesh of panel 1 is shown in Figure 4-28. Altogether 11052 elements with the element type S8R were in the model. The element sizes were 2 mm near the crack tip fields and 4 mm in the other parts.

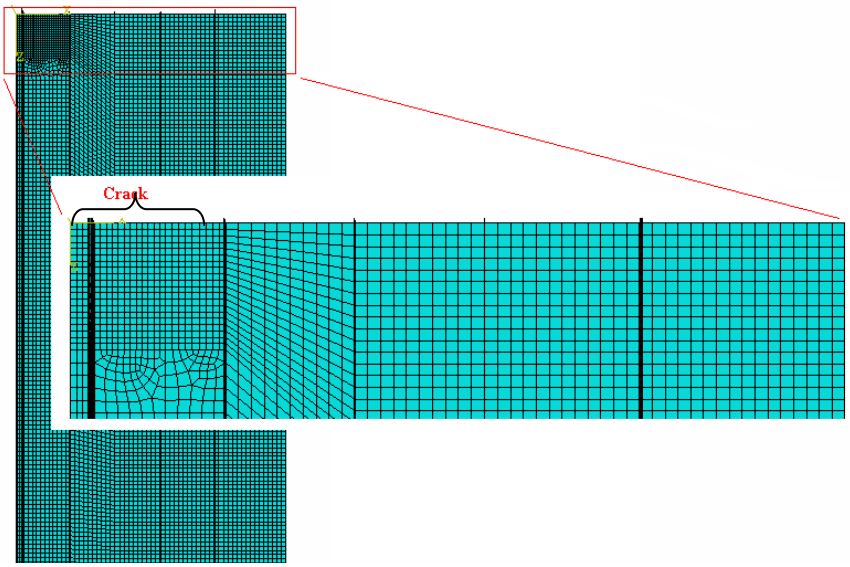

Figure 4-28 2D element mesh of panel 2

In the beginning the stress state and distribution were checked in order to confirm that the edge loads and constrains were accurate. The calculation results are shown in Figure 4-29.

Finally, the SIF values of different crack lengths were calculated. When the crack reached the stiffener, the propagation rate in skin and stiffener was supposed to be 1:1. The same assumption was used in 3D model. This rate was also assumed to be other values, which was not discussed in this thesis. The results are given in Table 4-10 and drawn in Figure 4-30.

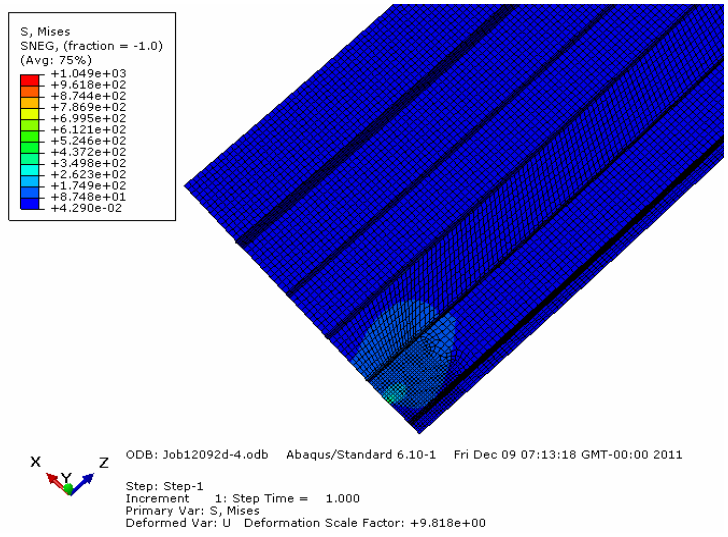

Figure 4-29 Stress distribution diagram of Panel 2 (2D)

Table 4-10 SIF values with different crack length of Panel 2 (2D)

a (mm)	K ($MPa\sqrt{m}$)	β
25	27.103	1.392
30	28.108	1.317
35	29.342	1.273
40	30.262	1.228
45	30.384	1.163
50	28.389	1.031
55	39.971	1.384
60	46.915	1.555
70	48.726	1.495
80	45.549	1.307
85	44.83	1.248
89.75	40.247	1.091
91.75	41.984	1.125
93.75	43.549	1.155
97.75	63.575	1.651
110	67.443	1.651
120	62.221	1.458
125	61.489	1.412
130	55.513	1.250

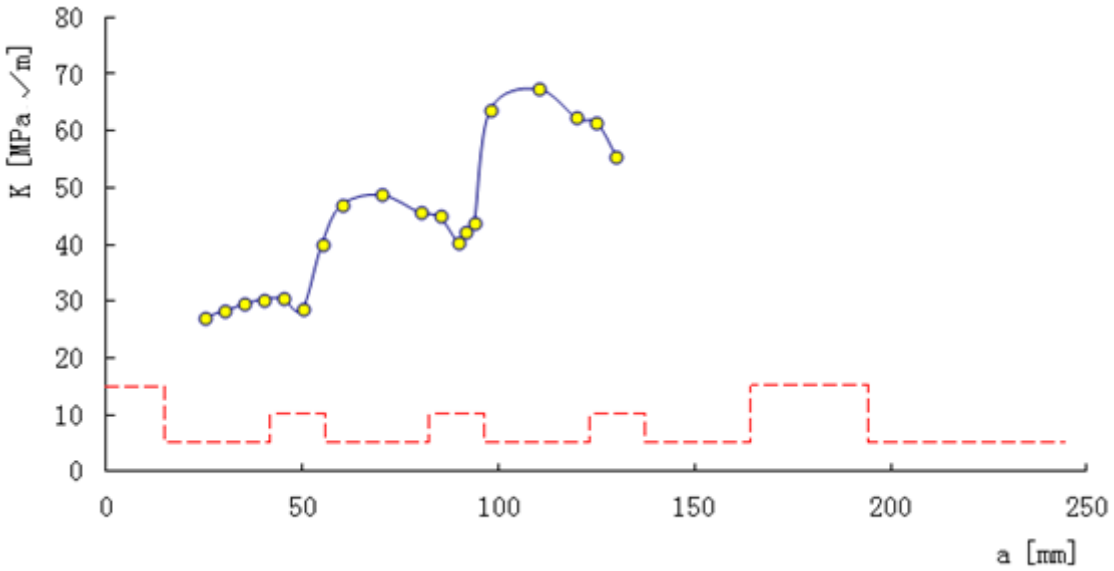

Figure 4-30 SIF curve of Panel 2 (2D)

The geometry factor β values of different crack lengths are plotted in Figure 4-31.

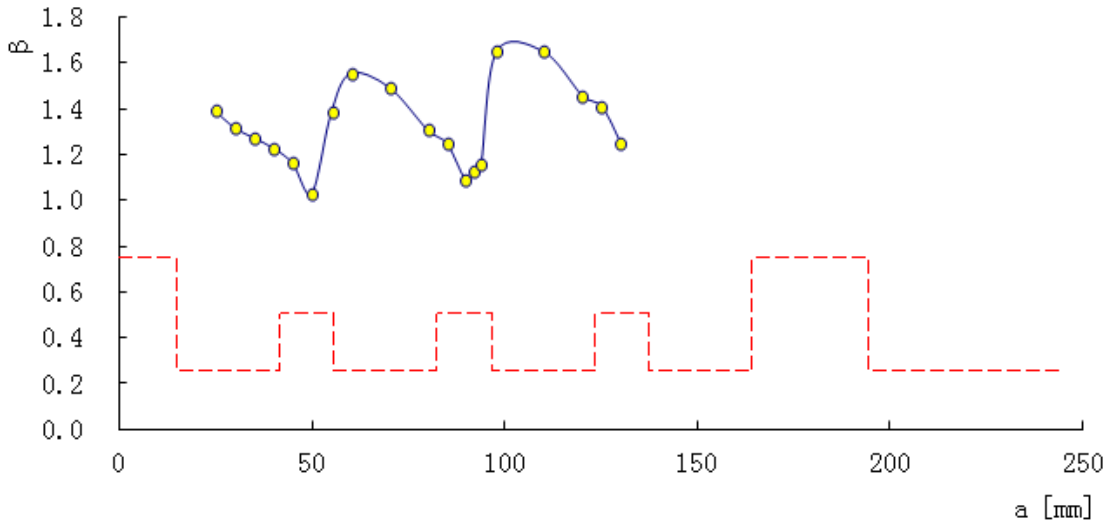

Figure 4-31 Geometry factor β curve of Panel 2 (2D)

4.3.1.4 Crack Growth Life Prediction Results

AFGROW tabular input was used in life prediction. When using AFGROW Tabular input method, Uniform amplitude loading (σ_{max}=69,5MPa,R=0.08) was chosen. Theβ values which were calculated in former calculation, were inputted

by user. The model taken to calculation is shown in Figure 4-32. At the beginning, crack length is 25mm, and width 224.6mm.

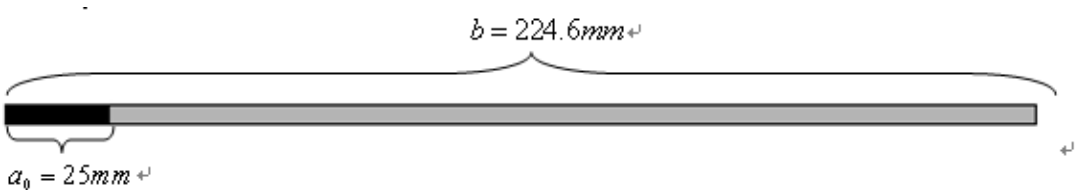

Figure 4-32 AFGROW crack growth model of Panel 2

Crack propagation stopped when the crack length reached the final crack length a=130mm. The method of Tabular input used the same data with the experiment [30], as shown in Figure 4-33.

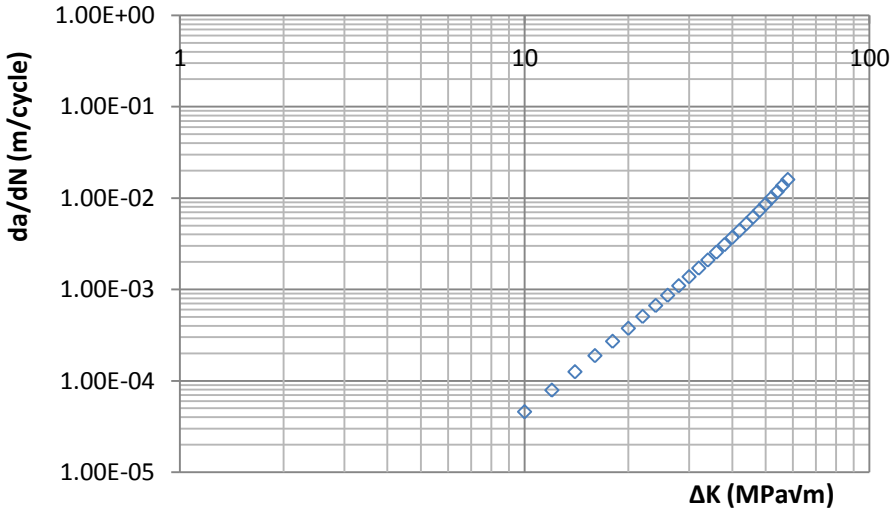

Figure 4-33 $\Delta K - da/dN$ curve of Al 2027-T351

The CGL prediction results of Panel 2 were presented in Table 4-11 and plotted in Figure 4-34.

Table 4-11 Prediction results of crack growth life of Panel 2 (2D)

Method	Crack Growth Life (Cycles)	Differential Ratio
Experiment	49000	
Using da/dN data	44167	-9.86%

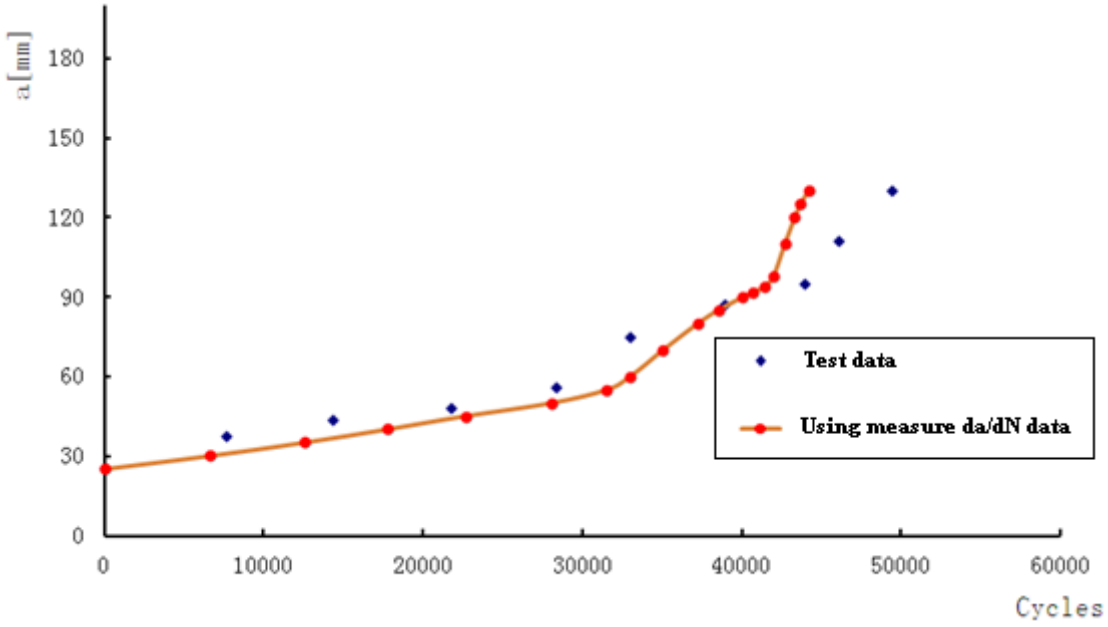

Figure 4-34 Prediction of crack growth curves and experiment

4.3.2 3D models

4.3.2.1 Model building

According to the geometry and loading condition, a quarter of the panel is modelled in favour of calculation.

ABAQUS 6.10-1 was used in model building. The load and boundary conditions was shown in Figure 4-35.Two types of boundary conditions are added into the geometry. In Y-Z symmetry, X displacements and Y and Z rotations are constrained. In X-Y symmetry, Z displacements and X and Y rotations are constrained except the crack location. A pressure load with the stress 69.5MPa is applied in Z direction on the top surface.

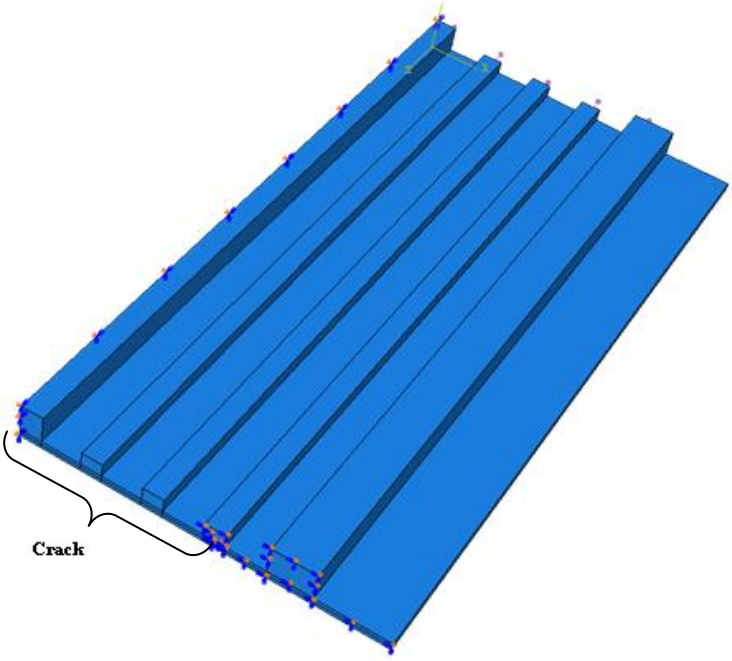

Figure 4-35 3D model of Panel 2 (one quarter)

4.3.2.2 Convergence test

In order to get a proper grid size to do the calculation of panel 2, half crack a= 30mm was taken to do the research to find out the relationship between grid size and the result using DE method. Grid size length would cut down gradually from 8mm to 1mm. The calculation results are list in Table 4-12, and curves are plotted in Figure 4-36. Considering both accuracy and time consuming, element size 3mm was taken in the calculation.

Table 4-12 Convergence test results of panel 2 (3D)

r (mm)	K ($MPa\sqrt{m}$)
8	26.637
6	27.883
4	28.512
3	28.971
2	29.233

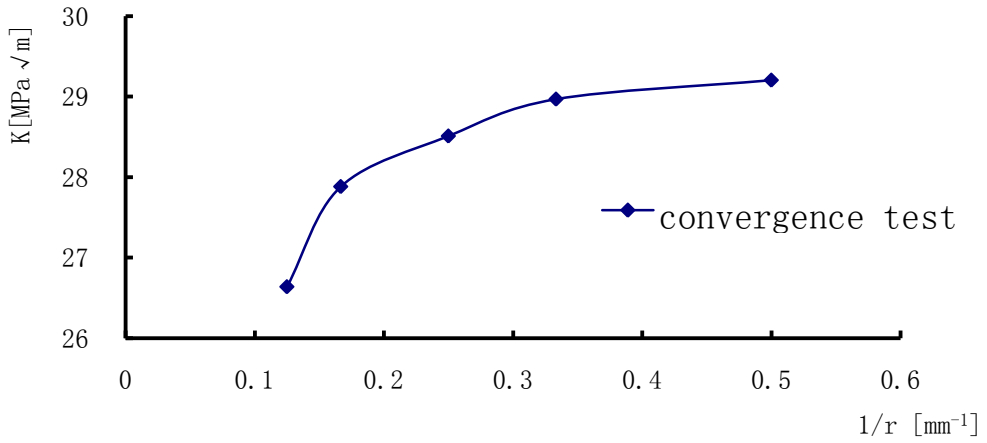

Figure 4-36 Convergence test curve of panel 2 (3D)

4.3.2.3 SIF result

The model is built and analyzed with the code pack ABAQUS 6.10-1. Altogether 22344 elements with the element type C3D20R are in the model. The element sizes are 3 mm. The mesh is drawn in Figure 4-37.

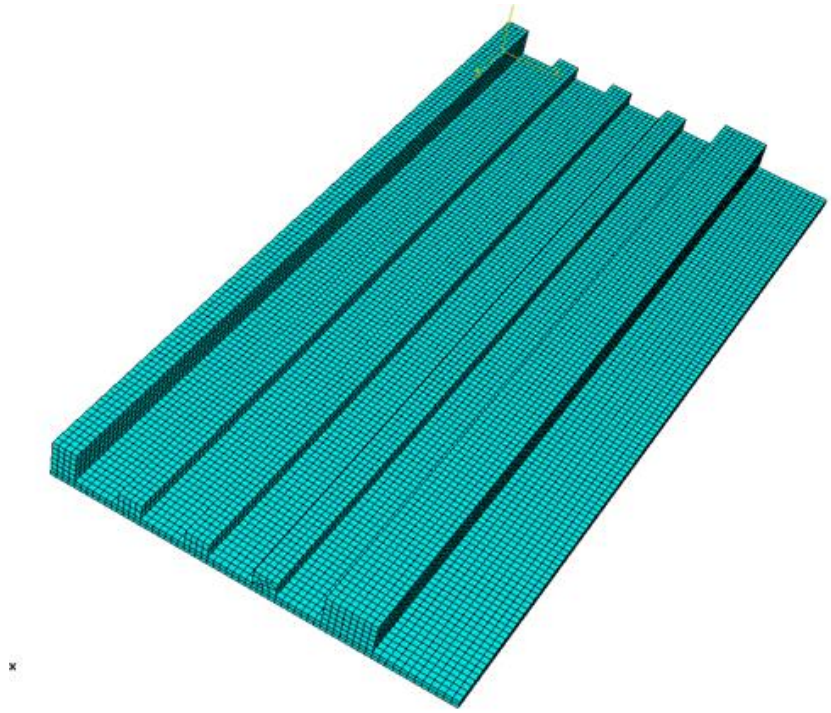

Figure 4-37 3D element mesh of panel 2

At first, the stress state and distribution is checked to confirm if the edge loads and constrains are accurate. The calculation results are shown in Figure 4-38.

Then, the SIF values of different crack lengths are calculated. The results are given in Table 4-13 and drawn in Figure 4-39 (compared with 2D results).

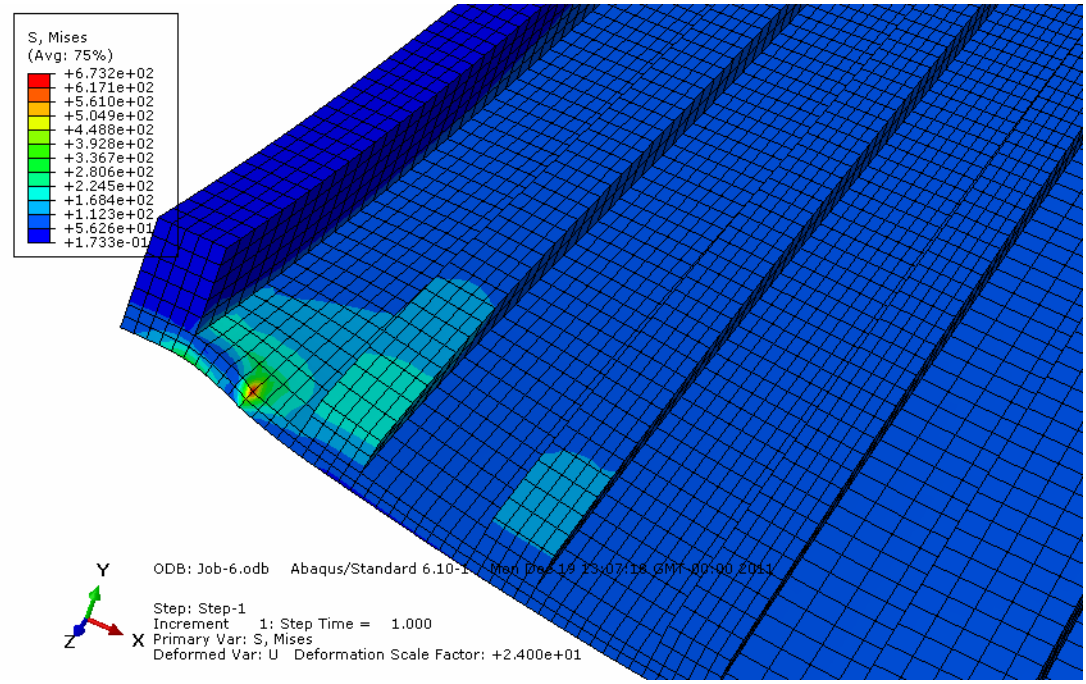

Figure 4-38 Stress distribution diagram of Panel 2 (3D)

Table 4-13 SIF values with different crack length of Panel1 (3D)

a (mm)	K ($MPa\sqrt{m}$)	β
25	29.206	1.499
30	28.971	1.358
40	27.802	1.128
50	24.792	0.900
60	41.823	1.386
65	42.932	1.367
70	43.577	1.337
80	43.664	1.253
90	34.270	0.927
100	59.669	1.532
105	59.821	1.499
110	59.481	1.456
120	57.774	1.354
130	45.098	1.015

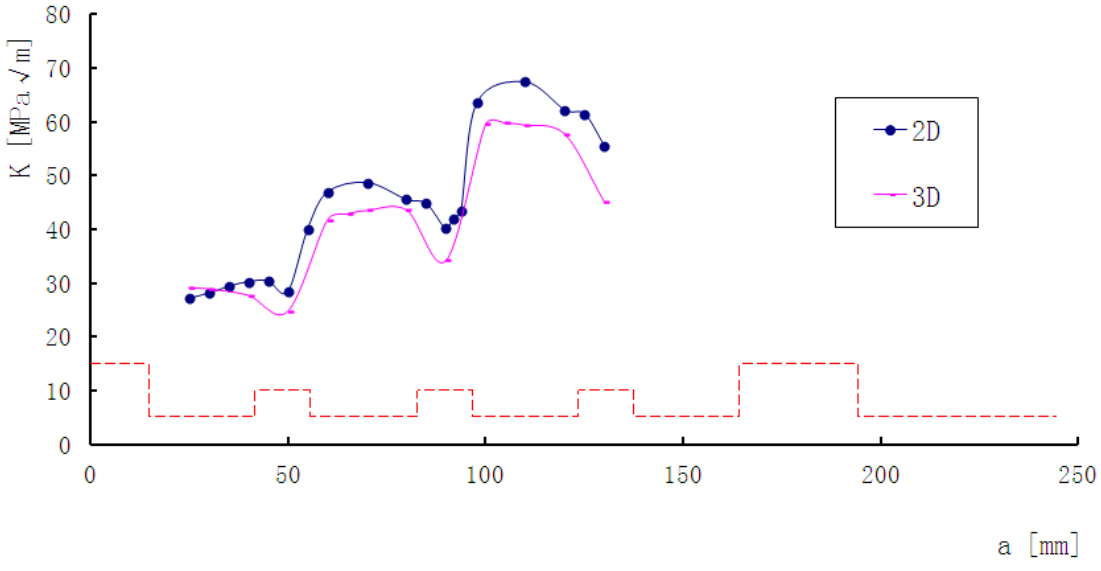

Figure 4-39 SIF results comparison of Panel 2 (2D and 3D)

The geometry factor β values of different crack lengths were plotted in Figure 4-40(compared with 2D results).

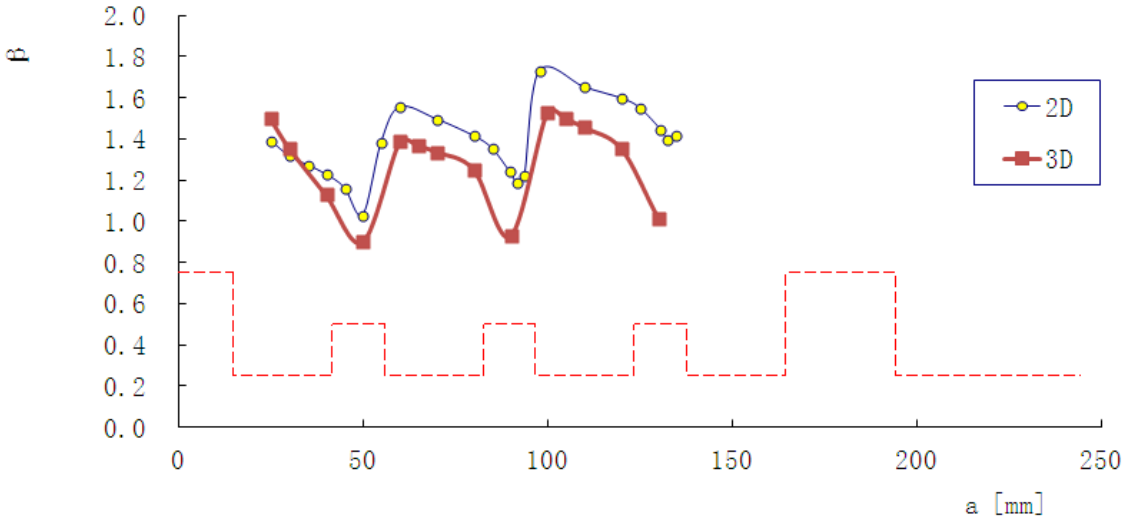

Figure 4-40 β values comparison of Panel 2 (2D and 3D)

The results indicate that, due to affection of stiffener, the SIF values cut down gradually until the crack reaches the central line of the stiffener. During the process of the crack through the stiffener, the SIF values increase rapidly.

4.3.2.4 Crack Growth Life Prediction Results

AFGROW tabular input was used in life prediction. When using AFGROW Tabular input method, Uniform amplitude loading (σ_{max}=69,5MPa,R=0.08) was chosen. Theβ value was defined by user, which calculated in former calculation. The model taken to calculation is shown in Figure 4-41. At the beginning, crack length is 25mm, and width 224.6mm.

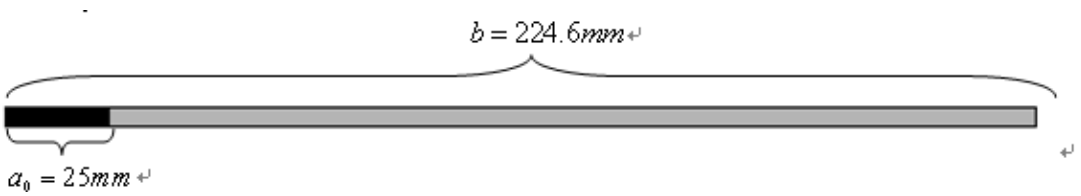

Figure 4-41 Crack growth model of Panel 2

Crack propagation stopped when the crack length reached the final crack length a=130mm.

The CGL (Crack Growth Life) prediction results of Panel 2 were presented in Table 4-14 and plotted in Figure 4-42 (compared with 2D model).

Table 4-14 Prediction results of crack growth life of Panel 2 (3D)

Method	Crack Growth Life (Cycles)	Differential Ratio
Experiment	49000	
Using da/dN data	58401	17.14%

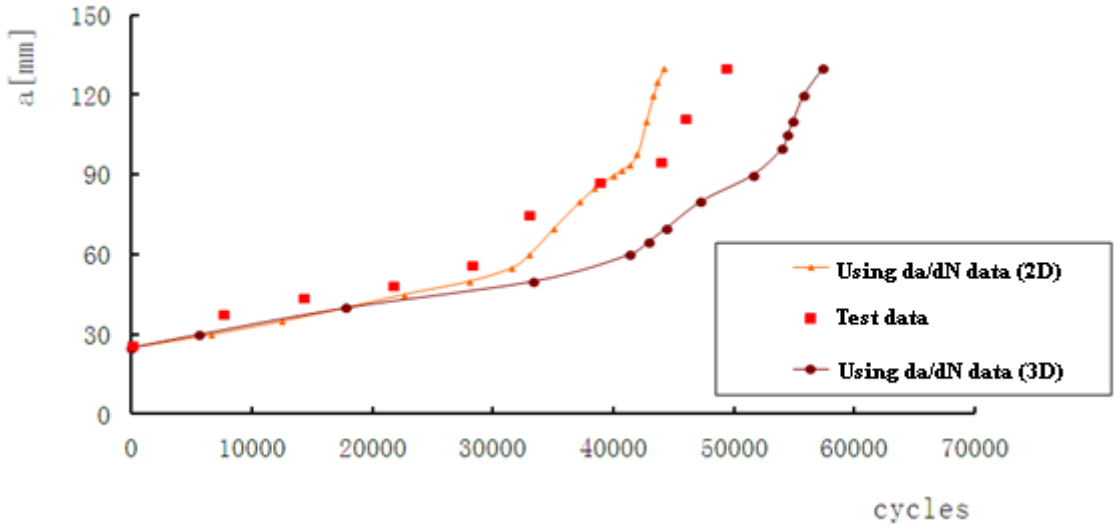

Figure 4-42 Crack growth curves (2D and 3D) and experiment

Before encountering the first stiffener, 2D and 3D results are almost the same and slightly small than the test results. When the crack reaches the stiffener, 2D results grow rapid. This phenomenal is probably caused by the 2D model defects, which cannot describe the crossing area of skin and stiffener very well. The disregard of the whole crossing region makes the SIF values higher than actual results. When using 3D model, the assumption in this region has significant influence in the final life prediction, which is discussed in detail in literature 20. In this article, the assumption of this region will be discussed in chapter 5.

4.3.3 New interactive procedure

During the previous calculation, when the crack crossed a stiffener, the crack growth rate of both panel and stiffener were supposed to be 1:1. But in the real

situation, it is not always the case. So, if the real crack growth rate at panel and stiffener can be calculated, it may get improvement in SIF results.

2D model was used in this new method. According the flow chart introduced in Figure 3-10, both SIF values of panel and stiffener were calculated when the crack reach the first stiffener. Then given a certain cycles, crack growth at both stiffener and panel could be calculated. New model could be built with new crack at panel and stiffener, and SIF values could be calculated. Repeated this work until the crack crossed the stiffener. The whole procedure of the crack cross the first stiffener was computed in Table 4-15.

Table 4-15 Procedure of the crack cross the first stiffener of Panel 2

Initial crack (mm)		K ($MPa\sqrt{m}$)		Cycles	Crack growth (mm)		New crack (mm)	
panel	stiffener	panel	stiffener		panel	stiffener	panel	stiffener
52.85	4.0	29.67	23.75	1000	1	0	53.85	4.0
53.85	4.0	28.64	24.88	1000	1	1	54.85	5.0
54.85	5.0	35.12	28.42	500	1	0	55.85	5.0
55.85	5.0	34.59	29.55	500	1	1	56.85	6.0
56.85	6.0	41.20	32.30	500	2	1	58.85	7.0
58.85	7.0	46.92	35.11	500	4	1	62.85	8.0
62.85	8.0	50.95	39.18	200	3	1	65.85	9.0

In short, it took a total of 4200 cycles when the crack crossed the first stiffener.

The same method was used when the crack crossed the second stiffener. And the whole procedure of the crack cross the second stiffener was computed in Table 4-16.

Table 4-16 Procedure of the crack cross the second stiffener of Panel 2

Initial crack (mm)		K ($MPa\sqrt{m}$)		Cycles	Crack growth (mm)		New crack (mm)	
panel	stiffener	panel	stiffener		panel	stiffener	panel	stiffener
93.75	4.0	41.55	31.54	500	2	0	95.75	4.0
95.75	4.0	38.90	34.35	500	1	1	96.75	5.0
96.75	5.0	48.02	39.43	200	2	1	98.75	6.0
98.75	6.0	57.66	44.94	200	3	1	101.75	7.0
101.75	7.0	65.40	57.88	100	3	2	104.75	9.0

In short, it took a total of 1500 cycles when the crack crossed the second stiffener.

When the crack tip was in the other place of the panel, the method used in SIF calculation was same with 2D model, and AFGROW was used in life prediction. The crack growth life of Panel 2 using new method was 45936 cycles and the result was plotted in Figure 4-43 (compared with 2D model). Compared with the experiment result, the result of new method got about 3.5% improvements than 2D model.

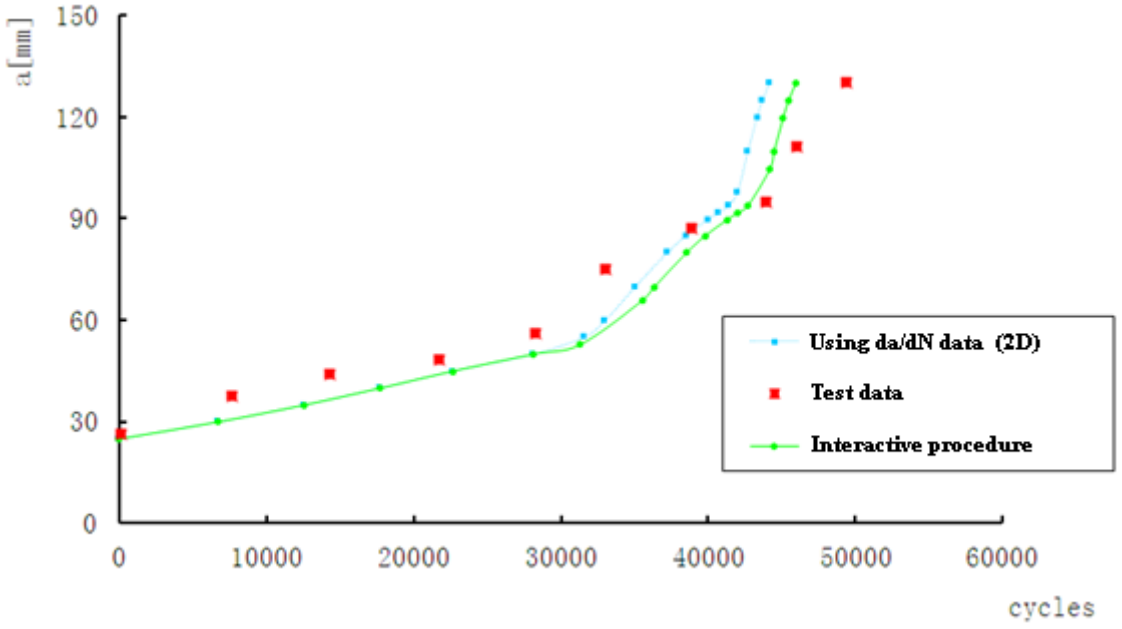

Figure 4-43 Crack growth curves of panel 2 using interactive method

4.4 Panel 3

4.4.1 2D Model

4.4.1.1 Model building

Considering the geometry and loading condition, only a quarter of the panel is modelled in favour of calculation.

Two types of boundary conditions are added into the geometry. In Y-Z symmetry, X displacements and Y and Z rotations are constrained. In X-Y symmetry, Z displacements and X and Y rotations are constrained except the crack location. A tensile load with the stress 100MPa is applied in Z direction on the top shell edge. The plane of shell reference is built in the central of the section of panel 3.

The model is built and analyzed using the ABAQUS 6.10-1 and its load and boundary conditions are shown in Figure 4-44.

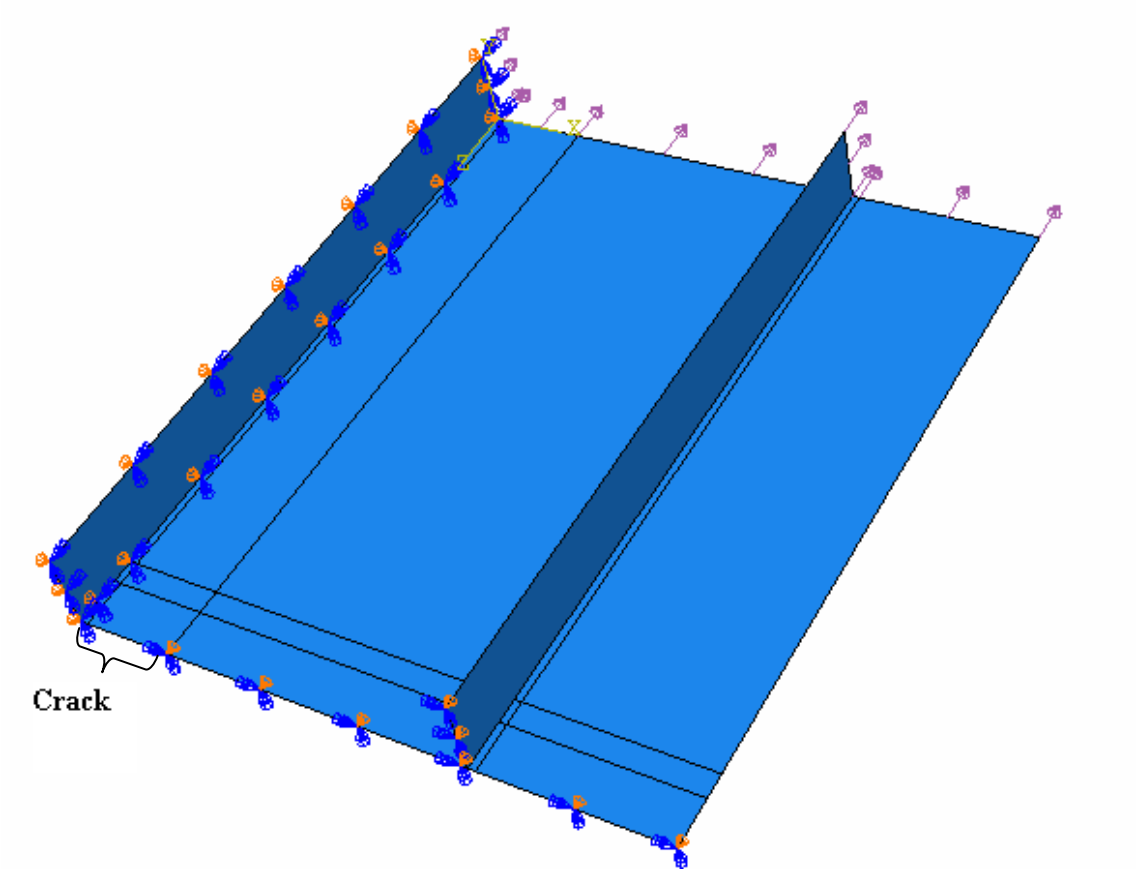

Figure 4-44 2D model of Panel 3 (one quarter)

4.4.1.2 Convergence test

In order to get a proper grid size to do the calculation of panel 3, half crack a= 40mm was taken to do the research to find out the relationship between grid size and the result using DE method. Grid size length would cut down gradually from 8mm to 1mm. The calculation results are list in Table 4-17, and curves are plotted in Figure 4-45. Considering both accuracy and time consuming, element size 3mm was taken in the calculation.

Table 4-17 Convergence test results of panel 3 (2D)

r (mm)	K ($MPa\sqrt{m}$)
1	43.608
2	43.383
3	43.153
4	42.736
6	42.088
8	42.250

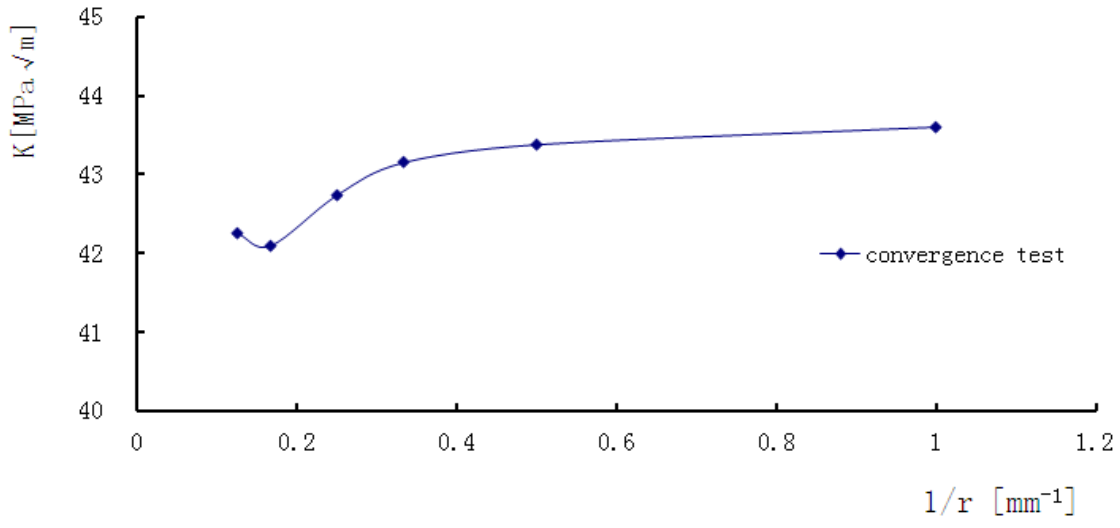

Figure 4-45 Convergence test curve of panel 3 (2D)

4.4.1.3 SIF result

ABAQUS 6.10-1 is used in model building and analysis. Altogether 4678 elements with the element type S8R are in the model. The element sizes are 3 mm around the crack and 6mm in the other parts. The mesh is drawn in Figure 4-46.

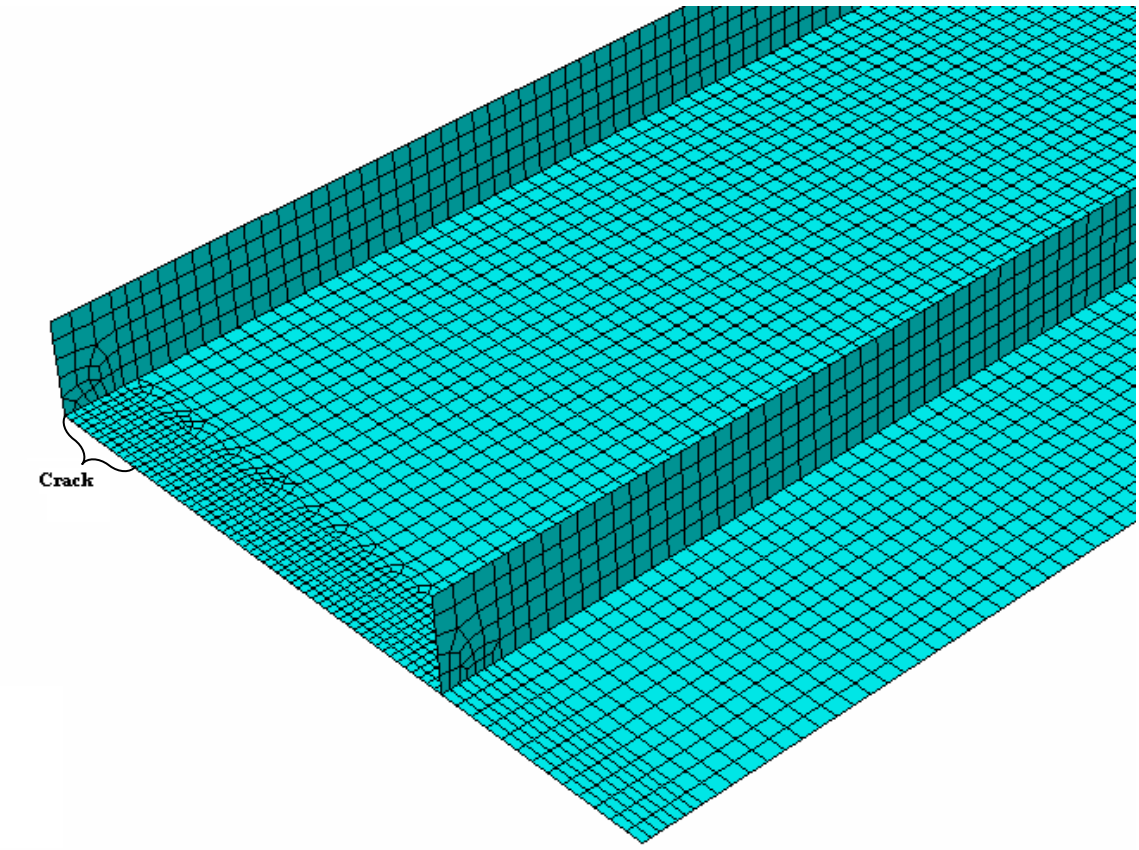

Figure 4-46 2D element mesh of panel 3

The stress state and distribution is checked to confirm if the edge loads and constrains are correct. The calculation results are shown in Figure 4-47.

Then, the SIF values of different crack lengths are calculated. The results are given in Table 4-18 and drawn in Figure 4-48.

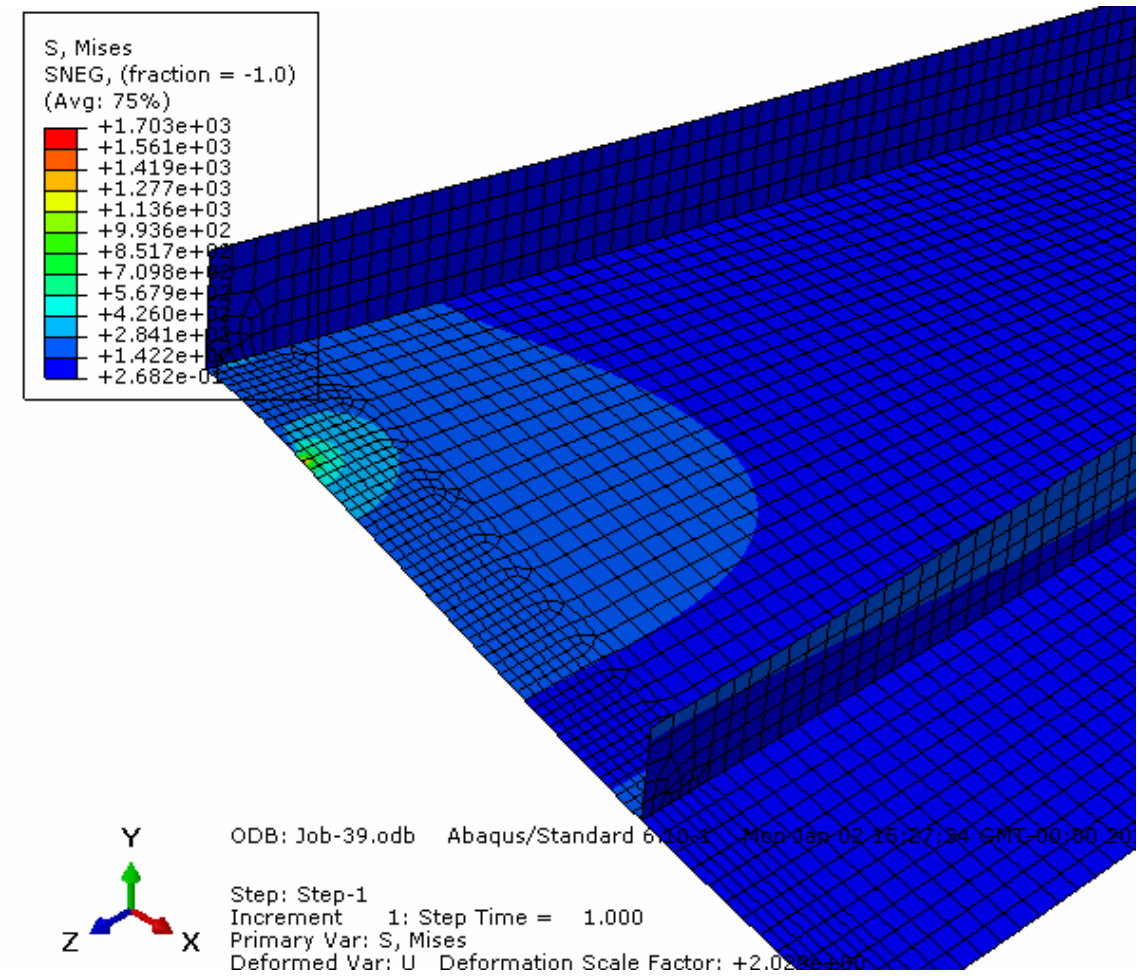

Figure 4-47 Stress distribution diagram of Panel 3 (2D)

Table 4-18 SIF values with different crack length of Panel 3 (2D)

a (mm)	K ($MPa\sqrt{m}$)	β
12	28.558	1.471
24	35.157	1.280
40	43.153	1.217
70	56.886	1.213
100	70.744	1.262
140	90.798	1.369
160	99.595	1.405

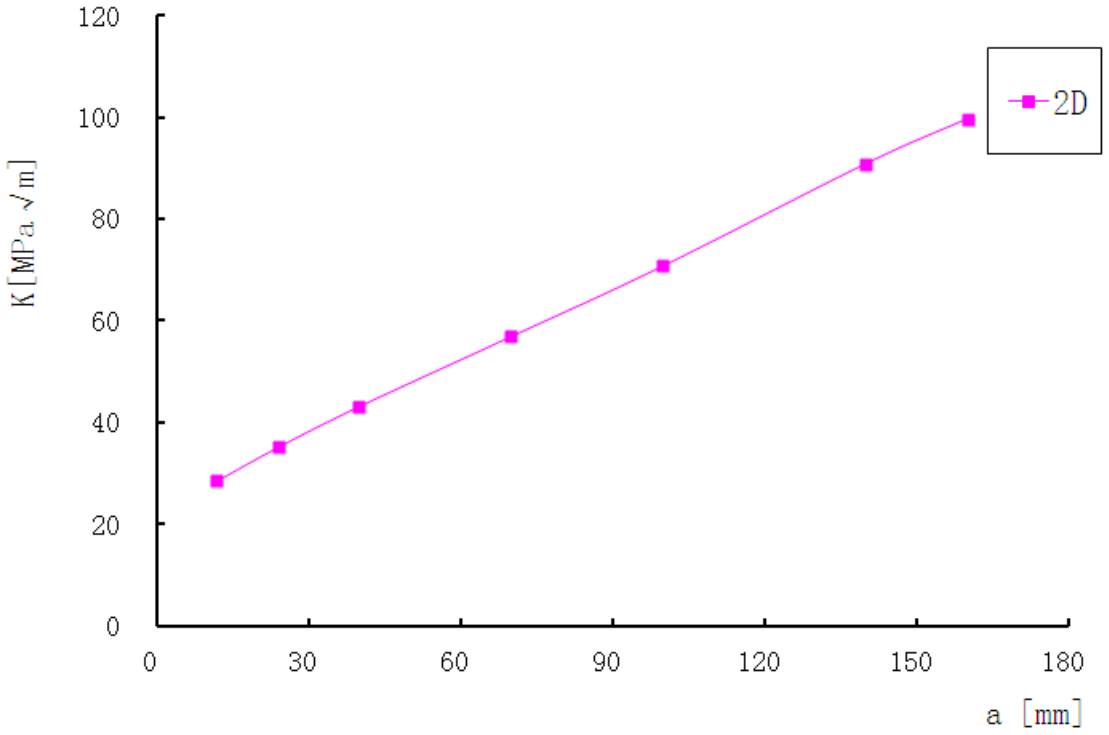

Figure 4-48 SIF curve of Panel 3 (2D)

The geometry factor β values of different crack lengths are plotted in Figure 4-49.

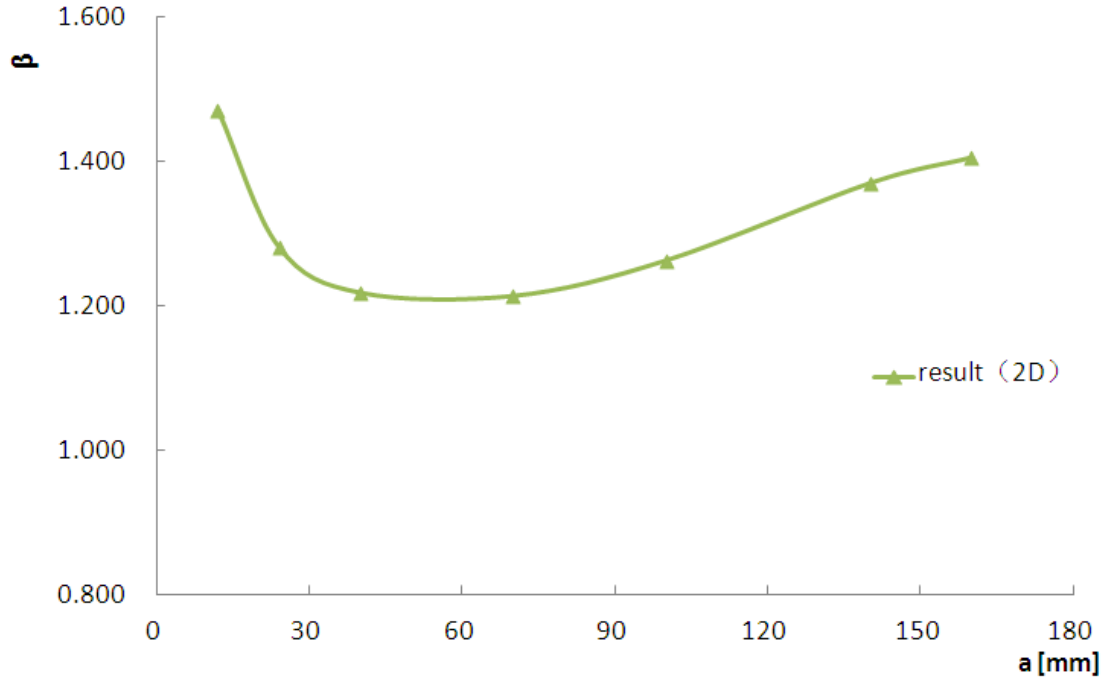

Figure 4-49 Geometry factor β curve of Panel 3 (2D)

4.4.1.4 Crack Growth Life Prediction Results

Paris law and AFGROW tabular input were used in life prediction. When using Paris law, C=0.534e-011 and n=3.9 were applied [29], and according to the Paris law equation $da/dN = C(\Delta K)^n$, crack growth life was calculated. When using AFGROW Tabular input method, Uniform amplitude loading ($\sigma_{max} = 100\text{MPa}$,) $R = 0.1$ was chosen. The β value was defined by user, which calculated in former calculation. At the beginning, crack length was $a_0 = 12\text{mm}$, and the calculation stopped when the crack reached 160mm. The crack growth life was 10985cycles when using Paris law and 9834 cycles when using AFGROW tabular input. The crack growth curves are plotted in Figure 4-50.

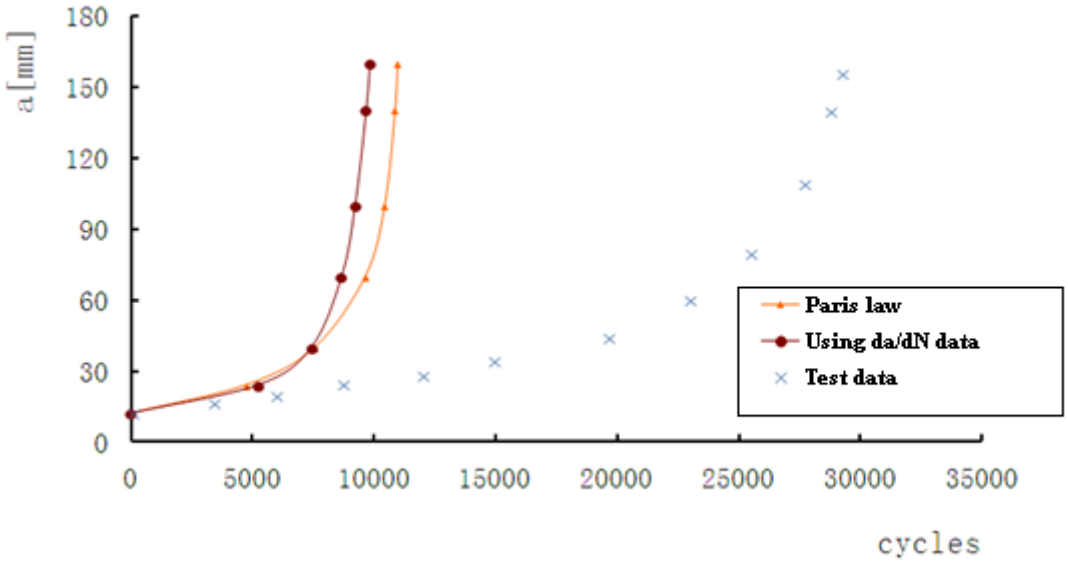

Figure 4-50 Prediction of crack growth curves

4.4.2 3D models

4.4.2.1 Model building

According to the geometry and loading condition, a quarter of the panel is modelled in favour of calculation.

Two types of boundary conditions are added into the geometry. In Y-Z symmetry, X displacements and Y and Z rotations are constrained. In X-Y symmetry, Z displacements and X and Y rotations are constrained except the

crack location. A pressure load with the stress 100MPa is applied in Z direction on the top surface.

The model with load and boundary conditions was shown in Figure 4-51.

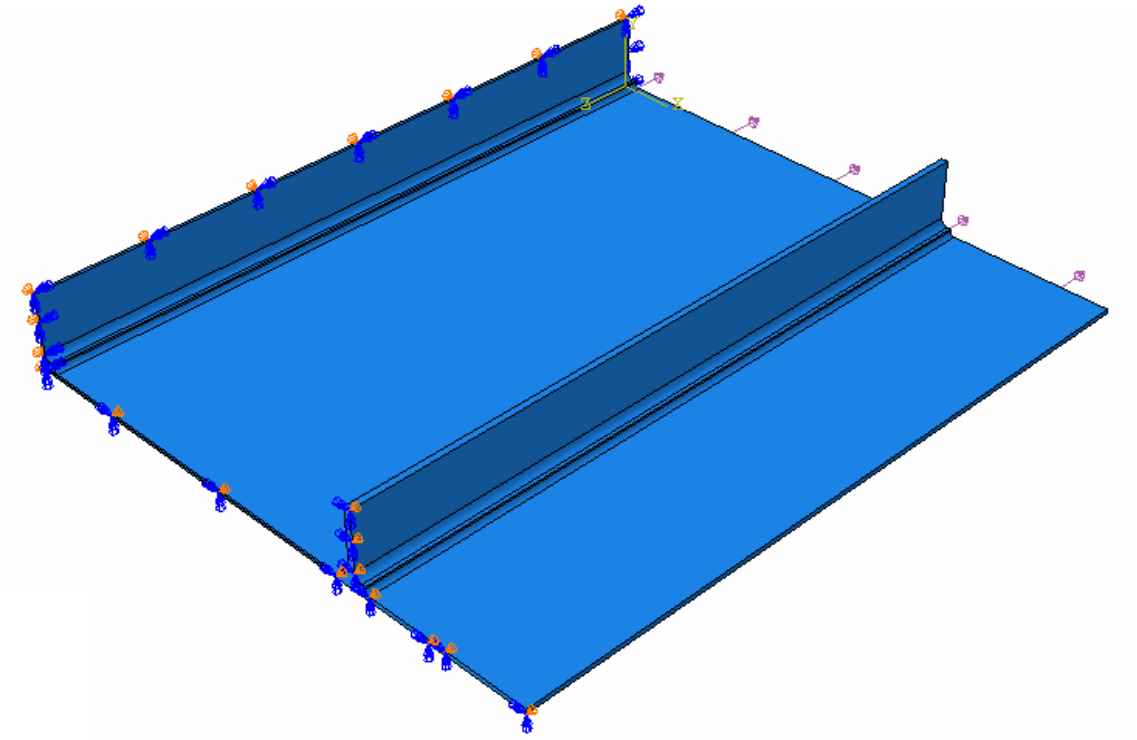

Figure 4-51 3D model of Panel 3 (one quarter)

4.4.2.2 Convergence test

In order to get a proper grid size to do the calculation of panel 3, half crack a= 40mm was taken to do the research to find out the relationship between grid size and the result using DE method. Grid size length would cut down gradually from 8mm to 1mm. The calculation results are list in Table 4-19, and curves are plotted in Figure 4-52. Considering both accuracy and time consuming, element size 3mm was taken in the calculation.

Table 4-19 Convergence test results of panel 3 (3D)

r (mm)	K ($MPa\sqrt{m}$)
8	44.163
6	43.961
4	43.873
3	43.759
2	43.674

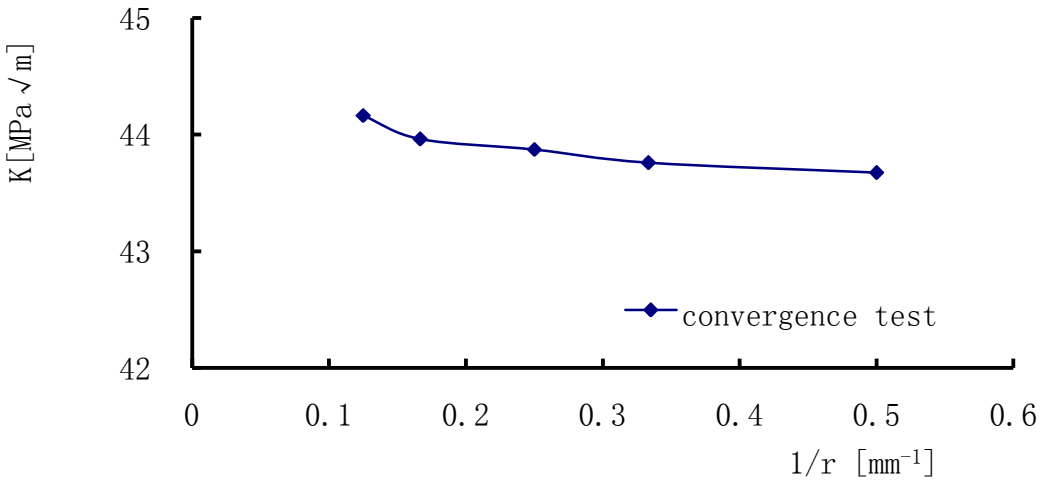

Figure 4-52 Convergence test curve of panel 3 (3D)

4.4.2.3 SIF result

The mesh of panel 3(3D) is shown in Figure 4-53. Altogether 23520 elements with the element type C3D20R were in the model. The element sizes were 3mm.

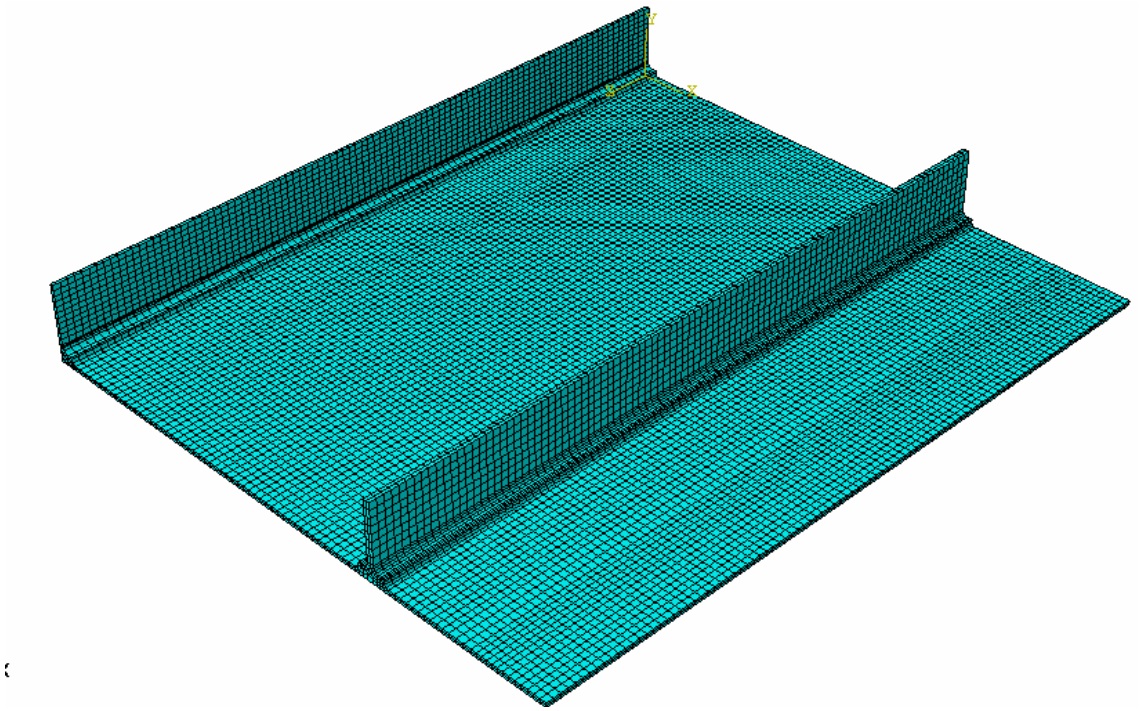

Figure 4-53 3D element mesh of panel 3

At first, the stress state and distribution was checked to confirm that the edge loads and constrains were correct. The calculation results are shown in Figure 4-54.

Then, the SIF values of different crack lengths are calculated. The results are given in Table 4-20 and drawn in Figure 4-55.

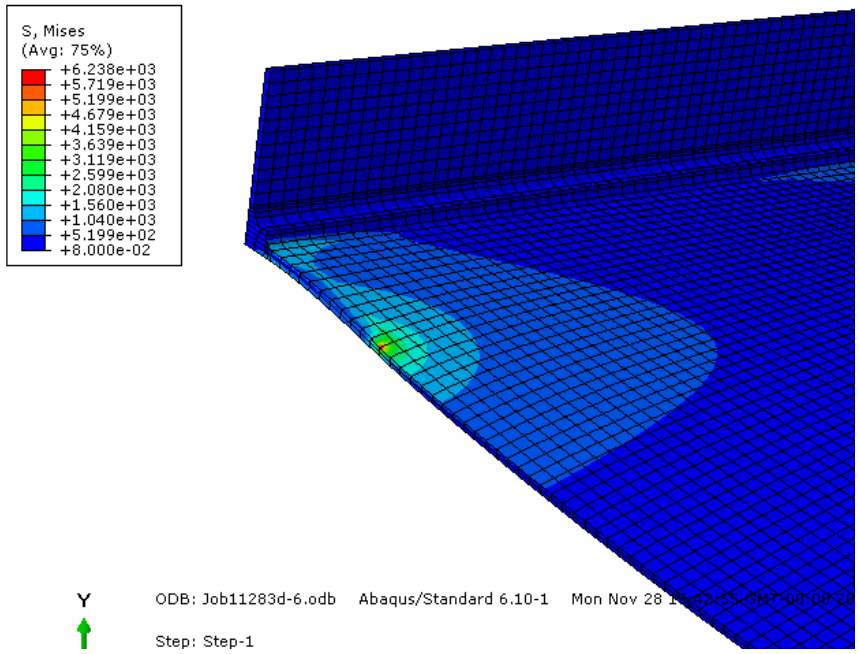

Figure 4-54 Stress distribution diagram of Panel 3 (3D)

Table 4-20 SIF values with different crack length of Panel 3 (3D)

a (mm)	K ($MPa\sqrt{m}$)	β
12	29.861	1.538
24	35.821	1.305
40	43.759	1.234
70	57.559	1.227
100	71.467	1.275
140	91.660	1.382
160	100.523	1.418

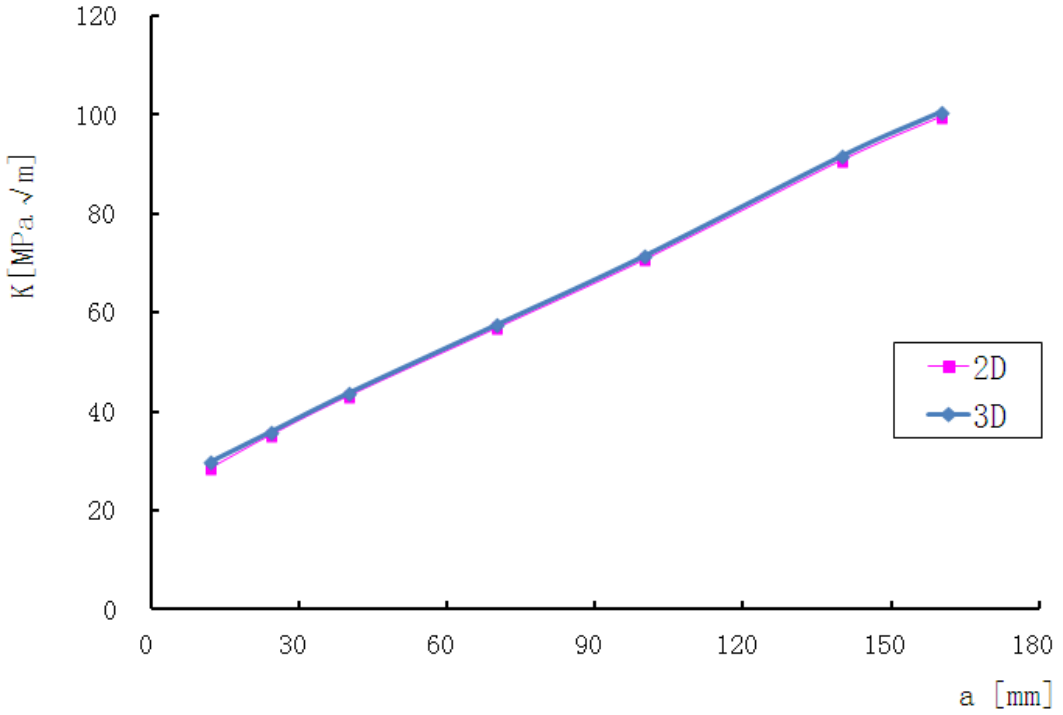

Figure 4-55 SIF curve of Panel 3 (2D and 3D)

The geometry factor β values of different crack lengths compared with the 2D results are plotted in Figure 4-56.

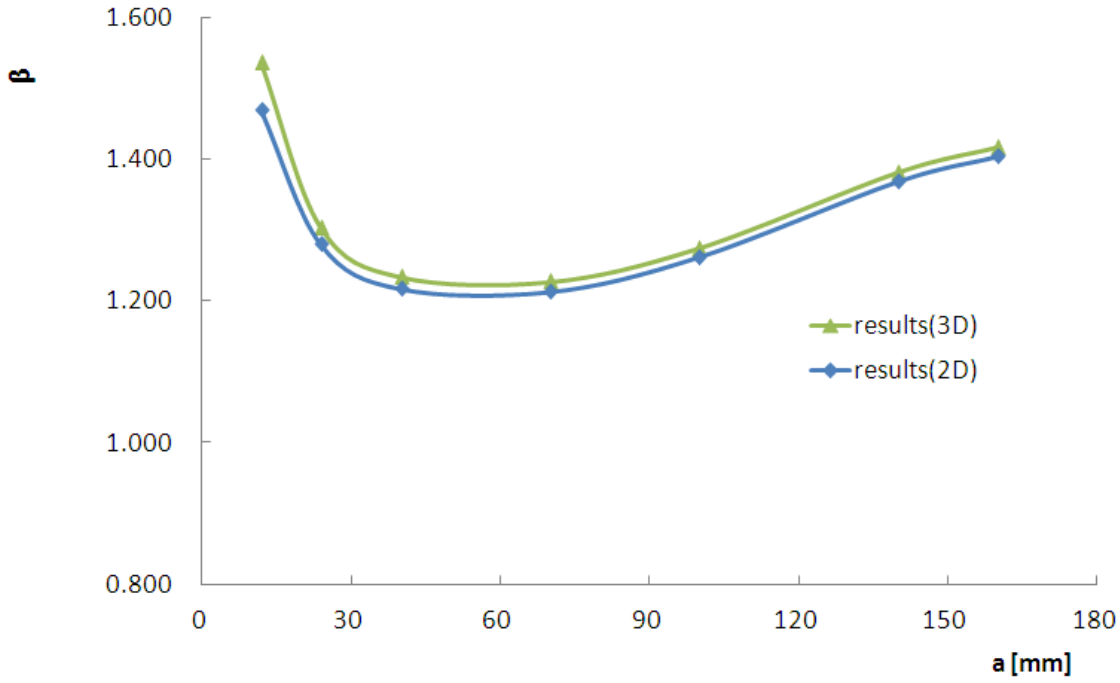

Figure 4-56 Geometry factor β curve of Panel 3 (2D and 3D)

4.4.2.4 Crack Growth Life Prediction Results

Paris law and AFGROW tabular input were used in life prediction. When using Paris law, C=0.534e-011 and n=3.9 were applied [29], and according to the Paris law equation $da/dN = C(\Delta K)^n$, crack growth life was calculated. When using AFGROW Tabular input method, Constant loading ($\sigma_{max} = 100\text{MPa}$,) $R = 0.1$ was chosen. The β value was defined by user, which calculated in former calculation. At the beginning, crack length was $a_0 = 12\text{mm}$, and the calculation stopped when the crack reached 160mm. The crack growth life was 10103cycles when using Paris law and 8766 cycles when using AFGROW tabular input. The crack growth curves are plotted in Figure 4-57.

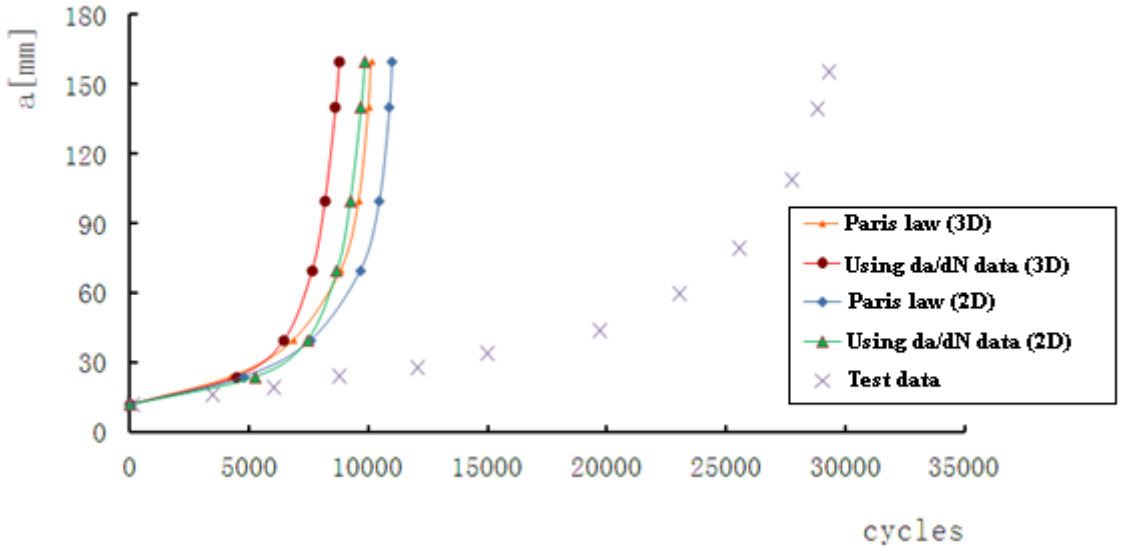

Figure 4-57 Prediction of crack growth curves [33]

The results show that, all 2D and 3D model with Pairs law and Tabular input methods get similar crack growth cycles, which are less than test results. High stress lever and very thin in thickness maybe the main reasons cause the results not as good as the previous panels. So，It is very important to calculate the plastic zone of this thin panel.

According to Irwin's first estimate of the plastic zone size [34], the plastic zone size is equal to the distance r_y, see Figure 4-58. And the equation is in 4-1.

$$r_y = \frac{1}{2\pi}\left(\frac{K_I}{\sigma_{ys}}\right)^2 \qquad \textbf{(4-1)}$$

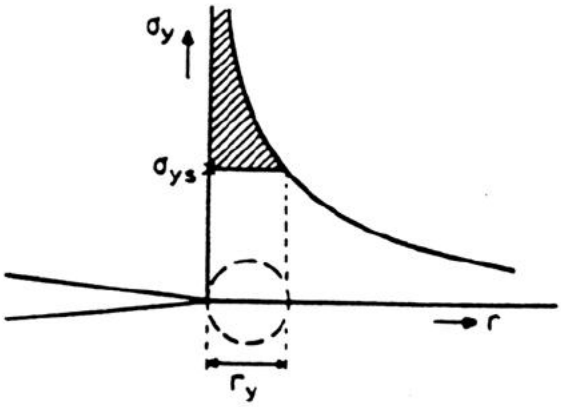

Figure 4-58 Irwin's first estimate of the plastic zone size

The actual plastic zone size must be larger than r_y , since the load represented by the shaded area in figure 4-58 must still be sustained. Irwin proposed that this plasticity makes the crack behave as if it were larger than its actual physical size, in Figure 4-59. And he gave the modification in 4-2.

$$r_p = 2r_y = \frac{1}{\pi}\left(\frac{K_I}{\sigma_{ys}}\right)^2 \qquad \textbf{(4-2)}$$

r_p is the corrected plastic zone size.

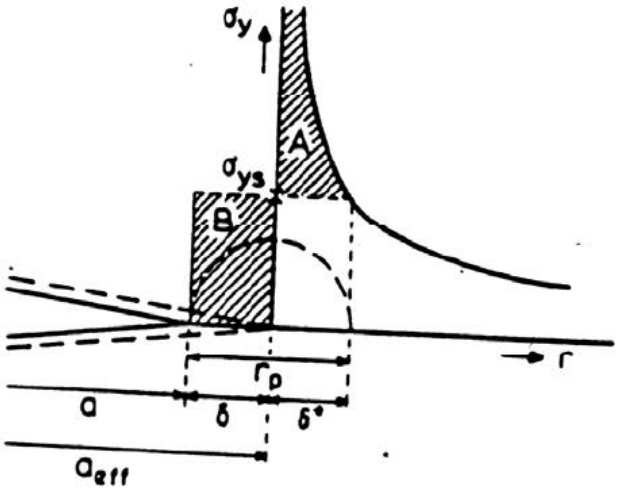

Figure 4-59 Irwin's second estimate of the plastic zone size

The plastic zone of panel 3 at several points were calculated and listed in table 4-21.

Table 4-21 Crack length and the corresponding plastic zone

a (mm)	Plastic zone size	
	r_y (mm)	r_p (mm)
12	1.34	2.69
24	1.93	3.87
40	2.89	5.77
70	4.99	9.98
100	7.70	15.39
140	12.66	25.32

According to results in table 4-21, r_p is much bigger than thickness t. Hence, the life prediction of panel 3 is not as good as previous two panels when using previous methods.

As introduced in chapter 3, Nasgro equation is also an effective method in crack growth prediction, especially the crack closure model, which considers the affection of plastic zone. Hence, Nasgro equation with crack closure model is also used in the life prediction of model 3. During the calculation, some constant data are modified according to literature 29, c=0.53E-9, n=3.9, q=0.1 compared with c=9.22E-9, n=3.353, q=1 in AFGROW database. Figure 4-60 gives the results of Nasgro equation. It is 29301(2D)and 26606(3D) cycles separately compared with test result 29270cycles.

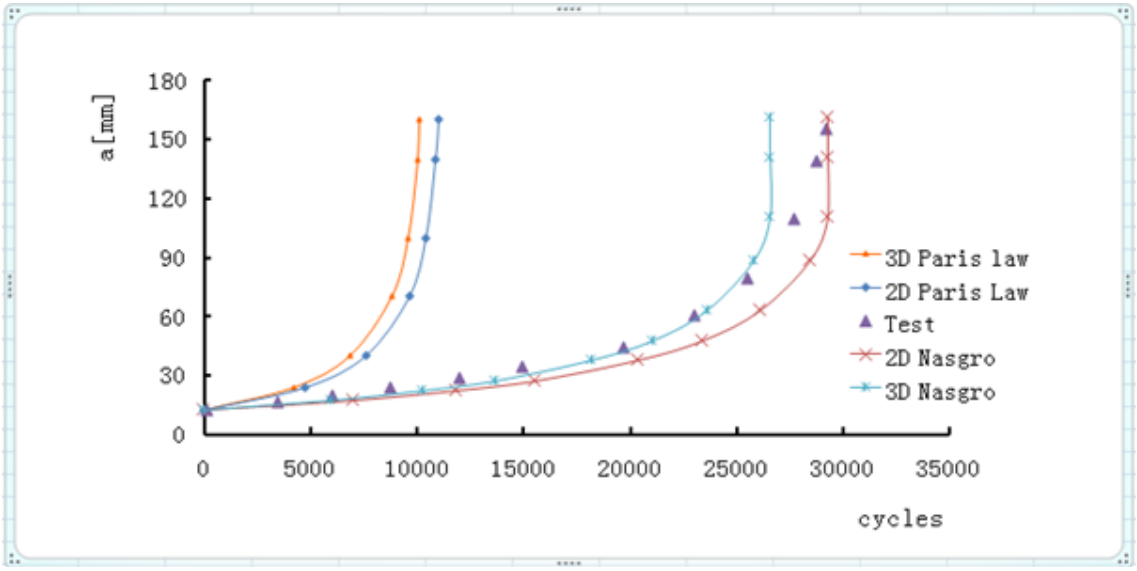

Figure 4-60 Prediction of crack growth curves using Nasgro equation [33]

It is obviously that Nasgro equation with crack closure model gets very good results in thin panel's crack growth life prediction.

5 Discussion

5.1 Methods discussion

5.1.1 Boundary Condition

Boundary condition should exactly represent the experiment condition and must be carefully modelled. The loading is specified as stress-controlled in the finite element models. The loading is carried out as displacement-controlled in the experiment. So define the applied stress is an important parameter in SIF calculation and it will influence the SIF values directly.

5.1.2 2D and 3D model

2D and 3D methods were used in this article in SIF calculation. 2D model was the first choice because it was easier to build and quicker to analyze for its fewer number of elements compared with 3D model. The calculation results also showed that the SIF values from 3D model were always slightly bigger than 2D model results when the crack did not reach the stiffener. While the crack reached the stiffener, 2D model could not describe the situation, and the crossing region was neglected. Hence, the results might not be accuracy.

In summarise, when the crack is far from the stiffener, 2D and 3D model are both valid for the SIF calculation, and 2D model seems more efficient. While the crack reaches the stiffener, especially in the crossing region, due to the model restrictions of 2D model. It is better to choose 3D model.

5.1.3 Assumptions

Two assumptions were made in the calculation. The first one was that the crack front was assumed to be straight for 3D model. It meant that along the thickness direction, the crack propagation rates would be the same. This assumption made easier the simulation of crack. While in the real situation, this was not always the case. When the crack was short, crack in the stringer side

grew faster than flat side. This phenomenon was described in literature [20] and drawn in Figure 2-7. It was also encountered during the calculation of three integral panels. The second one was the crack growth rates in skin and stringer were assumed to be the same, although it might be different with different structures and materiel.

5.1.4 New interactive method

In order to overcome the error caused by the second assumption, new interactive method was introduced in calculation. When applying this new method, the crack growth in skin and stringer would be calculated respectively. When crossing the first stringer, the crack grew 17mm in the panel and 9mm in the stiffener, and the growth rate was about 2:1. When crossing the second stringer, the crack grew 15mm in the panel and 9mm in the stiffener, and the growth rate was about 1.7:1. So, although it would cost more time in calculation, it made the result more accuracy.

5.2 Al 2024-T351 da/dN curve discussion

When using AFGROW tabular input method in Panel 1's life calculation, the errors of the results were more than 40%. They were much higher than the results calculated by Paris law. The situation might be caused by the da/dN curve of Al 2024-T351 (Figure 5-1 ASTM data), because these points could not be connected into a straight line. Hence, another curve of Al 2024-T351 was selected in life prediction, and it was come from FAA test result [31], as shown in Figure 5-1.

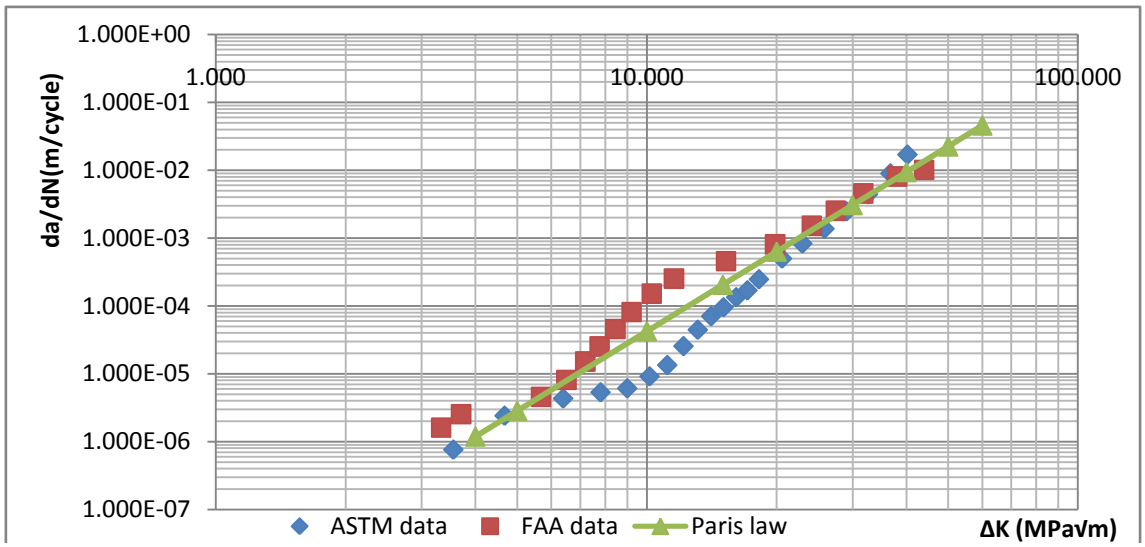

Figure 5-1 $\Delta K - da/dN$ **curve of Al 2024-T351 [31]**

The results of the calculation are shown in Figure 5-2. The results were 62885 cycles (2D model) and 60795 cycles (3D model), and the error was about -20%, compared with the test result.

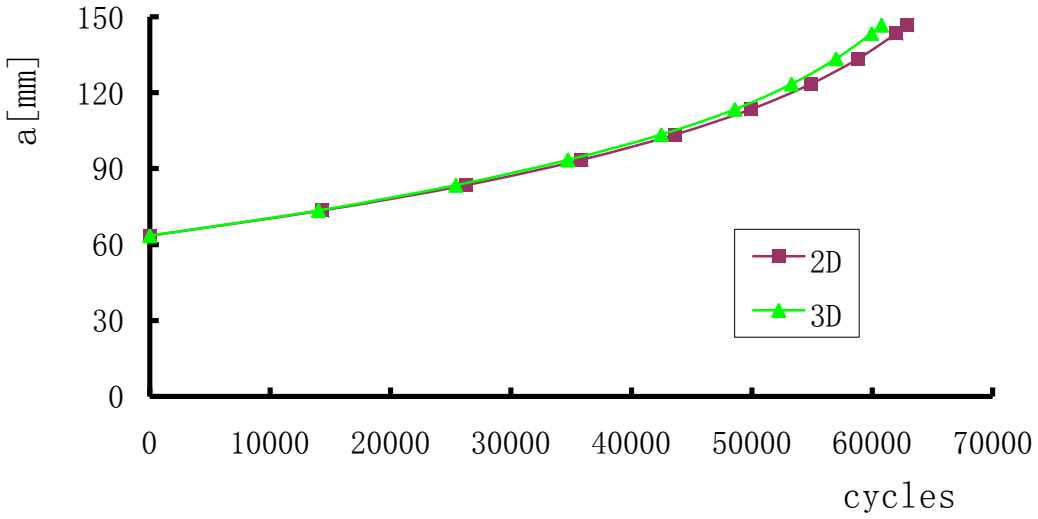

Figure 5-2 Crack growth curves of Panel 2

5.3 Cross-region description

There would be many kinds of assumptions when the crack grew to the cross-region of panel and stiffener in panel 2. In this thesis, it was ignored when using 2D model, because of the model restrictions. While using 3D model, the

assumption of the crack is shown in Figure 5-3. In the stiffener, the crack was supposed to be a quarter–circle. And in the panel, the crack was supposed to be a line, with the same length of the radius of the quarter–circle. Then, the cracks grew respectively in the panel and the stiffener with the same speed, until through the stiffener completely.

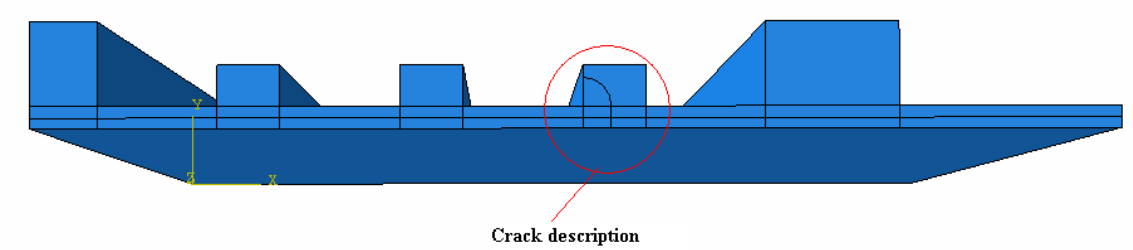

Figure 5-3 Crack assumption of Panel 2 (3D)

Compared with the test result, the final crack growth life is about 17% error when choosing this assumption. So, this kind of assumption is reasonable in the use of engineering.

5.4 Crack Growth Life Results Discussion

The crack growth lives of three panels are not predicted very accurate, especially for the panel3 only half cycles of the test data. .

There could be two reasons why the crack growth life predictions are not accurate. The first one is that the SIF results are calculated based on finite element model. Due to limitations of time and hardware, it is hard to get very accurate values, while the prediction results are rather sensitive with these values. Another one is the limitation of methods used in life prediction procedure. Each method has advantage and restrictions. So It is very hard for each panel choosing proper method.

6 Conclusion and future work

6.1 Conclusion

In this thesis, three different integral metallic skin-stringer panels are analyzed with 2D and 3D method. The analysis includes two steps: calculation of stress intensity factor and crack propagation analysis. The whole process show that although the results are not accurate to some extents, most of the results are acceptable in the use of engineering compared with the test results. Following conclusions are based on the analysis of this article.

1. Both 2D and 3D models with displacement method are good methods in calculation of stress intensity factor.
2. Compared with 3D model, only one forth of elements is needed in 2D model, it can save much time in calculation.
3. In the area away from the stiffener, the SIF values calculated from 3D model are slightly bigger than 2D values. While in the skin-stringer joint region, 3D model shows better accuracy than 2D model.
4. New interactive procedure can get more accuracy results than 2D model although it spends more time in calculation.

6.2 Future work

Due to the time limit, the author could only finish part of this program. There are many parts for improvement and recommendations for the future work as follow:

1. Since not well modelled with panel 3, new method could be used in stress intensity factor calculation of this panel, such as compounding method [32], which may get accuracy values.
2. It is very hard to get fine mesh, when the crack grows to the skin-stringer crossing area. Do more research in this area, and calculate the stress intensity factor in this region is very important.
3. New interactive method is only used in 2D method; it can also be used in 3D model, which may also improve calculation results.

REFERENCES

1. J.Munroe, K.Wilkins, and M.Gruber, “Integral Airframe Structures (IAS)—Validated Feasibility Study of Integrally Stiffened Metallic Fuselage Panels for Reducing Manufacturing Costs”, NASA/CR-2000-209337, May 2000.

2. Chen CS, Wawrzynek PA, Ingraffea AR. “Crack growth simulation and residual strength prediction in airplane fuselages”. NASA/CR-1999-209115; 1999

3. R.G.Pettit, J.J.Wang, and C.toh,”Validated Feasibility Study of Integrally Stiffened Metallic Fuselage Panels for Reducing Manufacturing Costs”, NASA/CR-2000-209342, May 2000.

4. Grigory I. Nesterenko TsAGI, Russia "Comparison of Damage Tolerance of Integrally Stiffened and Rivetted Structures", ICAS 2000 Congress.

5. Der Veen V, Eherstrom JC, Muzzolini R. “Monolithic airframe structure: materials and methods for reduced cost reduced weight and improved damage tolerance”. In: Proc. 44th AIAA materials and structures conference, paper AIAA-2003-1457; April 2003.

6. Zhang X, Boscolo M, Figueroa-Gordon D, Allegri G, Irving PE. “Fail-safe design of integral metallic aircraft structures reinforced by bonded crack retarders”. Engng Fract Mech 2009;76:114–33.

7. Heinimann M, Bucci RJ, Kulak M, Garratt M. “Improving damage tolerance of aircraft structures through the use of selective reinforcement”. In: 23rd ICAF symposium, Hamburg; June 2005.

8. J.Maclin，“Performance of Fuselage Pressure Structure”，1991 International Conference on Aging Aircraft and Structural Airworthiness, Washington D.C.，November19-21，1991，NASA Conference Pub 3160(1992).

9. T.Swift, “The Applications of Fracture Mechanics in the Development of the DC-10Fuselage”,in Fracture Mechanics of Aircraft Surtctures,AGARD-AG-176 by H.Liebowitz, Neuilly sur Seine, France，PP.226-287，1974.

10. T.Swift, “Damage Tolerance in pressurized Fuselage”,11th Plantema Memorial Lecture, 14th Symposium of the ICAF, New Materials and Fatigue Resistant Aircraft, Ottawa, Canada, 1987.

11. R.G.Pettit, J.C.Newman, and M.S.Domack, “Crack Turning Damage Tolerance Approach of integrally Stiffened Structure”，19th ICAF Symposium, Edinburg, June, 1997.

12. Sanders J. “Effect of a stringer on the stress concentration due to a crack in a thin sheet”. NASA TR R-13; 1959.

13. Rooke D, Cartwright D. “Compendium of stress intensity factors”. London: HMSO;

1976.

14. Dexter R, Pilarski P, Mahmoud H. “Analysis of crack propagation in welded stiffened panels”. Int J Fatigue 2003;25(9 – 11):1169 – 74.

15. Vlieger H. “The residual strength characteristics of stiffened panels containing fatigue cracks”. Engng Fract Mech 1973;5(2):447 – 70.

16. Utukuri M, Cartwright D. “Stress intensity factors for a crack near finite boundaries in multiply stiffened sheets”. Theor Appl Fract Mech 1991;15(3):257 – 66

17. Moreira, P. M. G. P., S. D. Pastrama, et al. (2009). "Three-dimensional stress intensity factor calibration for a stiffened cracked plate", Engineering Fracture Mechanics 76(14): 2298-2308.

18. Raju I, Newman J. “Three dimensional finite-element analysis of finite-thickness fracture specimens”, TN-D-8414, NASA Center for AeroSpace Information (CASI); 1977.

19. Kwon S, Sun C. Characteristics of three-dimensional stress fields in plates with a though-the-thickness crack. Int J Fract 2000;104:291 – 315.

20. M. Fossati, D. Colombo, A Manes, M. Giglio, “Numerical modelling of crack growth profiles in integral skin-stringer panels”, Engineering Fracture Mechanics 78, 2011, 1341 – 1352.

21. Knott, J F, “Fundamentals of Fracture Mechanics”, Butterworths, 1973.

22. Xie De, Qian qin, and Li Changan, “Numerical Methods in Fracture Mechanics and Engineering Applications”, Science Press, 2009 (Published in Chinese).

23. Rice J R, “A Path Independent Integral and the Approximate Analysis of Strain Concentration by Notches and Cracks”, Journal of Applied Mechanics, 1968, 35, 379-386.

24. Paris, P C and Erdogan,F, “A critical Analysis of Crack Propagation Laws”, Journal of Basic Engineering, Vol.85, 1960, 528-534.

25. Forman, R G, Keary, V E, and Engle, R M, “Numerical Analysis of crack Propagation in Cyclic-Loaded Structures”, Journal of Basic Engineering, Vol.89, 1967, 459-464.

26. NASGRO technical manual, September 2002, http://www.nasgro.swri.org/ (accessed 05/2011).

27. Ingo Scheider, and Wolfgang Brocks (2008), “Residual Strength Prediction of a Complex Structure Using Crack Extension Analyses”, *Engineering Fracture Mechanics*, vol.75, pp 4001-4017.

28. Marks Heinimann, Mark James (2006), “Panels for Phase 1 of Analytical Round

Robin on Integral Structures", ALCOA.

29. Zheng Xiaoling, Zhang Minfu, "Civil Aircraft Structural Durability and Damage Tolerance Design Manual", Aviation Industry Press, 2003 (Published in Chinese).

30. M.Giglio, A.Manes, and M.Fossati, "Analysis of the Cracks Propagation in a Integral Stiffened Panel", IGF 19, MILAN.

31. Fatigue Crack Growth Database for Damage Tolerance Analysis, DOT/FAA/AR-05/15, Office of Aviation Research Washington, D.C. 20591.

32. Pastramaˇ S et al. Compounded stress intensity factors: introduction to the method and the case of cracked stiffened plates. In: 10th Portuguese conference on fracture, Guimaraes, Portugal; 2006.

33. D Quinn, A Murphy, and L Cervi, 'Fatigue Performance of Aircraft Panels with Novel Skin Buckling Containment Features", Journal of Aerospace Engineering; 225 (7), pp. 791-806， 2011.

34. Irwin, G.R., Analysis of Stresses and Strains Near the End of a Crack Traversing a Plate, Trans. ASME, J. Applied Mechanics, vol.24, pp. 361-364, (1957).

APPENDIX A

Flying Wing Aircraft Conceptual Design

ABSTRACT

From March to early September 2011, the author paid main attention in a group design project (GDP) of the conceptual design of a 200-seat flying wing aircraft. So the author would like to give a brief introduction of the GDP work.

There are four stages in the GDP conceptual design process. The first stage is market analysis, from March to June 2011. In this stage, information is collected from aircraft manufacturers, operators, and design companies to find out what kind of aircraft is actually needed. The second stage is conventional aircraft design, from June to middle July. During this period, a 250-seat middle-range aircraft is designed with the range 4000 Nautical miles and Mach0.80. As family issue, a long-range conventional aircraft is also designed with the same wings, but the range changes to 7000 Nautical miles and Mach0.85. The third stage is from July to early August. At this time, the flying-wing aircraft design is finished with the range 7000 Nautical miles and Mach0.82. The last stage is document preparing and final presentation mainly in the August.

That is all the GDP work, and the next step detail design of the flying wing aircraft will be performed by another design group.

1 Introduction

The main objective of this Group Design Program is to design a new generation commercial aircraft which may be used both Chinese domestic market and global market in future. Therefore, Flying Wing aircraft should be designed to meet these two markets' requirements.

During the conceptual design process from March to September, all the research work is applying civil aircraft design technology to obtain a set of parameters, sizing configuration, and so on. Simultaneously, all the above results will be conservation in computer and be delivered to the next design group as the design inputs.

In order to achieve our objective, all the AVIC students were involved in the program. Every student was responsible for one part of each stage of the whole project and they were divided into several small groups. Each group had to work together, collect information and exchange their views. When facing with difficult problems, students could get help from supervisors of the group.

The major responsibility of the author is market research and analysis at first phase. Then do 3-D drawing of conventional aircraft and cabin structural of flying Wing aircraft in the next two phases. At last, the author prepares paper about market analysis for final presentation.

2 Market survey and analysis

During the conceptual design stage, the first design task of Flying Wing aircraft design group is to survey and analyze the current and future civil aviation market. At the end of this phase, the initial design requirements such as target market, design range, seat capacity, service time, flight speed, operating requirements, airport, and family issue should be defined.

2.1 Target market

Global gross domestic product (GDP) growth drives the aircraft demand. According to the Boeing Company's long-term market prediction, the global economic growth will gradually increase 3.2% per year in 20 years (see figure 2-1) [1]. Especially in Asia, the speed of economic growth is much higher than any other place of the world. Table 2-1 gives the data predicted by Boeing and China commercial about the average GDP growth rate in next 20 years.

Simultaneously, the world passenger traffic is expected to grow by 4.8% per year according to Airbus prediction over the 2009-2029 periods (see figure 2-2) [2]. COMAC compares the fleet percentage between 2009 and 2029 (see figure 2-3) [3], and China will have the most increase in next 20 years.

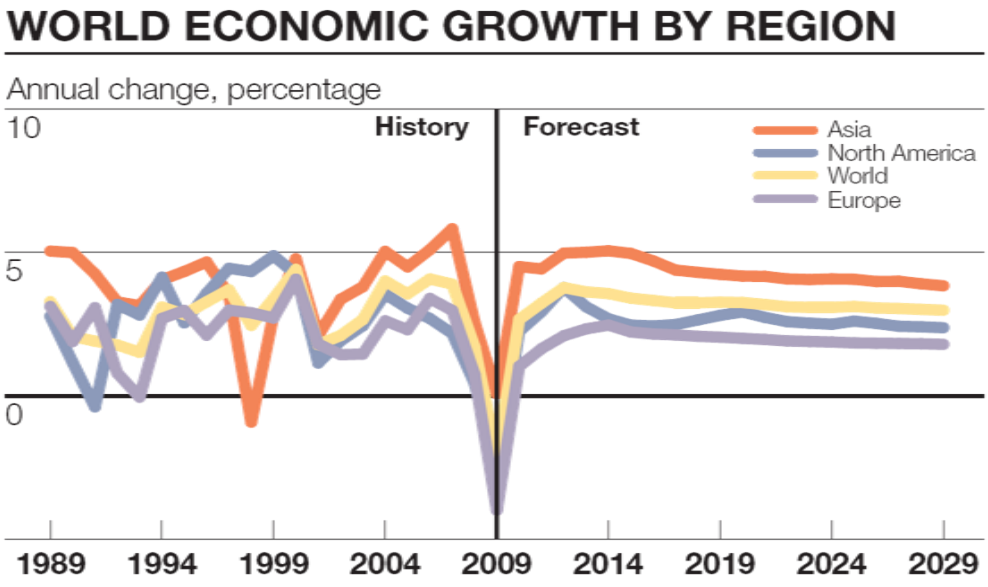

Figure2-1 World economic growth [1]

Table2-1 Average GDP growth rate in next 20 years

company	Asia Pacific	North America	Europe	Middle East	Latin America	CIS	Africa	China	World
Boeing	4.6	2.7	1.9	4.0	4.0	3.3	4.4	7.3	3.2
China commercial	4.4	2.63	1.96	4.84	3.84	3.16	5.21	5.87	3.71

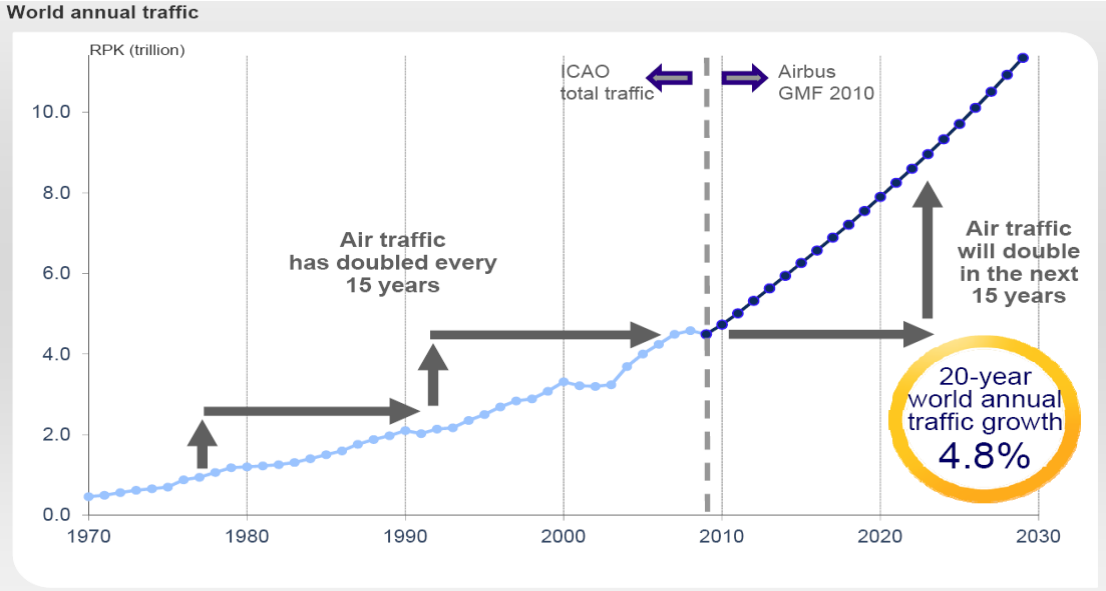

Figure2-2 World air traffic growth [2]

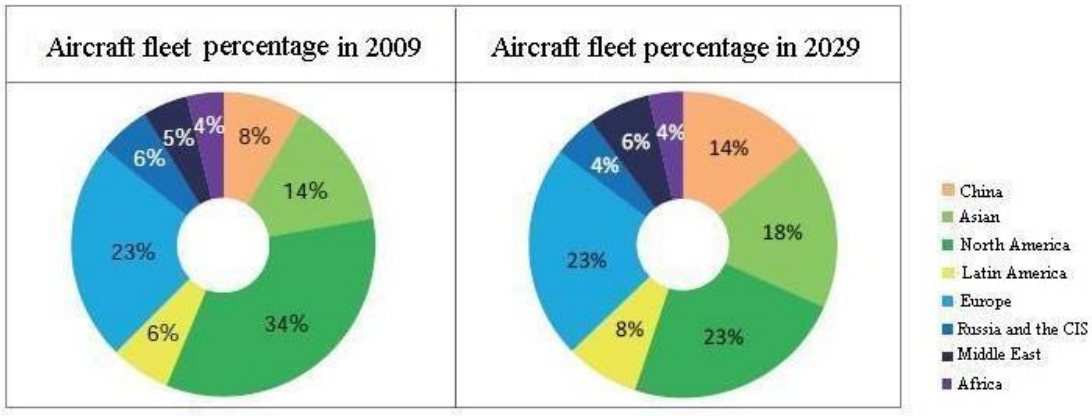

Figure2-3 Percentage of aircraft fleet in 2009 and 2029 [2]

To sum up, accompanied by the GDP growth, the demand for new passenger aircrafts will grow at a rate of 4.8 percent per year in next 20 years. Besides, Chinese domestic transportation market is the most vivid in the world civil aircraft market. Therefore, it is possible to design our Flying Wing aircraft to fly

in Chinese domestic market firstly. Then Europe and North-America market should also be considered because of large market occupation.

2.2 Seat capacity

According to Boeing Company's research, nowadays, single-aisle aircraft occupies 61 percent of the total aircraft fleet (see Figure2-4). The single-aisle fleet will be double in the next 20 years from 11,580 to 25,000 airplanes and represent 69 percent of the total fleet. In Asia, due to the rise of economies, the average growth rate will reach 4.4 percent.

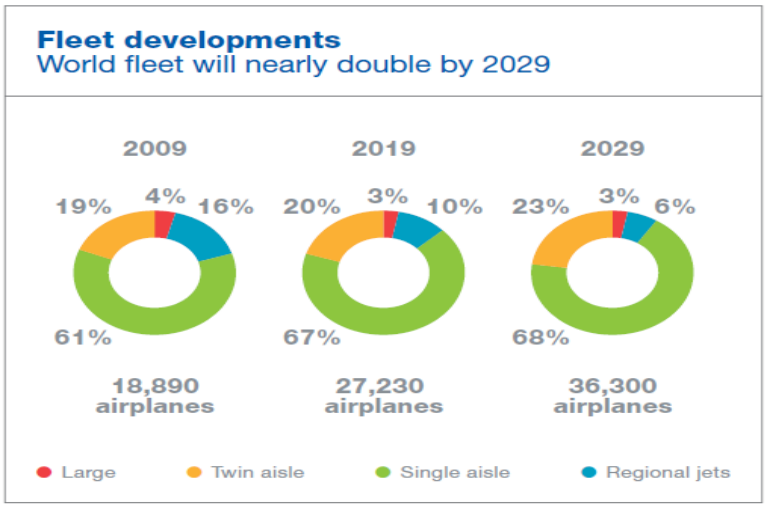

Figure2-4 Occupation of all kinds' airplanes

Boeing, Airbus and COMAC all give their prediction about the deliveries of various airplanes and their value from 2009 to 2029[1] [3] [5] (see Table2-2). According to their prediction, Twin aisle aircraft occupies the biggest value.

Table2-2 Aircraft deliveries and their value

	Global Aircraft Deliveries and Value							
	Large		Twin aisle		Single aisle		Regional jet	
	Deliveries	Value Billion	Deliveries	Value Billion	Deliveries	Value Billion	Deliveries	Value Billion
Boeing	720	220	7,100	1,630	21,160	1,680	1,920	60
Airbus	1,740	576	6,240	1,344	17,870	1,280		
COMAC			6,916	1,682.3	19,921	1,580.5	3,396	133.5

The strategy of China is another reason should be considered when design a new airplane. According to the research (see figure 2-5 [3]), the whole process of Chinese design its own aircraft can be divided into four stages. The first stage is regional jet, and ARJ21 has been successful designed. The second stage is single aisle, and China are preparing for C919 designing now. The third stage should be a twin aisle airplane to meet the biggest value market.

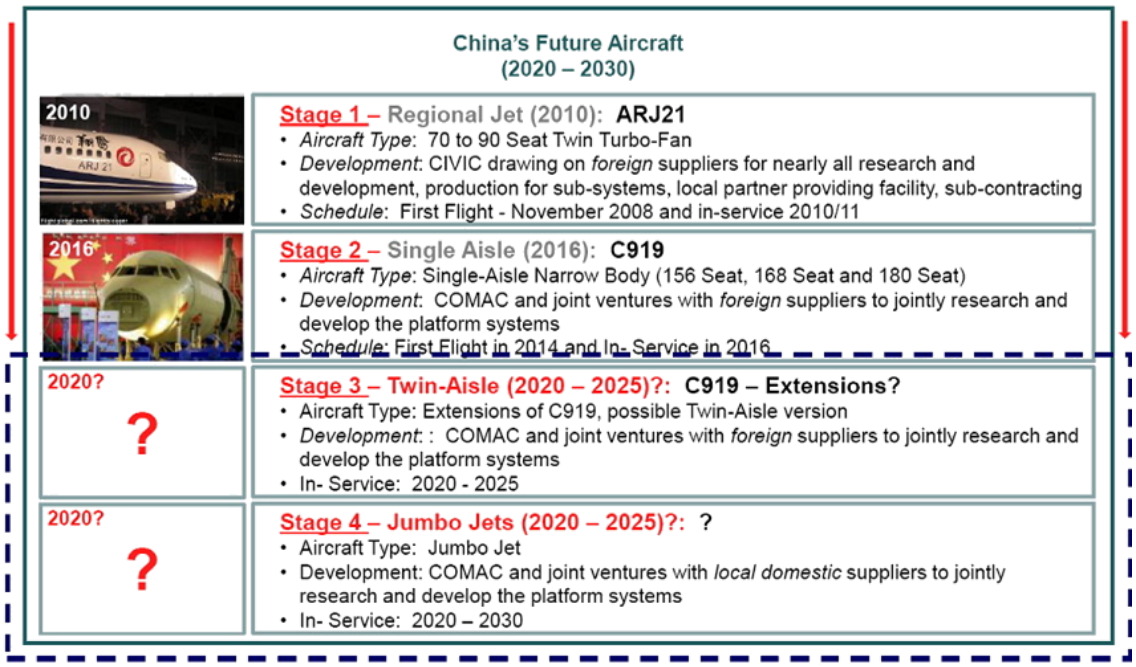

Figure2-5 Stages of china aircraft development

In conclusion, regional jet ARJ21, seat capacity 70-90, will put into service soon. Single aisle C919, seat capacity 150-180, is under development. Therefore, the Flying Wing aircraft should be from 200 to 250 seats.

2.3 Operators research

The research is about all kinds of 150-250 seat aircraft and the operators who are using those airplanes. Considering the main market is domestic China, the research is concentrated in Chinese operators.

2.3.1 Overview of the 150-250 seat aircraft

At present, many 150-250 seat civil aircraft are in service, including Airbus A320 family, Boeing 737 family, some McDonnell Douglas aircraft (M82, M90) and

Russian aircraft (TU5), which will be presented in Table 2-3. The ranges of those aircraft are shown in Figure 2-6.

Table2-3 150-200 seat aircraft

Type		Seats	Company
A320series	A318-100	107（Ⅱ） 117（Ⅰ）	Airbus
	A319-100	124（Ⅱ） 142（Ⅰ）	
	A320-200	150（Ⅱ） 180（Ⅰ）	
	A321-200	185（Ⅱ） 220（Ⅰ）	
B737series	B737-100	104（Ⅱ） 118（Ⅰ）	Boeing
	B737-400	146（Ⅱ） 168（Ⅰ）	
	B737-500	110（Ⅱ） 132（Ⅰ）	
	B737-600		
	B737-700	128（Ⅱ） 149（Ⅰ）	
	737-700ER		
	B737-800	162（Ⅱ） 189（Ⅰ）	
	B737-900ER	177（Ⅱ） 215（Ⅰ）	
M82、M90		About 150	McDonnell Douglas
TU5		About 150	Russia company

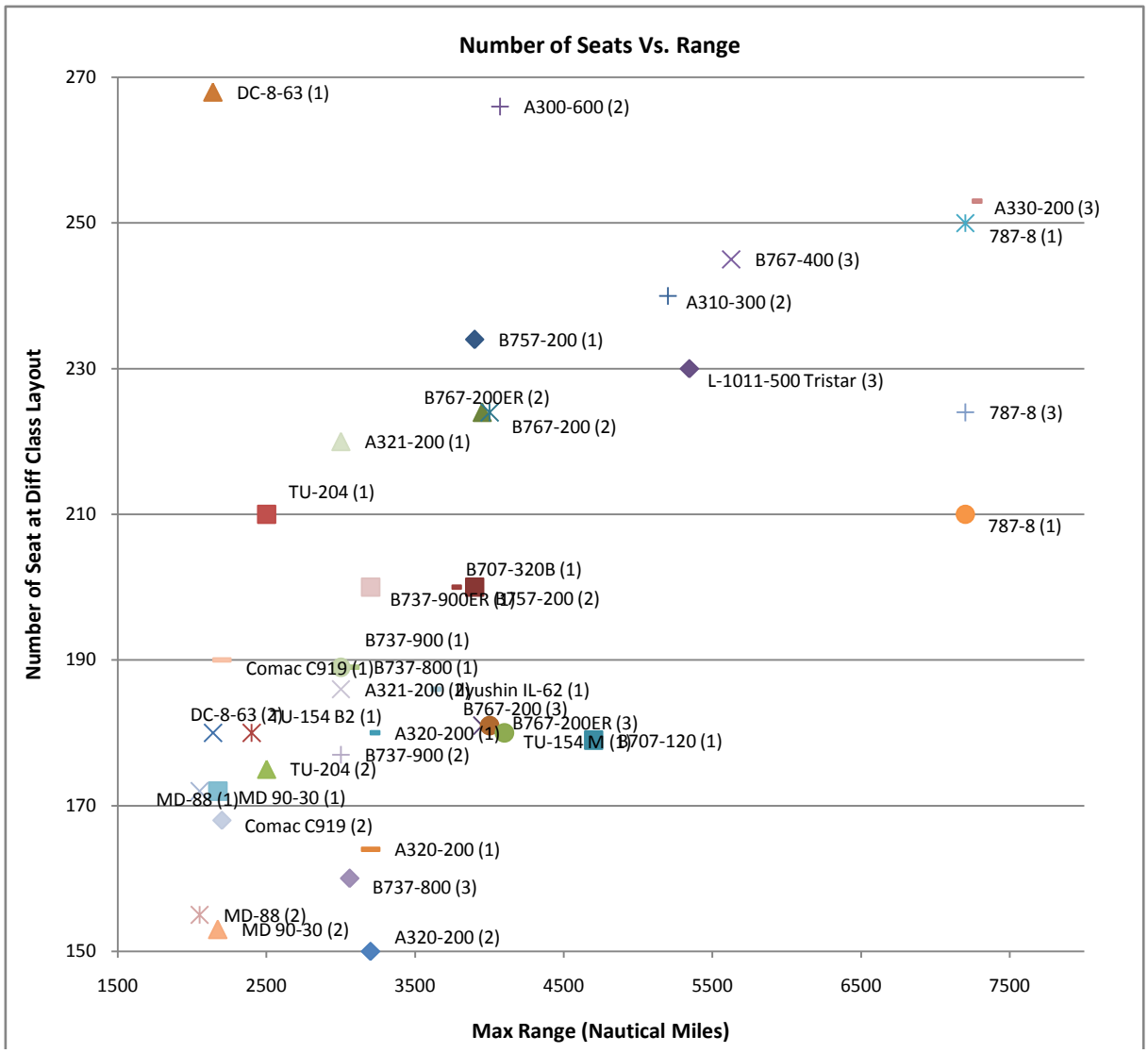

Figure2-6 150-250 seat aircraft and their range

2.3.2 Chinese operators

All together, there are 46 operators in China, and three of them are central enterprises companies which are much larger than others, Air China, China Eastern Airlines and China Southern Airlines. Some Local state-owned enterprises companies are also very large, such as Hainan Airlines, Sichuan Airlines and Shenzhen Airlines. Besides, some private enterprises also operate well, especially Spring Airlines, which grows much faster than other companies.

2.3.2.1 Air China

China Airlines was established in July 1988. It is one of the three largest Airlines in China with the employee more than 23,000, and Beijing is the company's headquarter. By the end of July 2009, it has 278 aircraft. Table 2-4 lists parts of the airplane. Domestic and International routes are drawn in Figure 2-7.

Table2-4 Parts of aircraft owned by Air China

Type	Number (ended July 2009)
A319	33
A320	5
A321	3
A330-200	20
A340-300	6
B737-300	38
B737-700	20
B737-800	47
B757-200	13
B767-200	3
B767-300	7
B777-200	10
B747-400	12

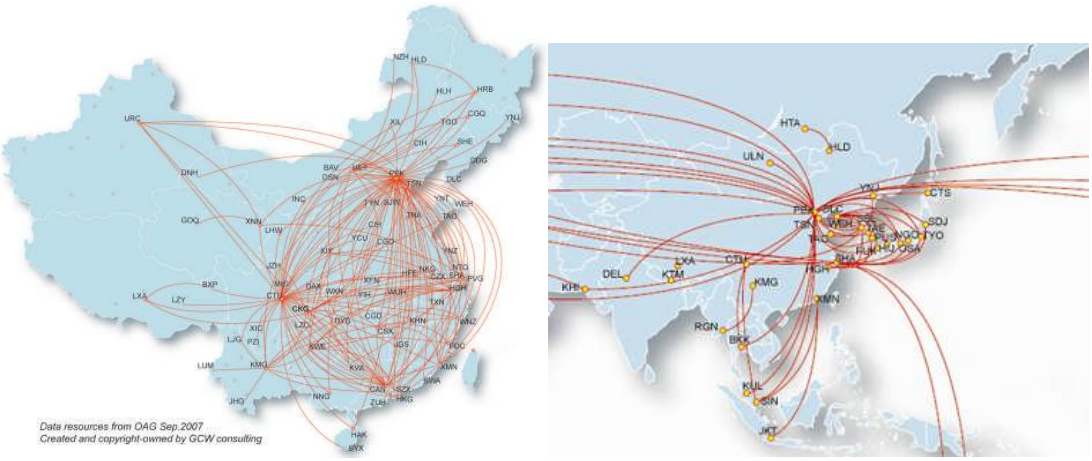

Figure2-7 Domestic and International routes of Air China

2.3.2.2 China Eastern Airlines

China Eastern Airlines was established in June 1988. It is the one of three largest Airlines in China with the employee more than 60,000, and Shanghai is the company's headquarter. By the end of January 2010, it has more than 330 medium-sized aircraft. China Eastern Airlines fleet includes major Airbus A300, A320, A330, A340, Boeing 737, Boeing 767, MD-90 and CRJ-200, ERJ-145, etc. Table 2-5 lists parts of the airplane. Domestic and International routes are drawn in Figure 2-8.

Table2-5 Parts of aircraft owned by China Eastern Airlines

Type	Number (ended April 2011)
A319-100	15
A320-200	97
A321-200	21
A330-200	5
A330-300	15
A340-300	5
A340-600	5
A300-600R	7
737-300	16
737-700	43
737-800	17
767-300ER	1
CRJ-200	5
ERJ-145	10

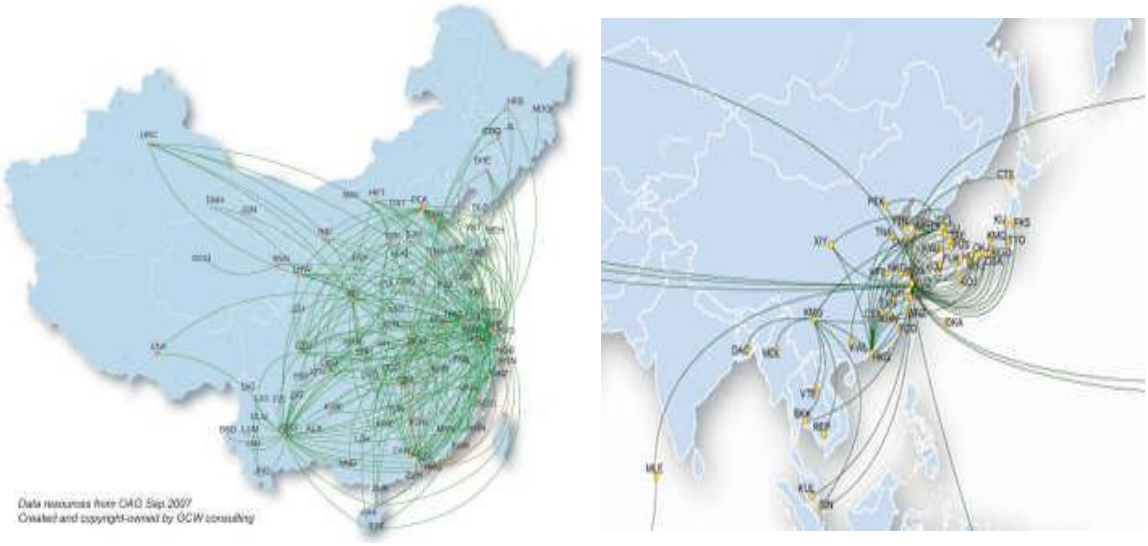

Figure2-8 Domestic and International routes of China Eastern Airlines

2.3.2.3 China Southern Airlines

China Southern Airlines was established in 1991. It is the one of three largest Airlines in China with the employee more than 13,000, and Guangzhou is the company's headquarter. By the end of January 2010, it has more than 400 medium-sized aircraft. China Eastern Airlines fleet includes major Boeing 777,747,757,737, Airbus A330, 321,320,319,300,380 etc. Table 2-6 lists parts of the airplane. Domestic and International routes are drawn in Figure 2-9.

Table2-6 Parts of aircraft owned by China Southern Airlines

Type	Number (ended May 2011)
A319-100	41
A320-200	64
A321-200	57
A330-200	9
A330-300	8
A380-800	5
A300-600R	3
737-300	25
737-700	31
737-800	50
757-200	15
777-200	4
777-200ER	6
777-200F	5
787-8	10
ATR72	5
ERJ145	6
MD-90	7

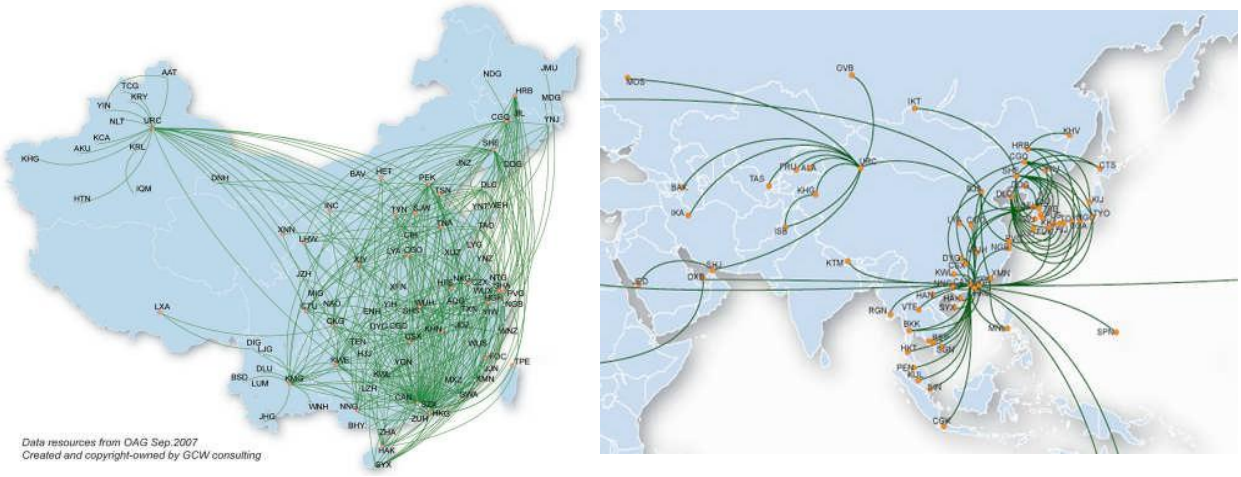

Figure2-9 Domestic and International routes of China Southern Airlines

2.3.2.3 China Hainan Airlines

China Hainan Airlines was established in January 1993. It is the fourth largest Airlines in China, and Haikou is the company's headquarter. By the end of February 2011, it has 258 aircraft most of them are Boeing 737 series aircraft. Table 2-7 lists parts of the airplane. Domestic routes are drawn in Figure 2-10.

Table2-7 Parts of aircraft owned by China Hainan Airlines

Type	Number (ended February 2011)
A319-100	29
A320-200	7
A330-200	7
737-300	7
737-300F	9
737-400	9
737-700	10
737-800	74
747-400F	4
Dornier 328	29
ERJ-145	24
ERJ-190	34

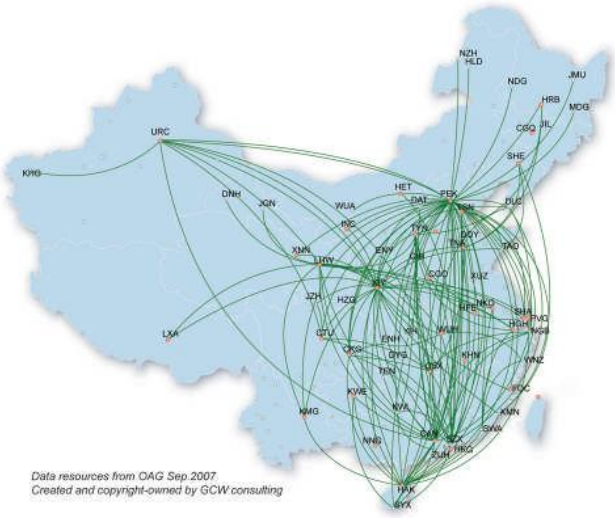

Figure2-10 Domestic routes of China Hainan Airlines

2.4 Design Range

The Figure 2-11 gives the 20-year traffic growth and 2029 world RPK predicted by Airbus. Domestic China will be the second large market in next 20 years.

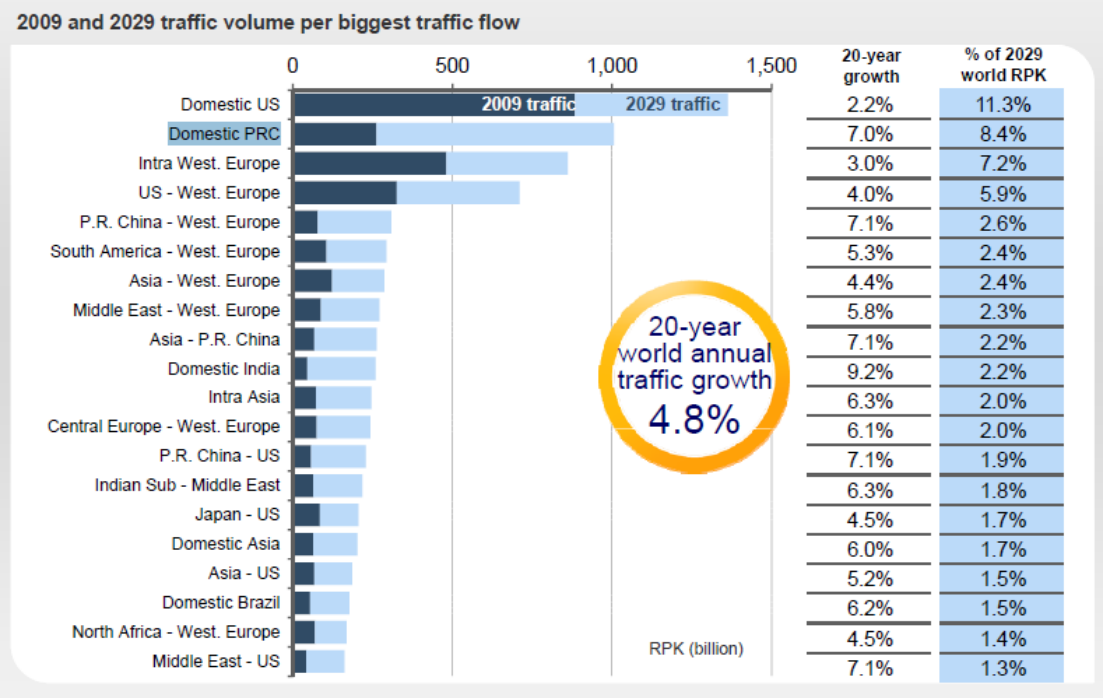

Figure 2-11 2009 and 2029 traffic volume[3]

When choosing the proper market, the first choice is domestic China, and it will occupy more than 7% of world RPK. The next goal is European and American, so the Flying Wing aircraft should be able to fly all around the world. Figure2-12 gives the place the Flying Wing aircraft can reach if the range is 7000 Nautical miles. It is enough for the aircraft reach Europe and North America. So the design range is 7000nm.

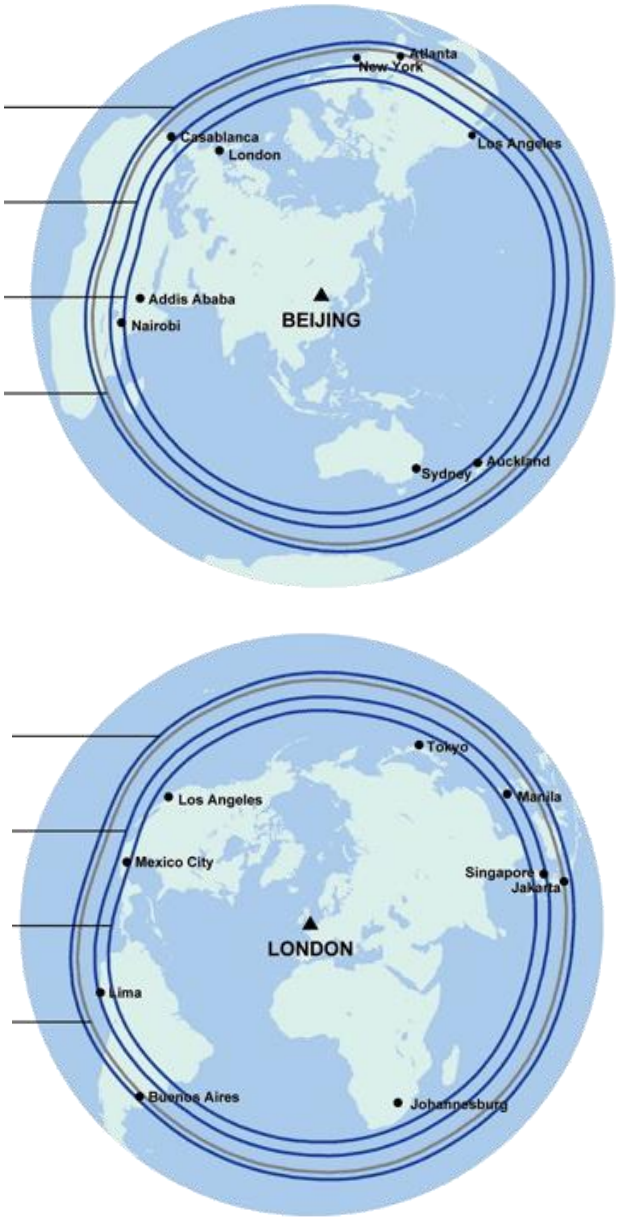

Figure2-12 Place Flying Wing aircraft can reach

2.4 Cruise Speed

According to the survey of same size aircraft B767 and A330, their cruise speed is M0.8 and M0.82 separately. B787 is a new advance aircraft with the cruise speed M0.85. So the cruise speed for Flying Wing aircraft will between M0.8 to M0.85.

2.5 Operating Requirements

It is obviously that fuel pays a very important role in the whole operating cost. According to Boeing's survey, the relationship between fuel and operating cost in recent years is shown in figure2-13 [8].

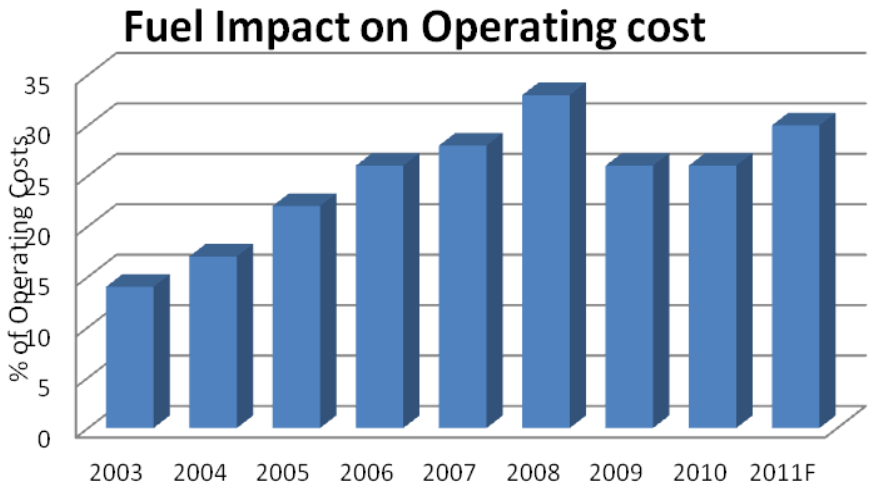

Figure2-13 Fuel and operating cost relationship

So, saving the oil means reducing the operating cost. The target of the airplane is 25% oil saving.

2.6 Airport Requirement

The classification of airport is shown in Figure2-14. Considering the figure of Flying Wing aircraft, 4E airports is required at least.

Code element 1		Code element 2		
Code number (1)	Aeroplane reference field length (2)	Code letter (3)	Wing span (4)	Outer main gear wheel span[a] (5)
1	Less than 800 m	A	Up to but not including 15 m	Up to but not including 4.5 m
2	800 m up to but not including 1 200 m	B	15 m up to but not including 24 m	4.5 m up to but not including 6 m
3	1 200 m up to but not including 1 800 m	C	24 m up to but not including 36 m	6 m up to but not including 9 m
4	1 800 m and over	D	36 m up to but not including 52 m	9 m up to but not including 14 m
		E	52 m up to but not including 65 m	9 m up to but not including 14 m
		F	65m up to but not including 80m	14m up to but not including 16m

a. Distance between the outside edges of the main gear wheels.

Figure2-14 Airport classification

Then next survey is about main airport in China, see figure 2-15 [9]. In all, 20 airports can be used for Flying Wing aircraft taking off and landing. The list is shown in Table 2-8.

Figure2-15 main airport in China [9]

Table 2-8 4E airport in China

	Airport	Passenger throughput	Increase over the previous year
1	Beijing Capital Airport	65,375,095	19.8%
2	Guangzhou Baiiyun Airport	37,048,712	10.8%
3	Shanghai Pudong Airport	31,921,019	13.1%
4	Shanghai Hongqiao Airport	25,078,538	9.6%
5	Shenzhen Biaoan Airport	24,486,406	14.4%
6	Chengdu Shuanliu Airport	22,637,762	31.3%
7	Wujiabao Airport	18,945,716	19.3%
8	Xi'an Xianyang Airport	15,294,947	28.3%
9	Hangzhou Xiaoshan Airport	14,944,715	17.9%
10	Chongqing Jianbei Airport	14,038,044	26.0%
11	Xiamen Airport	11,327,871	20.7%
12	Wuhan Tianhe Airport	11,303,767	22.8%
13	Changsha Huanghua Airport	11,284,282	33.5%
14	Nanjing airport	10,837,222	22.0%
15	Qingdao Airport	9,660,129	17.8%
16	Dalian Zhoushuizi Airport	9,550,365	16.4%
17	Haikou Meilan Airport	8,390,478	2.0%
18	Sanya Phoenix Airport	7,941,345	32.2%
19	Shenyang Tao Xian airport	7,504,828	10.2%
20	Zhengzhou Airport	7,342,427	24.7%

2.7 Manufacture research

The survey is mainly concentrated in AVIC manufacture companies. Since 1950, more than 30 types of civilian and military aircraft have been manufactured in those companies. In recent years, AVIC also has participated in subcontract work of B747, B757, B787, A310, A320, A330, A340, A350; MD-90 and FALCON2000/7X, G150/250, Figure2-16 [1] gives the Boeing 737 work-share in China.

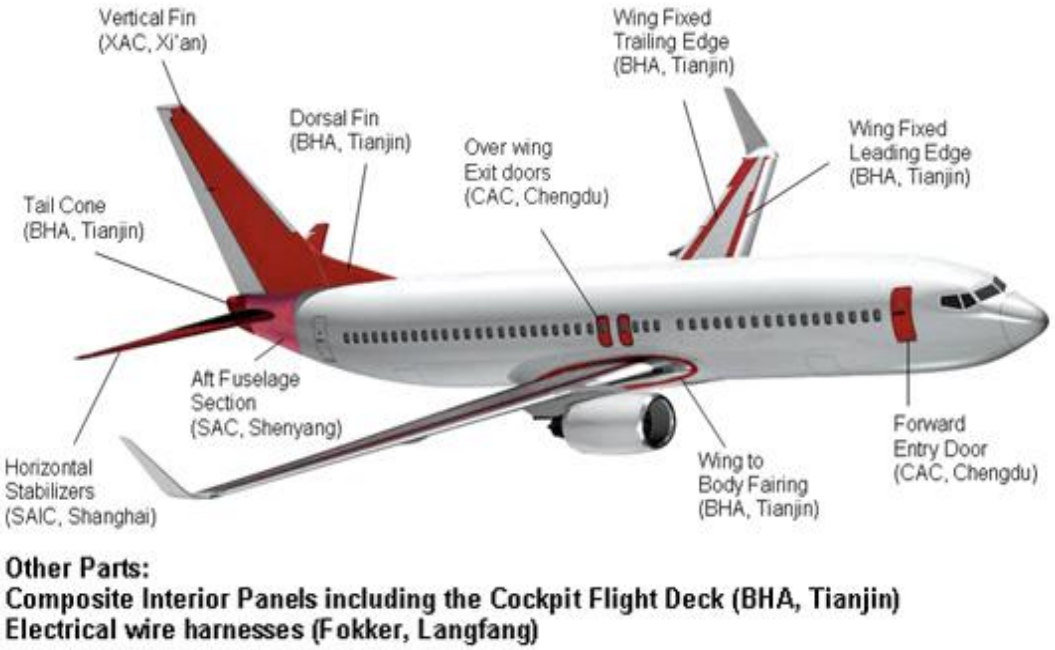

Figure2-16 Boeing 737 work-share in China [10]

China has advantage Components manufacturing capacity. Titanium alloy heat shaping, Shot penning forming and strengthening, hydro-forming of aircraft sheet metals, fatigue resistance manufacturing and connecting technology, and composite material manufacturing technology are all widely used in Components manufacturing. In C919, the use of composite materials will account for 20% [7].

2.8 Conclusion

According to our research, it seems that Boeing and Airbus share most of the aircraft manufacturing market in the range of 150-250 seating-capacities. However, new manufacturers are emerging to break this duopoly. A seating capacity of 150-200 is more popular among airlines. Operating costs seem to be the main driver to buy an aircraft rather than the seating-capacity of the aircraft. Most aircraft manufacturers tend to increase the percentage of composite materials to manufacture major components (fairings, part of the wings, cockpit). Airbus and Boeing tend to have more collaboration with other countries (India, Brazil), in particular with China. Considering the whole domestic and international demands, the Flying Wing airplane should be:

a) A twin-aisle, 250 seats international aircraft;

b) 7500 nm range, M 0.80-0.85 cruise speed;

c) Taking-off and Landing at 4E airports;

d) Better fuel efficiency;

e) Flexible operating capabilities;

f) Be able to manufacture in China.

3 Cabin Structure

Compared with conventional cylindrical pressurized fuselage, Non-circular pressurized fuselage brings two problems in cabin design. Firstly, with the increase in the number of passengers, emergency evacuation window will reduce. Secondly, non-circular cabin will increase moment stress greatly, causing an increase in structure weight. Figure 3-1 illustrates a cylindrical and a square box fuselage under internal pressure. It is clear that high stress is a serious problem for a non-circular cabin.

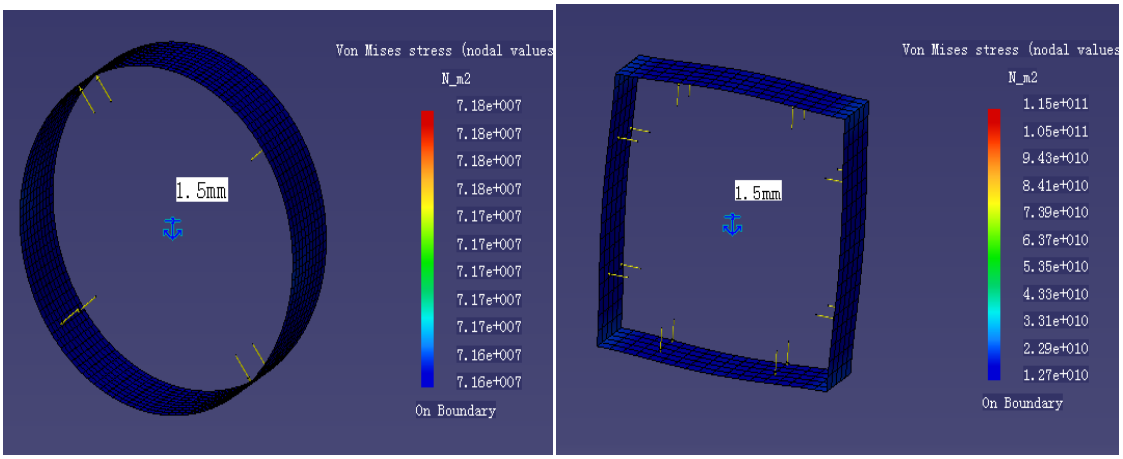

Figure 3-1 A cylindrical and a square fuselage under internal pressure

In order to solve the problem and reduce the stress and weight, four kinds of fuselage structure are discussed in cabin structure design process of Blended-Wing-Body (BWB) aircraft [11], including Conventional multi-bubble, Columned multi-bubble, Ribbed/honeycomb panel and Y-braced panel, which are presented in Figure 3-2. During the process of Cabin Structure of flying wing aircraft, last two layouts are through heated discussions. The advantages of Honeycomb panel are easy to layout and its high cabin space availability, while the disadvantages are also significant that it is very difficult to manufacture and maintain. When it turns to Y-braced panel, it reduces the bending at the joint of the roof and cabin walls and its skin provides higher bending stiffness without adding significant weight penalty. And it is easier to maintain than previous one. The evaluations of four structures are presented in Table 3-1.

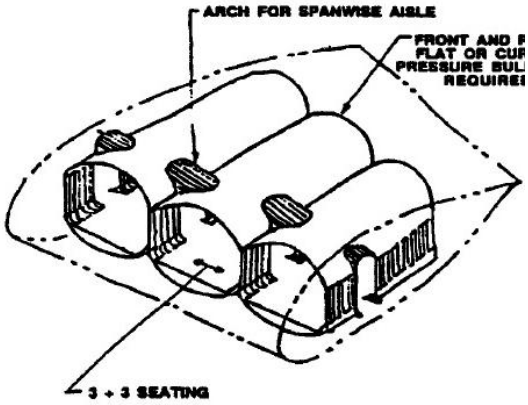

Conventional multi-bubble

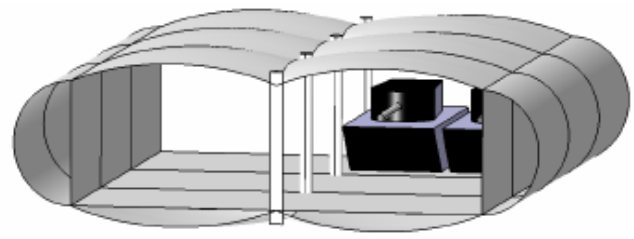

Columned multi-bubble

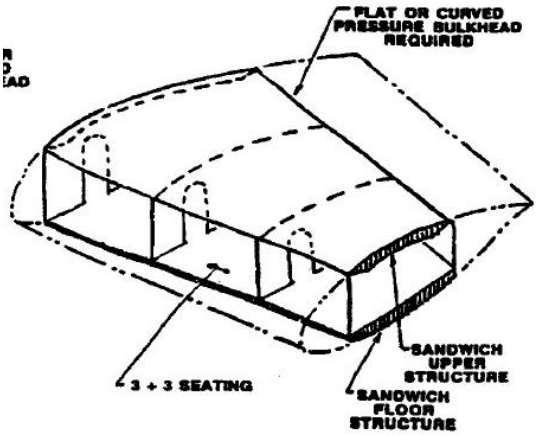

Ribbed/honeycomb panel

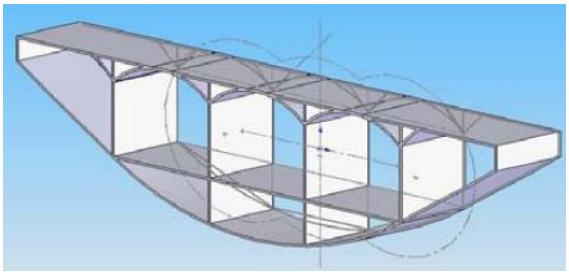

Y-braced panel

Figure 3-2 Four kinds of cabin structures

Table 3-1 Evaluations of four structures

	multi bubble		integrated structure	
	conventional	columned	Ribbed	Y-braced
Technique	★★★★	★	★★	★★★
Manufacture	★★★★★	★★	★★	★★★
Weight	★★	★★★★	★★	★★★★
Effective space	★	★★	★★★★	★★★
Maintenance	★★★	★★	★★	★★★

According the results of discussing, Y-braced panel is chosen in cabin structure. Figure 3-3 describes the Y-braced panel in the inner wing.

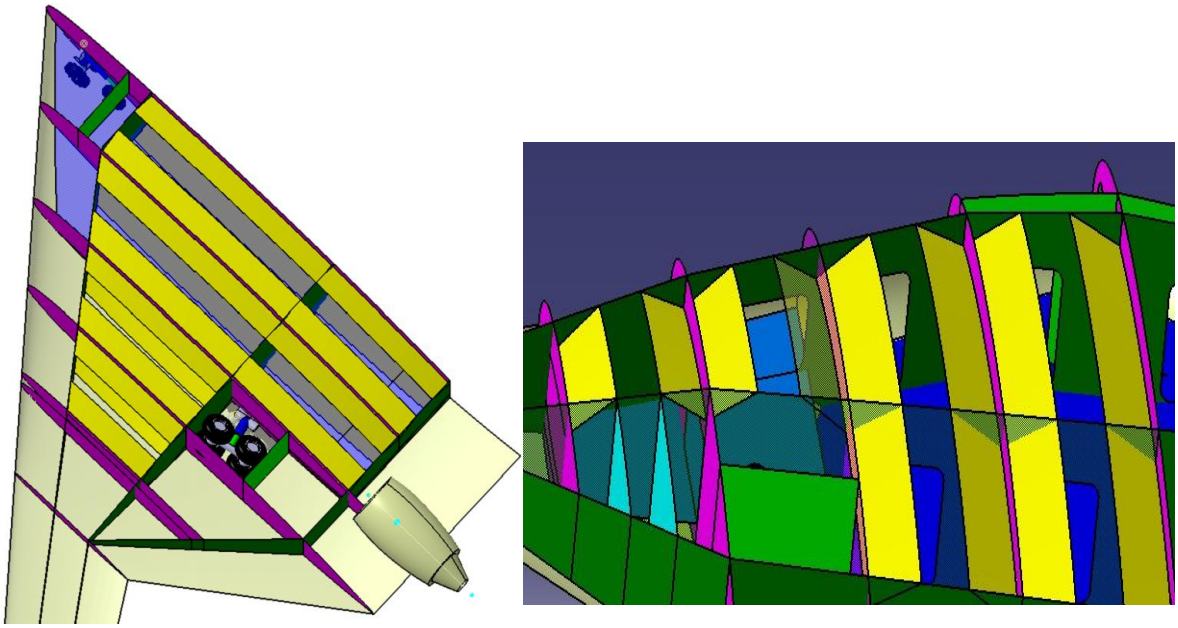

Figure 3-3 Y-braced panel in the inner wing

3 Conclusion and future work

Appendix A covers parts of the work that author has done during the conceptual design process of flying wing aircraft. All the work is finished by several groups of students who devote their time and energy to do the research.

Next stage is preliminary design progress. The future work will concentrated on more detail parameters of the flying wing aircraft.

REFERENCE

1. The Boeing Company, WORLD AIR CARGO FORECAST 2010-2011.

2. ICAO, Environmental Report 2010, P20-21.

3. Airbus, Global Market Forecast 2010-2029, December 13th 2010 www.airbus.com (accessed 04/2011).

4. Boeing, Global Market Forecast 2011-2030 www.boeing.com (accessed 04/2011).

5. COMAC, Global Market Forecast 2009 – 2029.

6. Aviation Industry Development Research Centre of China, China Market Outlook for Civil Aircraft 2007-2026, China Aviation Industry Corporation I, Beijing, China, 2007.

7. http: //www.planespotters.net

8. http://www.flickr.com/photos/jimyvrroutemap/sets/

9. http://himg2.huanqiu.com/attachment2010/101116

10. http://www.wikipedia.org

11. Blended-Wing-Body (BWB) Fuselage Structural Design for Weight Reduction, NASA Langley Research Centre, Hampton, VA.